AD-A155 472 DUCTILE FRACTURE OF DYNAMICALLY LOADED NAVAL STRUCTURES-COMPACT TENSION S.. (U) DAVID W TAYLOR NAVAL SHIP RESEARCH AND DEVELOPMENT CENTER BET.. 1/2

UNCLASSIFIED E A RASMUSSEN ET AL. FEB 85 DTNSRDC/84/071 F/G 20/11 NL

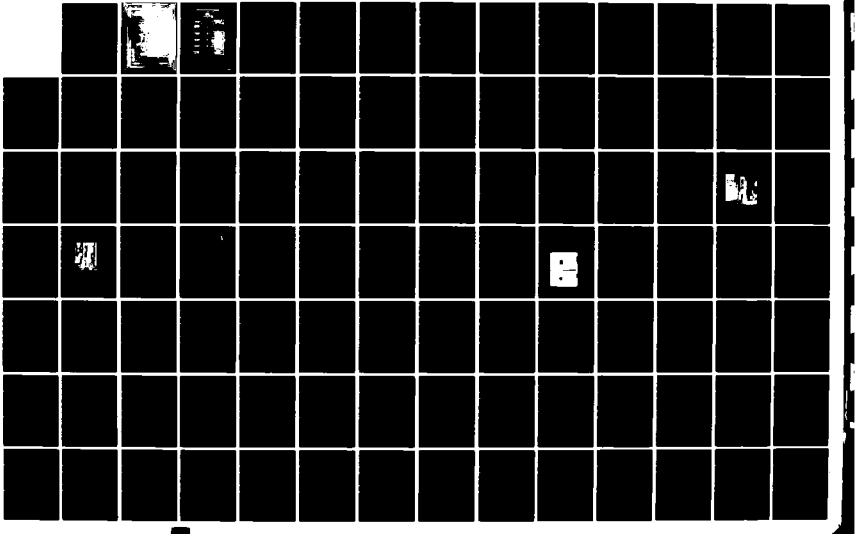

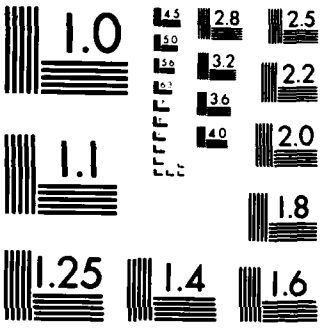

MICROCOPY RESOLUTION TEST CHART
NATIONAL BUREAU OF STANDARDS 1963-A

J-integral also increases (usually in a nonlinear fashion). When J reaches its critical value, J_{IC}, crack growth will initiate. With a further increase in

UNCLASSIFIED

SECURITY CLASSIFICATION OF THIS PAGE (When Data Entered)

REPORT DOCUMENTATION PAGE	READ INSTRUCTIONS BEFORE COMPLETING FORM
1. REPORT NUMBER DTNSRDC-84/071	2. GOVT ACCESSION NO. A155 492 / 3. RECIPIENT'S CATALOG NUMBER
4. TITLE (and Subtitle) DUCTILE FRACTURE OF DYNAMICALLY LOADED NAVAL STRUCTURES—COMPACT TENSION SPECIMEN TESTS AND ANALYSES	5. TYPE OF REPORT & PERIOD COVERED Final Report 6. PERFORMING ORG. REPORT NUMBER
7. AUTHOR(s) Erik A. Rasmussen William E. Carr L. Nash Gifford	8. CONTRACT OR GRANT NUMBER(s)
9. PERFORMING ORGANIZATION NAME AND ADDRESS David W. Taylor Naval Ship Research and Development Center Bethesda, Maryland 20084-5000	10. PROGRAM ELEMENT, PROJECT, TASK AREA & WORK UNIT NUMBERS (See reverse side)
11. CONTROLLING OFFICE NAME AND ADDRESS Naval Sea Systems Command Washington, D.C. 20362	12. REPORT DATE February 1985 13. NUMBER OF PAGES 136
14. MONITORING AGENCY NAME & ADDRESS(if different from Controlling Office)	15. SECURITY CLASS. (of this report) UNCLASSIFIED 15a. DECLASSIFICATION/DOWNGRADING SCHEDULE

16. DISTRIBUTION STATEMENT (of this Report)

APPROVED FOR PUBLIC RELEASE: DISTRIBUTION UNLIMITED

17. DISTRIBUTION STATEMENT (of the abstract entered in Block 20, if different from Report)

18. SUPPLEMENTARY NOTES

19. KEY WORDS (Continue on reverse side if necessary and identify by block number)

Fracture Mechanics
Finite Element Methods
Inelastic Dynamic Fracture
J-Integral
Compact Tension Specimen

20. ABSTRACT (Continue on reverse side if necessary and identify by block number)

A combined experimental/analytical research program aimed at extending the static J-integral to the case of dynamic inelastic fracture is described. This program was a first step toward the goal of quantifying the fracture response of naval structures containing flaws subjected to dynamic loading. One-inch thick HY-80 baseplate was used because of its known toughness and its widespread application in naval structures.

(Continued on reverse side)

DD FORM 1 JAN 73 1473 EDITION OF 1 NOV 65 IS OBSOLETE
S/N 0102-LF-014-6601

UNCLASSIFIED
SECURITY CLASSIFICATION OF THIS PAGE (When Data Entered)

(Block 10)

Program Element 61152N
Project Task Area ZR 023 0301
Work Unit 1720-410

(Block 20 continued)

For the experimental work, a drop weight test fixture was designed that permitted controllable, high rate loading of precracked compact tension specimens. A series of specimens was tested, and applied load, load point displacements, and back face strains were routinely measured with improving confidence and accuracy as the program progressed. The final measure required to obtain a critical value of the J-integral was the time, load or load point displacement at which fracture initiated. This proved to be the most difficult event to measure. After much trial and error, a multiple specimen approach was adopted in which specimens were loaded up to and just beyond the point of crack initiation. Using this method, an apparent dynamic J_{IC} for HY-80 steel was "bracketed". The resulting value was approximately 1000 in.-lb/in.^{2} versus an average static J_{IC} of 1110 in.-lb/in.^{2} for the same plate.

For the analytical work, two-dimensional finite element analyses were performed in conjunction with the experiments in an effort both to further develop analytical techniques for dynamic fracture problems and to provide information on the specimen response in this test program. The complex state of stress and the presence of side grooves in the specimens complicated the application of two-dimensional analyses. These problems were overcome, but the precision of the analyses performed remains uncertain pending further verification, perhaps using three-dimensional analysis methods.

The analyses performed displayed variable correlation with the experimental results. This variability was dependent on the yield stress input to the analysis. Surprisingly large differences in load point displacement resulted from small changes in yield stress. The analyses also showed the load point displacement to be very sensitive to the modeled crack depth. Changes of less than 1% in the ratio of crack length to specimen width resulted in load point displacement variations of roughly 40%. This sensitivity to stress-strain properties and crack depth was thought to be largely due to the deeply cracked nature of the specimens in this program, but remains a point of concern and interest due to the potential effect on similar fracture analyses.

TABLE OF CONTENTS

	Page
LIST OF FIGURES	iv
LIST OF TABLES	vii
NOTATION AND ABBREVIATIONS	viii
ABSTRACT	1
ADMINISTRATIVE INFORMATION	1
INTRODUCTION	2
BACKGROUND	3
EXPERIMENTAL TEST PROGRAM	9
TEST SPECIMEN	9
TEST APPARATUS	11
INSTRUMENTATION	12
Applied Load	15
Load Point Displacement	18
Detection of Crack Initiation	20
Summary of Instrumentation Design	26
TEST PROCEDURE AND RESULTS	26
FINITE ELEMENT ANALYSES	42
GENERAL	42
REVIEW OF PRELIMINARY ANALYSIS	43
SUBSEQUENT STUDIES	50
DISCUSSION	72
SUMMARY AND CONCLUSIONS	84
ACKNOWLEDGMENTS	87
APPENDIX - FURTHER INSTRUMENTATION DETAILS	89
REFERENCES	121

LIST OF FIGURES

	Page
1 - Physical Interpretation of the J-Integral for a Compact Tension Specimen	5
2 - The Arbitrary Path Γ About a Crack Tip	6
3 - Calculation of J from a Load-Displacement Record	8
4 - Geometry of the Modified Compact Tension Specimen	10
5 - Typical Acceleration Pulses from Preliminary Load Rate Tests	13
6 - Drop Weight Test Fixture for Very Rapid J_{IC} Testing	14
7 - Initial Instrumentation for Obtaining J_{IC} (Load Cell and Displacements D1 and D2 or D2')	18
8 - Calibration of Test Fixture Load Cell	19
9 - Characteristics of Side Grooves Placed in the Compact Tension Specimen	22
10 - Procedures Using Bondable Gages to Detect Crack Propagation	23
11 - Potential and Current Lead Attachment Locations	25
12 - Set-Up in Cyclic Load Machine for Fatigue Cracking Compact Tension Specimens	28
13 - Drop Test Set-Up	31
14 - Instrumentation Diagram for Dynamic J-Integral Tests	32
15 - Typical Oscillograph Record of Dynamic Test Data	33
16 - Digitized Record of Applied Load versus Time for Specimen JC-32	34
17 - Digitized Record of Load Point Displacement (LPD) versus Time for Specimen JC-32	35
18 - Load versus Load Point Displacement for Specimen JC-32	37
19 - J-Integral versus Time for Specimen JC-29	38
20 - Details of Fracture Surfaces for a Severely Tested Specimen	39

Page

21 - Measurements Typically Obtained after Separating Specimen..... 40

22 - ADINA Two-Dimensional Finite Element Idealization..... 45

23 - Specimen JC-6 Load versus Load Point Displacement for Static Finite Element Solutions..... 46

24 - Specimen JC-6 Load versus Load Point Displacement for Dynamic Finite Element Solutions..... 47

25 - Dynamic Finite Element Plastic Zone Growth for Specimen JC-6..... 49

26 - Input Load Histories for Finite Element Analyses..... 51

27 - Actual and Idealized Side Groove Geometry..... 53

28 - Actual and Idealized Material Stress/Strain Relations..... 58

29 - Experimental and Finite Element Load Point Displacement versus Time Results for Specimen JC-27..... 60

30 - Experimental and Finite Element Load Point Displacement versus Time Results for Specimen JC-23..... 61

31 - Finite Element Model of Loading Clevis..... 63

32 - Effect of Clevis on Finite Element Load Point Displacement Response for Specimen JC-23..... 64

33 - Effect of Clevis on Finite Element Load Point Displacement Response for Specimen JC-27..... 66

34 - Experimental and Finite Element Load Point Displacement versus Time Results for Specimen JC-22..... 69

35 - Experimental and Finite Element Load Point Displacement versus Time Results for Specimen JC-15..... 71

36 - Effect of Crack Depth on Specimen JC-27 Load Point Displacement Response..... 80

37 - Effect of Crack Depth on Specimen JC-23 Load Point Displacement Reponse..... 81

38 - Crack Depth versus Compliance for a Side Grooved Compact Tension Specimen..... 82

Page

A. 1 - Sensitivity Change in LPD Sensor Before and After Use in Test..... 91

A. 2 - Procedure for Calibrating Fotonic Displacement Sensor..... 93

A. 3 - Typical Characteristics of the Fotonic Sensor..... 93

A. 4 - Fotonic Sensor Calibrations for Different Target Conditions..... 95

A. 5 - Sensitivity of Fotonic Sensor for Simulated Test Condition..... 95

A. 6 - Validation of Fotonic Sensor Used for LPD Measurement..... 97

A. 7 - Initial Method for Determination of Crack Initiation..... 99

A. 8 - Attempt to Measure Crack Initiation with Sensor Located in Ligament..... 100

A. 9 - Attempts to Measure Crack Initiation with Sensor Located in Notch..... 100

A.10 - Example Showing Erroneous Indication by Crack Detection Gages (No Crack Extension)..... 103

A.11 - Example Showing Good Correlation Between Crack Detection Gages (No Crack Extension)..... 104

A.12 - Example Showing Discrepency Between Crack Detection Gages (Crack Extension Measured in Specimen)..... 105

A.13 - Load Required to Open "Krak" Gage after Precracking..... 107

A.14 - Moiré Fringes Produced During a Severe Specimen Test..... 109

A.15 - Comparison of Measurements from High Speed Film and LPD Sensor for Specimen JC-15..... 110

A.16 - Circuitry for Potential Difference Measurements..... 113

A.17 - Effects of Current Probe Location on Output Voltage..... 113

A.18 - Specimen Potential Drop Characteristics for Present Test and Referenced Results..... 114

A.19 - Potential Difference Signatures from Two Specimen Tests..... 116

Page

A.20 - Applied Load and Corresponding Potential Difference Histories for Specimen JC-32..... 117

A.21 - Comparison of Potential Difference Record with Applied Load for Tests at Comparable Conditions..... 118

LIST OF TABLES

1 - Sequence and Parameters for Dynamic J-Integral Tests..... 16

2 - Instrumentation or Techniques Used with Each Specimen to Obtain Load Point Displacement and Detection of Crack Initiation..... 27

3 - Summary of Specimen Preparation..... 30

4 - Summary of Test Results..... 41

5 - Analytical J-Integral Values for Specimen JC-6..... 48

6 - Load Point Displacements by Compliance and Finite Element Methods for Side Grooved and Full Thickness Specimens..... 54

7 - Load Point Displacement by Compliance and Finite Element Methods for a Side Grooved Specimen Varying Young's Modulus..... 56

8 - Summary of Finite Element Analyses..... 73

9 - Summary of Experimental J_{IC} Results..... 75

NOTATION AND ABBREVIATIONS

A_T	Area under the load-load point displacement curve
a	Crack depth
a_o	Initial crack depth
B	Specimen thickness
BFS	Back face strain
C	Compliance (load point displacement/load)
COD	Crack opening displacement
CT	Compact tension
DCPD	Direct current potential drop
DTNSRDC	David Taylor Naval Ship Research and Development Center
d	Distance between observed moiré fringes
ds	Differential length along a path
E	Young's modulus
G	Elastic strain energy release rate
J-Integral	A measure of the intensity of the stress and strain fields near the crack tip--the rate of change of total potential energy of a cracked body with respect to the developing crack surface area
$\dot{J}$	Rate of change of the J-integral with respect to time
J'	Generalization of the J-integral including dynamic effects
J_{IC}	Critical value of the J-integral at which crack initiation occurs
LD	Ligament displacement
LLD	Load line displacement
LPD	Load point displacement
ms	millisecond
n_j	Components of the unit normal vector

P	Spacing of master grid for moiré fringe technique
P_l	Load level
PD	Potential difference
ΔT	Parameter characterizing inelastic dynamic fracture
T_i	Tractions acting on a contour
U	Potential energy
u_i	Displacement components
V_a	Potential difference between two points on the specimen center line
W	Specimen width
W	Strain energy density
x,y	Cartesian coordinates
Y	A particular distance from the slit in a specimen
α	Geometric constant
Γ	Any closed path surrounding the crack tip
ε_{ij}	Strain components
θ	Angle of specimen half rotation
ν	Poisson's ratio
σ_{ij}	Stress components

ABSTRACT

A combined experimental/analytical research program aimed at extending the static J-integral to the case of dynamic inelastic fracture is described. This program was a first step toward the goal of quantifying the fracture response of naval structures containing flaws subjected to dynamic loading. One-inch thick HY-80 baseplate was used because of its known toughness and its widespread application in naval structures.

For the experimental work, a drop weight test fixture was designed that permitted controllable, high rate loading of precracked compact tension specimens. A series of specimens was tested, and applied load, load point displacement, and back face strains were routinely measured with improving confidence and accuracy as the program progressed. The final measure required to obtain a critical value of the J-integral was the time, load or load point displacement at which fracture initiated. This proved to be the most difficult event to measure. After much trial and error, a multiple specimen approach was adopted in which specimens were loaded up to and just beyond the point of crack initiation. Using this method, an apparent dynamic J_{IC} for HY-80 steel was "bracketed". The resulting value was approximately 1000 in.-lb/in.^{2} versus an average static J_{IC} of 1110 in.-lb/in.^{2} for the same plate.

For the analytical work, two-dimensional finite element analyses were performed in conjunction with the experiments in an effort both to further develop analytical techniques for dynamic fracture problems and to provide information on the specimen response in this test program. The complex state of stress and the presence of side grooves in the specimens complicated the application of two-dimensional analyses. These problems were overcome, but the precision of the analyses performed remains uncertain pending further verification, perhaps using three-dimensional analysis methods.

The analyses performed displayed variable correlation with the experimental results. This variability was dependent on the yield stress input to the analysis. Surprisingly large differences in load point displacement resulted from small changes in yield stress. The analyses also showed the load point displacement to be very sensitive to the modeled crack depth. Changes of less than 1% in the ratio of crack length to specimen width resulted in load point displacement variations of roughly 40%. This sensitivity to stress-strain properties and crack depth was thought to be largely due to the deeply cracked nature of the specimens in this program, but it remains a point of concern and interest due to the potential effect on similar fracture analyses.

ADMINISTRATIVE INFORMATION

This project was initiated and supported primarily by the David W. Taylor Naval Ship Research and Development Center (DTNSRDC) Independent Research Program, Element 61152N, Task Area ZR 023 0301, Work Unit 1720-410.

INTRODUCTION

The initiation and growth of cracks in critical naval structures has always been a concern to those who design scantlings and select materials and fabrication procedures. Many designs, however, notably lack quantitative consideration of defects ("How harmful is a given flaw under given loading?"). Instead, reliance has been placed on very tough (defect tolerant) materials, high quality welding, rigid weld inspection, and follow-on weld surveillance. This state of affairs, and ongoing research to improve the situation, have been discussed by a number of Navy researchers.[1-5]*

Cracklike defects in tough materials have not been addressed quantitatively because adequate technology simply does not yet exist. Because the materials in question are extremely tough, the relatively well-established principles of linear elastic fracture mechanics are not often applicable except in fatigue analysis. The emerging science of nonlinear fracture mechanics, on the other hand, shows great promise for dealing quantitatively with cracks in tough materials, that is, for assessing the margin of safety associated with a given flaw for a given static or dynamic load.

Within the past decade, research in nonlinear fracture mechanics has concentrated largely on static loading, with the so-called "J-integral"[6] becoming widely accepted as a fracture toughness measure. Standard procedures[7] were developed for J-integral testing under static conditions, and such tests have been conducted routinely at this Center for some time.[8] The early rationale behind this work was the development of methods for fracture toughness testing of more ductile metals, which are beyond the linear elastic (plane strain) constraints

---

*References are listed on page 121.

imposed by ASTM Standard E399.[9] Subsequently, it was recognized[10] that the J-integral also could serve as a fracture initiation criterion in real cracked structures (as opposed to standard test specimens), provided one could calculate its value as a function of applied load.

The loading of most interest for many naval structures is dynamic, however, and this area of nonlinear fracture mechanics has been subject of practically no research other than the recent work described in References 11 through 14. This report describes a basic experimental and analytical research program aimed at extending the J-integral approach to the analysis of inelastic fracture initiation under dynamic loading. Our research was motivated by the following questions:

1. Can the J-integral concept be used to characterize inelastic fracture initiation under dynamic loading conditions?
2. How can the critical value of J (J_{IC}) be measured under dynamic loading conditions?
3. Is J_{IC} dependent on loading rate for steels typically used in submarine hull construction?

Such questions, it was found, are not easy to answer. This report covers "trial and error" research conducted over 4 years. Considerable detail of the experimental and analytical programs is included so that future researchers may benefit from our experiences, both good and bad.

BACKGROUND

The J-integral is used in nonlinear fracture mechanics to measure the intensity of the stress and strain fields near the tip of a crack that tend to drive the crack forward. As loading on a cracked structure is increased, the

J-integral also increases (usually in a nonlinear fashion). When J reaches its critical value, J_{IC}, crack growth will initiate. With a further increase in load, stable crack growth or unstable crack propagation (complete fracture) will occur, depending on the method of loading (displacement control versus load control) and on the structural compliance.

The J-integral is thus not a failure criterion. If the structure and loading cause crack growth to decrease the crack driving force (a common situation), then failure will not occur when J reaches J_{IC}.

Physically, the J-integral is defined as the rate at which total potential energy of a cracked body changes with respect to developing crack surface area, and is a nonlinear generalization of the elastic strain energy release rate G. It is defined for two-dimensional through-cracked structures as

$$J = -\frac{1}{B}\frac{\partial U}{\partial a} \tag{1}$$

where B is the thickness of the structure, U is the potential energy, and a is the crack depth. As shown in Figure 1 for compact tension specimens of unit thickness, $J\Delta a$ at the load level P_1 is simply the shaded area between the load-displacement curves for two specimens having crack lengths of a and $a + \Delta a$.[15]

In addition to this experimental interpretation, the J-integral has a mathematical definition as given by Rice[6] for two-dimensional bodies containing a mode I through crack:

$$J = \oint_{\Gamma} W dy - T_i \frac{\partial u_i}{\partial x} ds \quad (i = x,y) \tag{2}$$

Here Γ is any closed path surrounding the crack tip, W is the strain energy density $\left(W = \int_0^{\varepsilon_{ij}} \sigma_{ij}\, d\varepsilon_{ij}\right)$, T_i are the tractions acting on the contour ($T_i = \sigma_{ij}\, n_j$),

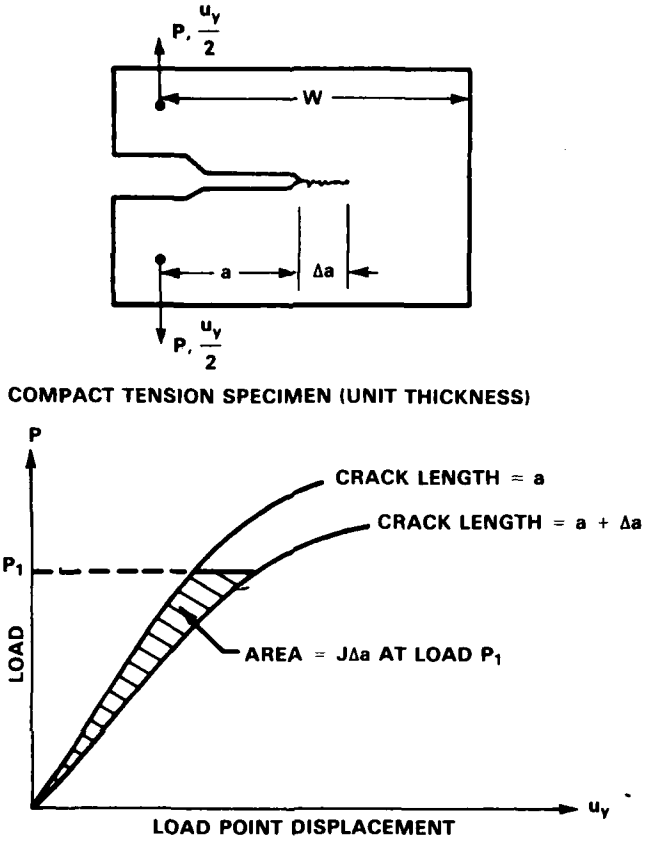

Figure 1 - Physical Interpretation of the J-Integral for a Compact Tension Specimen

ε_{ij} are strains, σ_{ij} are stresses, n_j are the components of the unit normal to the path, u_i are displacements, and x, y, and ds are as defined in Figure 2. Rice showed that for linear elastic bodies, and for bodies to which the deformation theory of plasticity applies, the J-integral is independent of the path chosen for its evaluation. For the more realistic incremental theories of plasticity, the J-integral is practically path-independent so long as the loading increases monotonically and remains nearly proportional. Thus the J-integral is an ideal parameter for calculating crack driving force, since the researcher may choose a path that is remote from

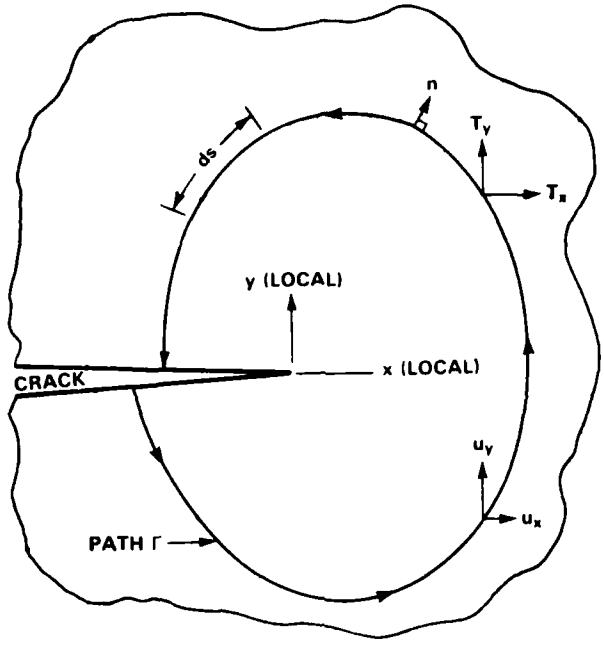

Figure 2 - The Arbitrary Path Γ About a Crack Tip

the crack tip, where accurate stress analysis is easier, rather than analyzing the vicinity of the crack tip, which is difficult. In general, nonlinear finite element analysis is used to calculate the J-integral as a function of increasing load in realistic structures (as opposed to test specimens). As an example, the DTNSRDC PAPST (Plastic Axisymmetric/Planar STructures) finite element computer program[16] has a built-in capability to calculate the J-integral on up to ten user-specified paths about a crack tip.

For compact tension specimens like that shown in Figure 1, the experimental value of the J-integral may be related to the load versus load point displacement curve in the manner shown by Merkle and Corten[17]:

$$J = \frac{2(1+\alpha)}{B(W-a)(1+\alpha^2)} \int_0^{u_y} P du_y + \frac{2\alpha(1-2\alpha-\alpha^2)}{B(W-a)(1+\alpha^2)^2} \int_0^{P} u_y dP \qquad (3)$$

In the above, $\int P du_y$ is the area under the load-displacement curve (work), $\int u_y dP$ is the complementary work, and α is given by

$$\alpha = \left[\left(\frac{2a}{W-a}\right)^2 + \frac{4a}{W-a} + 2\right]^{1/2} - \frac{2a}{W-a} - 1 \qquad (4)$$

where W and a refer to the specimen dimensions shown in Figure 1.

Under slow test, the critical value of J may be determined in a single specimen test by noting the load or load point displacement at which fracture begins. This is usually done by the unloading compliance method described by Joyce and Gudas,[8] wherein the load is decreased by about 10% periodically during a test to check for a change in elastic specimen compliance that indicates fracture initiation. The load-displacement record, together with Equation (3), then gives J_{IC}. In fact, for deeply cracked specimens, Equation (3) can be reduced to[18]

$$J = \frac{1 + \alpha}{1 + \alpha^2} \frac{2A_T}{B(W-a)} \qquad (5)$$

where A_T is the total area under the load-load point displacement curve diagrammed in Figure 3.

To summarize, we have outlined two uses of the J-integral in the static realm: (1) as an experimental parameter (beyond linear elastic fracture mechanics) for measuring the toughness of materials loaded into the elastic-plastic range, and (2) as a mathematical parameter that can be calculated for realistic elastic-plastic cracked structures. This duality affords a capability for design against fracture initiation by comparing calculated values of J against the experimentally measured critical value of the J-integral, J_{IC}. Until now, however, this idea has been largely confined to the static case.

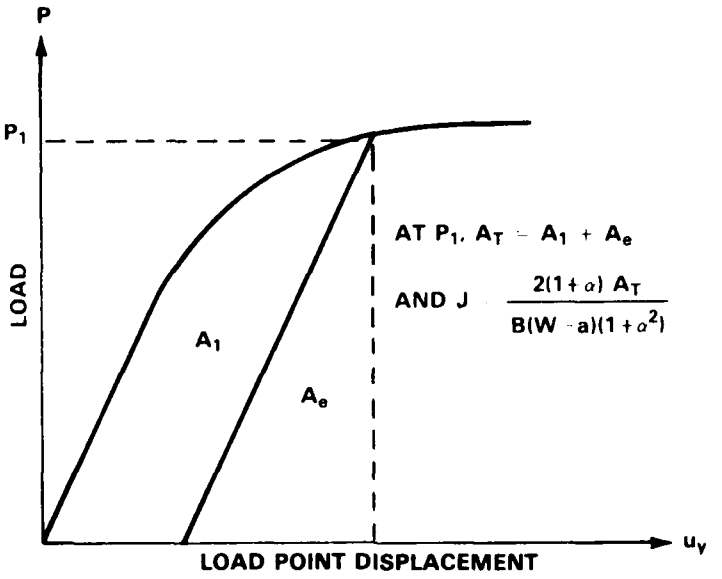

Figure 3 - Calculation of J from a Load-Displacement Record

In the work described in this report we sought to extend the J-integral concept to dynamic inelastic fracture of large-scale naval structures. The specific objectives of this research were as follows:

1. Design an experimental technique by which standard compact tension J_{IC} specimens may be rapidly loaded at various rates.

2. Develop instrumentation techniques capable of measuring fracture phenomena that occur in less than a millisecond. Specifically, load versus time and load point displacement versus time must be accurately measured in order to use equations like (4) and (5) to construct the curve of the J-integral versus time.

3. Develop a technique for determining when fracture begins in terms of time, load, or displacement in order to estimate the value of J_{IC} under dynamic conditions.

4. Validate analytical techniques (nonlinear dynamic finite element fracture analyses) to assist in guiding the experimental program and to make possible the calculation of J in realistic cracked ship structures.

5. Determine the difference, if any, between the values of J_{IC} under static and dynamic loading for typical (HY) steel structural materials.

Our approach and progress in achieving these goals are described in this report.

EXPERIMENTAL TEST PROGRAM

TEST SPECIMEN

The J-integral has been identified as an appropriate criterion for fracture initiation for many tough materials under static and quasi-static load conditions.[10] Our task was to determine this same property for dynamic load conditions at rates typical of those associated with an impact or an explosion attack on naval structures. The deep notch compact tension (CT) specimen used in these studies was similar to the type widely used to study material toughness, perhaps most notably the plane-strain fracture toughness properties as outlined in Reference 9. Basic dimensions for the specimen used in this work are shown in Figure 4, and manufacturing drawings are identified in Reference 19.

Alterations were made to the specimen during the test program. The alterations included modifying the holes to accept the instrumentation and machining side grooves to reduce undesirable shear lips that tend to develop on the specimen edges. A fatigue precrack had to be introduced into the specimen before the test. The controlled procedure outlined in Reference 9 was used to assure that a crack of proper depth and with a sharp tip was obtained so that the specimen would perform consistently and give valid data.

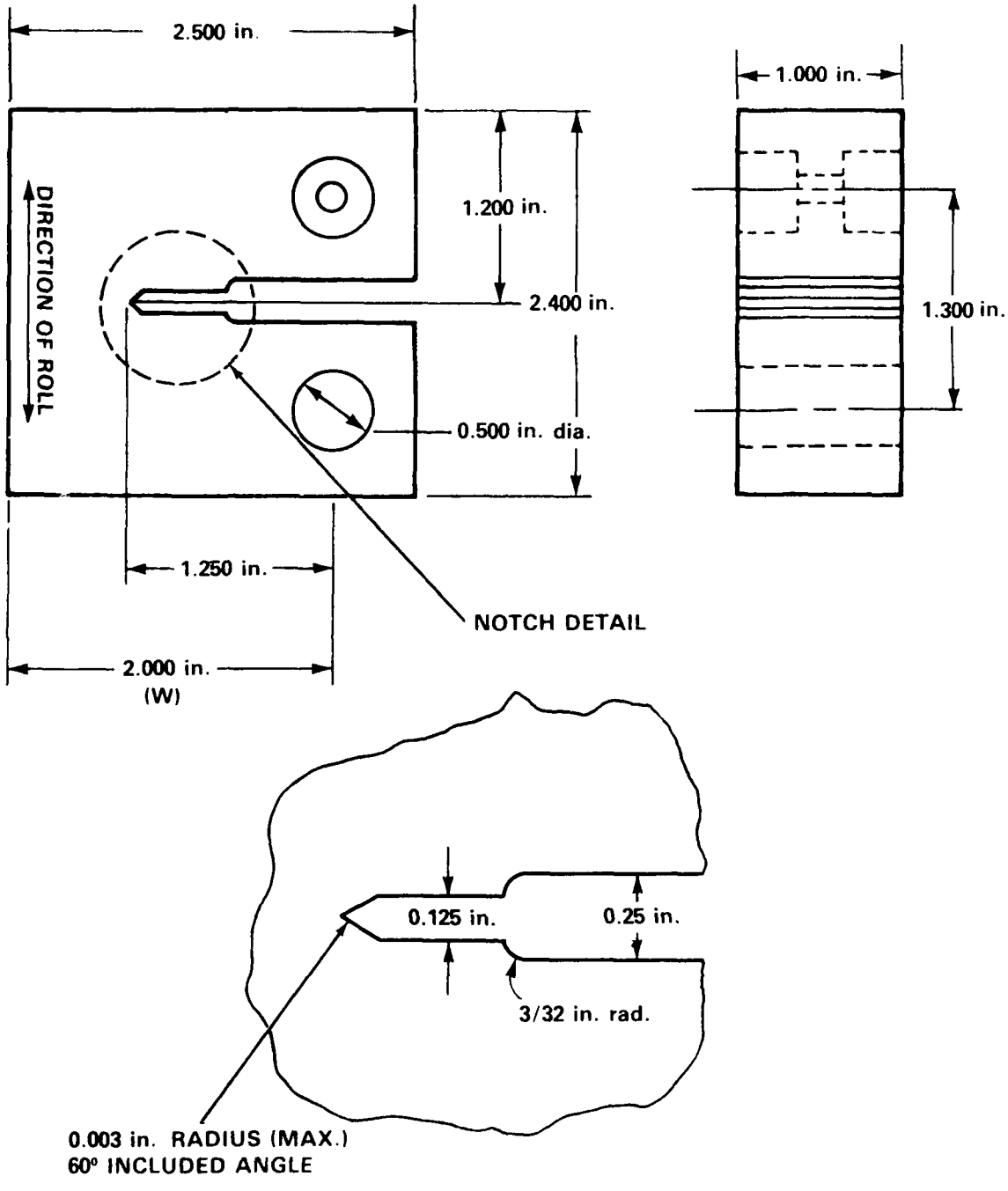

Figure 4 - Geometry of the Modified Compact Tension Specimen

TEST APPARATUS

After considering the various test conditions desired for this study, we decided that a drop test technique would be most appropriate. The specimen would be installed in a stationary fixture which a free-falling weight would strike thus loading the specimen in the opening mode. This approach was simple and offered many loading rate options. The applied load could be varied by choice of drop height and the size of the drop weight. Drop weights of 115, 60, and 30 lb were available. The heaviest weight was made of steel and the two lighter ones of aluminum. They were cylindrical, 8 in. in diameter, and were constructed with a longitudinal groove on each side to mate with a vertical guide track. An impact buffer could be placed between the fixture and the impacting weight. These buffers could be designed with different properties to act as load programmers providing even wider test variations.

Some preliminary work was done to determine the extent to which the loading could be controlled by varying certain test parameters, namely the impact device and the drop height. Several different materials, including nylon, adiprene (a rubber type material), and lead, were investigated. These materials were configured into various cross-sectional areas and thicknesses to give different stiffness characteristics. To investigate their dynamic characteristics these devices were then placed on a rigid steel base and were struck by a 60-lb weight dropped from two discrete heights. This facility was designed so that it could later be used in the test program. To determine the performances of these different arrangements, the deceleration pulse was measured at impact with an accelerometer positioned on top of the drop weight. These pulses are qualitative indications of the shape and duration of the generated force. They do not truly represent the actual test pulses, because

the dynamic characteristics of both the test fixture and of the specimen would alter the load pulses obtained. The shapes and the range of magnitudes and durations for the load pulses are shown in Figure 5.

An extremely rigid test fixture, which permitted the specimen to be loaded in an opening mode at impact, was designed and built. It was designed with tight tolerances so that essentially only an axial load would be applied. Special clevis pins to engage the specimen were used to eliminate clearance and prevent extraneous signals from occurring on the test measurements. Figure 6 is a sketch of this drop test fixture; Reference 20 identifies drawings used to fabricate the device.

INSTRUMENTATION

The J-integral is a measure of the intensity of stress and strain fields near a crack tip in a material at a given value of applied load. At some load, a critical condition known as J_{IC} is reached, where crack growth initiates. The J-integral can be conveniently obtained from a curve relating the applied load and the corresponding load point displacement. To determine J_{IC}, crack initiation must be determined as a function of time, displacement, or load.

Special instrumentation and techniques had to be developed to obtain these measurements because the tests were to be conducted under rapid load conditions. A large effort was involved with this phase, and frequently, certain procedures were found unsuccessful and alternate approaches were needed. The load point displacement and the crack initiation were particularly difficult to measure. A technique was finally developed whereby this displacement could be confidently measured, but the problem of detecting crack initiation in a single-specimen test was not solved satisfactorily. Without this capability, the alternative was to run a series of tests, with increasingly severe loading, and to determine the threshold of fracture.

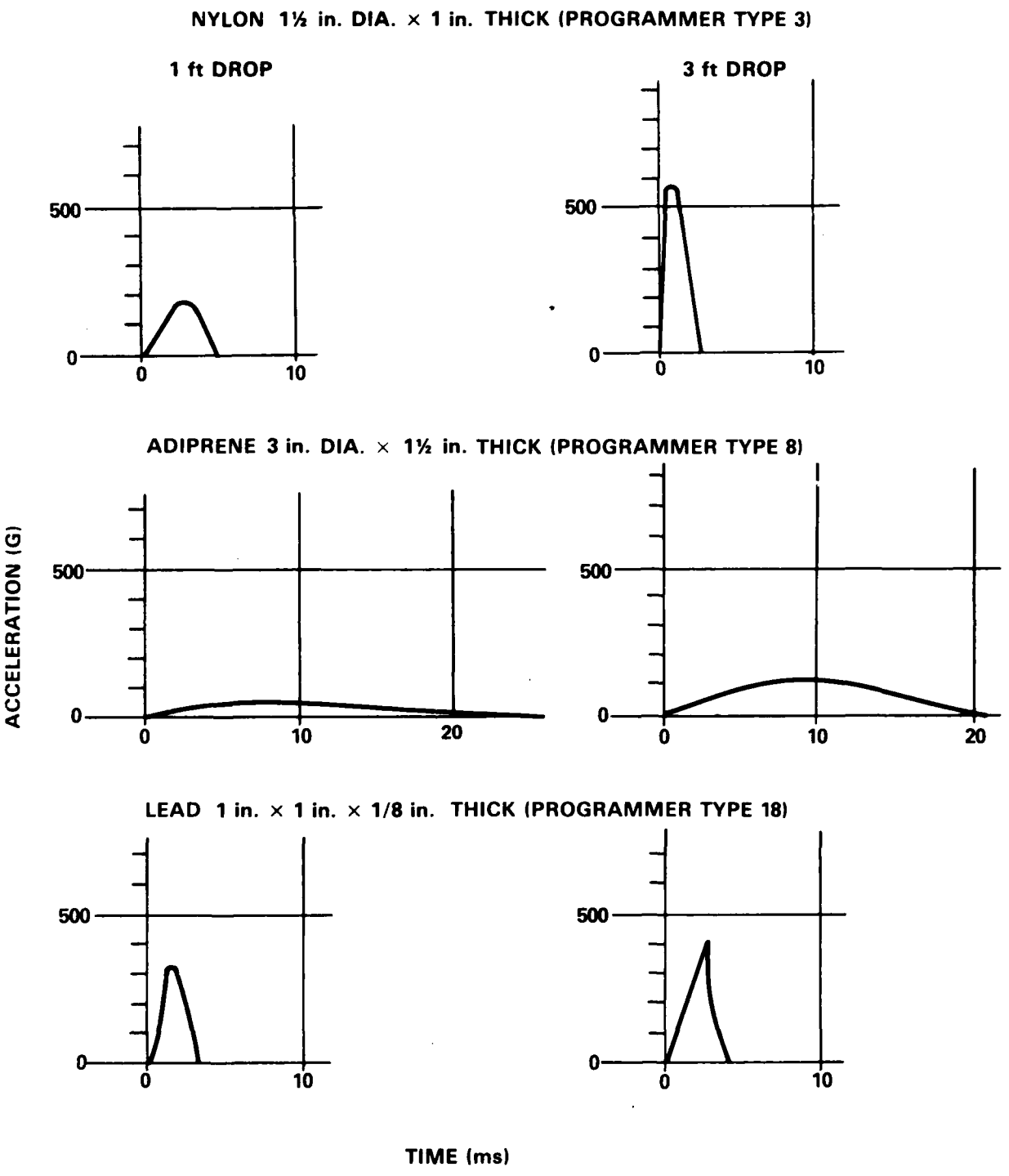

Figure 5 - Typical Acceleration Pulses from Preliminary Load Rate Tests

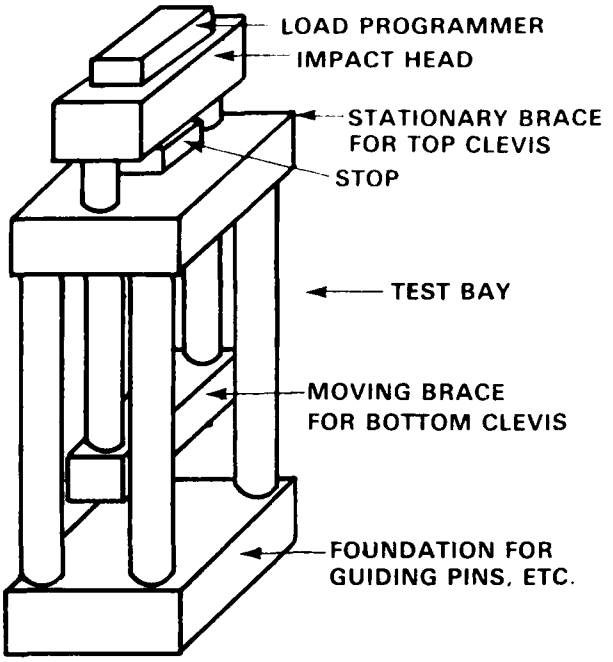

Figure 6a - Schematic of Test Fixture Mechanism

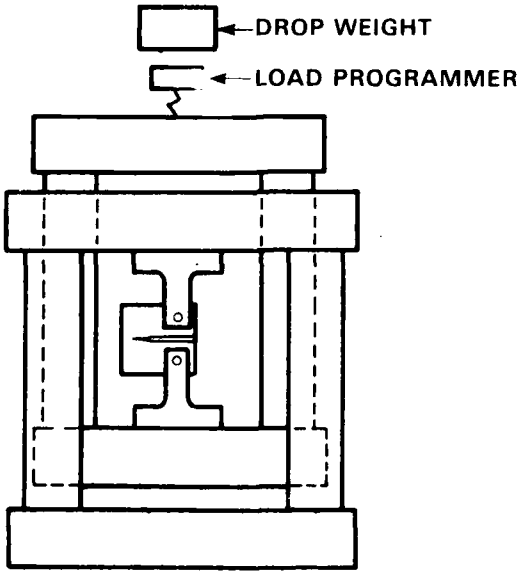

Figure 6b - View of J_{IC} Specimen in Test Fixture

Figure 6 - Drop Weight Test Fixture for Very Rapid J_{IC} Testing

The corresponding J-integral was then assumed to be the critical value, J_{IC}. This approach was used for two basically different load histories. At this writing, 26 HY-80 steel specimens have been tested and 42 separate drops made. Table 1 lists these specimens along with the essential parameters (drop height, drop weight, and impact device) for each test.

Following are discussions of the procedures and techniques used to obtain the essential measurements. Some procedures were quite successful from the start and remained essentially unchanged throughout the test series. Obtaining some of the more difficult measurements, however, required an evolutionary process of varying instrumentation and associated techniques. In the interest of clarity, the next sections describe only the most accurate and reliable of the measurement methods attempted. Detailed discussion of all the techniques and instrumentation used and the trials associated with obtaining valid data from them are provided in the appendix.

Applied Load

Figure 7 is a sketch of the test fixture and compact tension specimen. As shown, the load cell was located on the lower clevis stem and measured the force transmitted to the specimen. This cell consists of a strain gage bonded to each side of the stem. They operate as two active arms of a four arm Wheatstone bridge and are connected in opposite arms of the bridge to effectively cancel any bending components on the signal. The cross section of the clevis where the gages were attached had been reduced in order to increase the sensitivity of the bridge. This load cell was calibrated statically for loads up to 15,000 lb and the results are shown in Figure 8. Also shown in the figure is the projected sensitivity based on the cross section area of the stem; note the close correspondence between the two.

TABLE 1 - SEQUENCE AND PARAMETERS FOR DYNAMIC J-INTEGRAL TESTS

Specimen No.	Drop No.	Drop Weight (lb)	Drop Height (in.)	Element*
1	1	30	6	8
	2	30	12	8
	3	30	3	8
	4	30	6	8
	5	30	6	8
	6	30	12	8
	7	60	36	8
	8	115	36	8
2	1	115	36	8
3	1	60	36	8
4	1	60	36	8
5	1	115	36	3
6	1	115	36	3
7	1	115	36	3
8	1	115	6	3
10	1	60	6	3
11	1	60	5	3
14	1	60	7	3
13	1	60	9	3
15	1	60	8	3
16	1	60	12	3
18	1	60	3	3
	2	60	5	3

* See note at end of table

TABLE 1 (Continued)

Specimen No.	Drop No.	Drop Weight (lb)	Drop Height (in.)	Element*
18	3	60	12	3
	4	60	8	3
	5	60	8	3
19	1	60	8	3
	2	60	8	3
	3	60	8	3
	4	60	8	3
21	1	60	8	3
	2	60	8	3
20	1	60	8	3
	2	60	8	3
22	1	60	8	3
23	1	60	8	18
26	1	60	12	18
27	1	60	10	18
31	1	60	10	18
32	1	60	12	18
33	1	60	11	18
29	1	60	11	18

* Weight/fixture impact device: Type 8, 3 in. dia. × 1½ in. thick Adiprene; Type 3, 1½ in. dia. × 1 in. thick Nylon; Type 18, 1 in. × 1 in. × 1/8 in. thick lead.

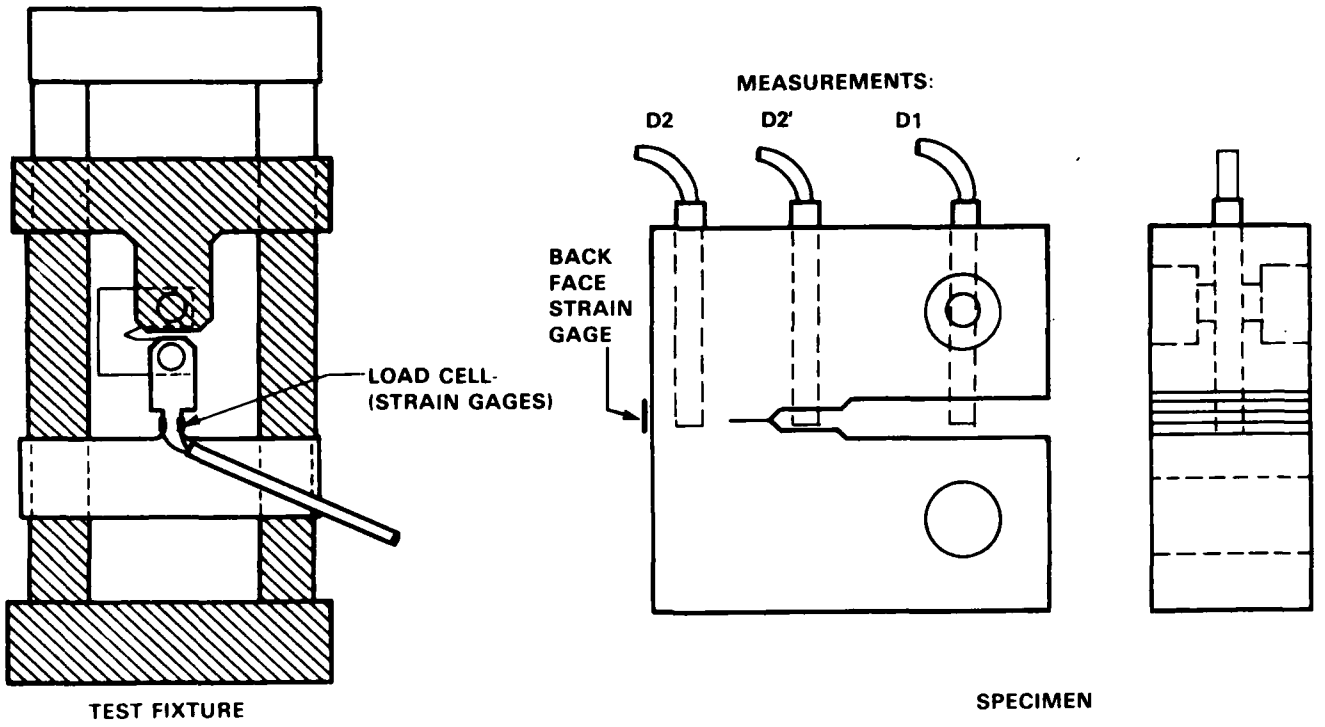

Figure 7 - *Initial Instrumentation for* Obtaining J_{IC}
(Load Cell and Displacements D1 and D2 or D2')

This static sensitivity was used to determine the force applied to the specimen during the dynamic tests.

Load Point Displacement

The second essential measurement was the load point displacement, LPD--also called the load line or the crack opening displacement (LLD and COD, respectively). This is measurement D1 in the schematic of Figure 7. Primary considerations for selecting this sensor were frequency response, displacement range, and size and ease of adapting to the test setup. A clip gage, which had been used in the past for this application under static loading, did not offer these desired features.

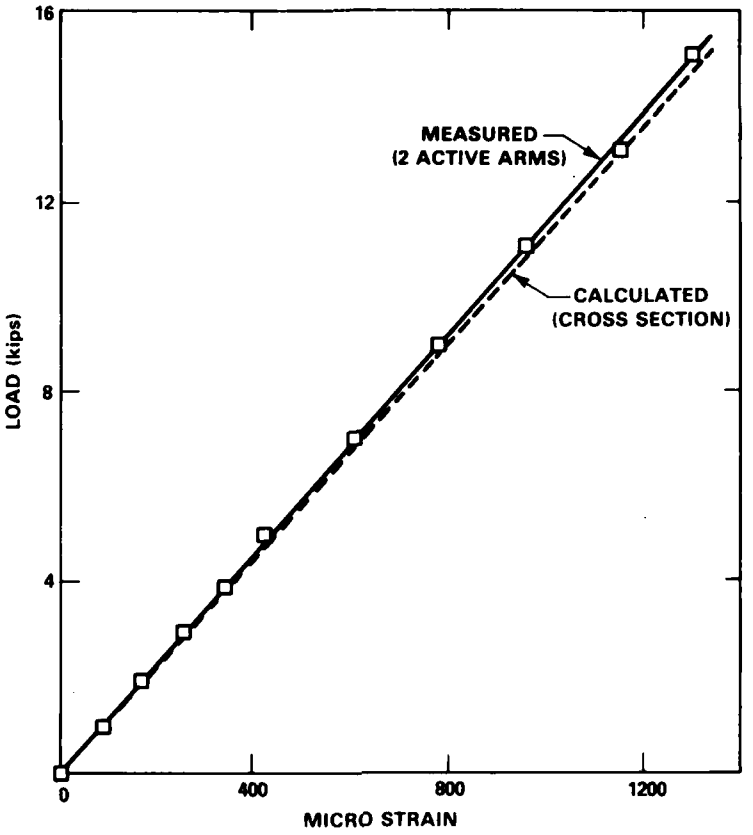

Figure 8 - Calibration of Test Fixture Load Cell

After attempts with a non-contact eddy-current displacement measuring system proved less than successful due to problems with the linearity of the sensor, a system using fiber optic transmitted and reflected light to determine load line displacement was used. Detailed descriptions of both of the systems and the calibration and test procedures tried for each are presented in the appendix.

The fiber optic system provided the most consistent results; the displacement measurements obtained using it were accurate to within 10%. This system, known as a Fotonic™ sensor, was manufactured by Mechanical Technology, Inc. The sensing probe contains two sets of fiber optic filaments arranged in concentric circles. One set

of filaments transmits light from the instrument to a target on the lower face of the specimen notch. The second set receives the reflected light and transmits it back to the sensor unit. There, the reflected light is converted to an electical signal that is proportional to the gap between the probe tip and reflecting surface.

A large effort was required to obtain a good calibration curve for the Fotonic sensor. The primary problem was that, because of sensor characteristics, the effective hinge length[21] of the compact tension specimen had to be considered during the micrometer calibration of the sensor. The opening of the notch faces produced a nonparallel reflecting surface which reduced the accuracy of the sensor. This was accounted for by using a steel rotating face during the calibration of the sensor so that the sensitivity curve obtained was representative of the test conditions. A complete description of this procedure is provided in the appendix.

Detection of Crack Initiation

The final measurement required to determine J_{IC} is an indication in real time of crack initiation in the specimen. Several techniques were tried but none was successful enough to give reliable data. As a consequence, part of the test program emphasized loading the specimen just to the threshold of crack initiation. Thus, the measured J-integral would correspond roughly to the desired J_{IC}.

Though not finally successful, an extensive effort was made to determine precisely when the crack extension began. Many of the techniques tried and types of instrumentation used showed promise for application in similar work. The effort is described completely in the appendix. The various techniques used and problems encountered in this work are described briefly below.

Initially, an eddy current displacement sensor like that used for the first few load point displacement measurements was placed in a hole in the ligament

section of the specimen just beyond the crack tip. Subsequently, the sensor was moved to the notch area of the specimen just before the crack tip. These locations are shown as D2 and D2' in Figure 7. We had hoped that these sensors would indicate crack initiation by showing a significant change in the slope of the ligament or notch displacement plotted versus the load point displacement response. No trend indicating crack initiation was determined because the sensor in the ligament was insensitive to crack extension until the crack reached the hole containing the sensor. Also, the notch-mounted sensor displayed no marked change in slope when plotted versus the load point displacement sensor.

The failure of the displacement response method shifted the emphasis to the use of more direct methods at or near the crack tip to determine initiation. Three different procedures were employed: crack detection strain gages, crack propagation gages and an optical moiré fringe method.

During the test program, we observed substantial plasticity at the side faces of the specimens. There was concern that this could influence the fracture characteristics. To eliminate this effect, V-grooves were machined on both sides of the specimen. Finally, to accommodate bondable gages, wide grooves with a radius at the bottom were used, although this arrangement perhaps was not as successful in eliminating the formation of shear lips upon fracture as the V-grooves. The configuration of the grooves is shown in Figure 9.

Figure 10 shows the arrangement of the crack detection and crack propagation gages. The crack detection gages were standard strain gages, applied to the specimen sides about 1/8 in. away from the visible crack tip. We hoped that the plastic strains measured near the crack tip would decrease markedly when crack extension occurred and that these gages would show this effect. Unfortunately, the gages

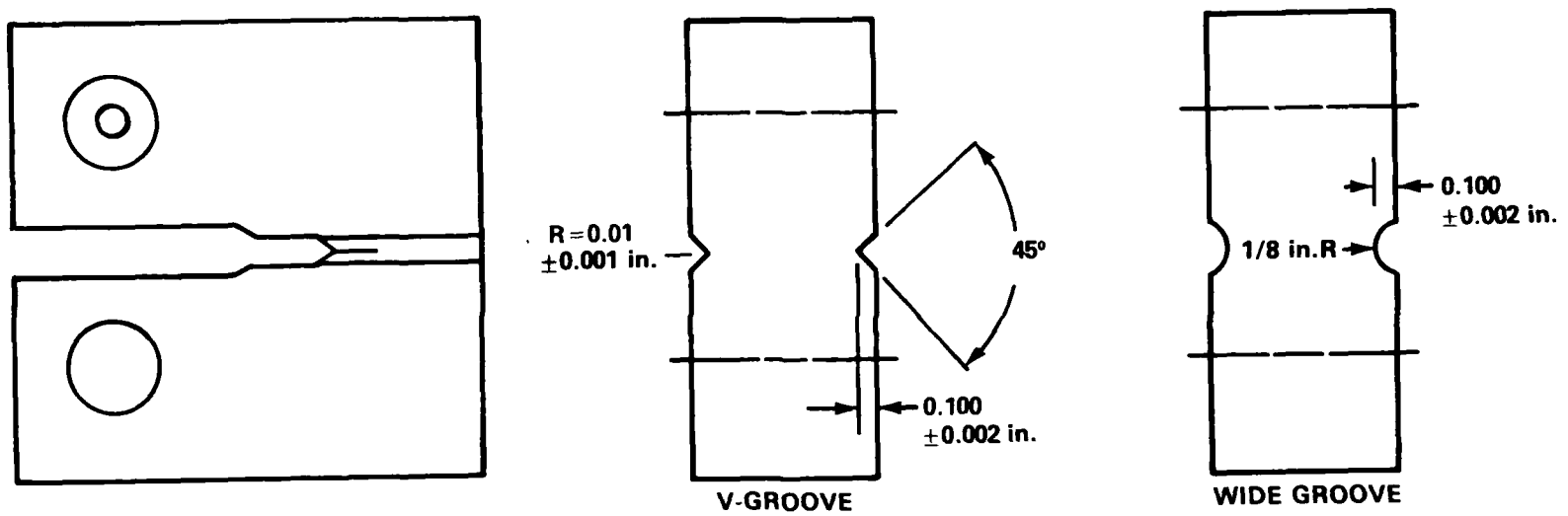

Figure 9 - Characteristics of Side Grooves Placed in the Compact Tension Specimen

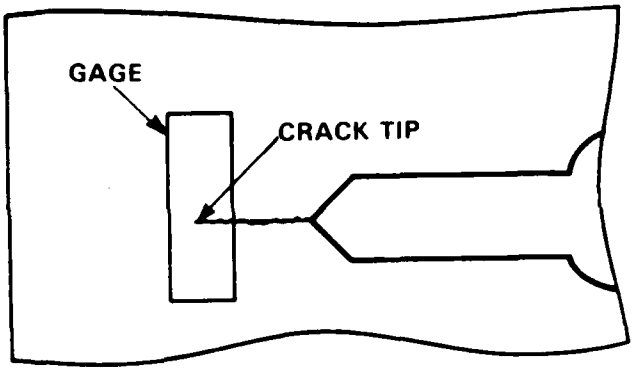

Figure 10a - Crack Propagation Gage
(Type MM TK-09-CPB02-005)

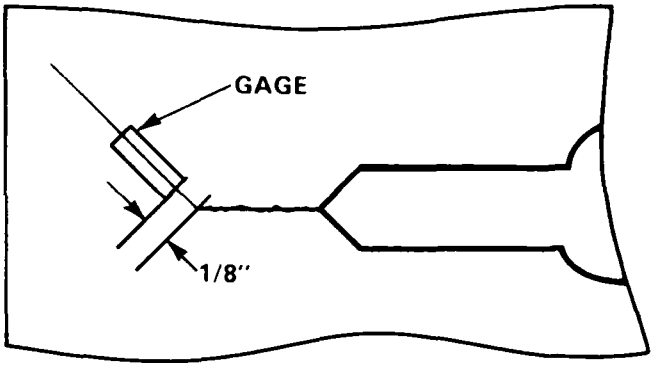

Figure 10b - Strain Gage on Flat Surface
(Type BLH FAE-03-12-56 ET)

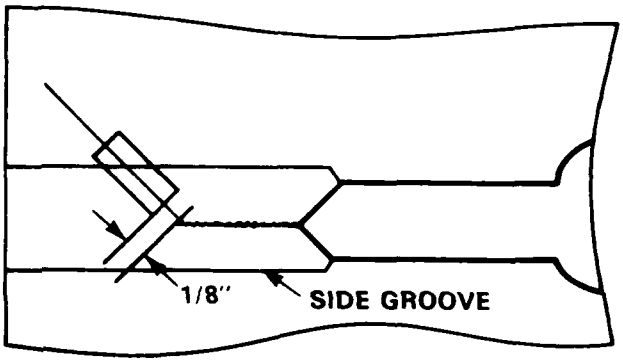

Figure 10c - Strain Gage in Wide Groove
(Type BLH FAE-03-12-56 ET)

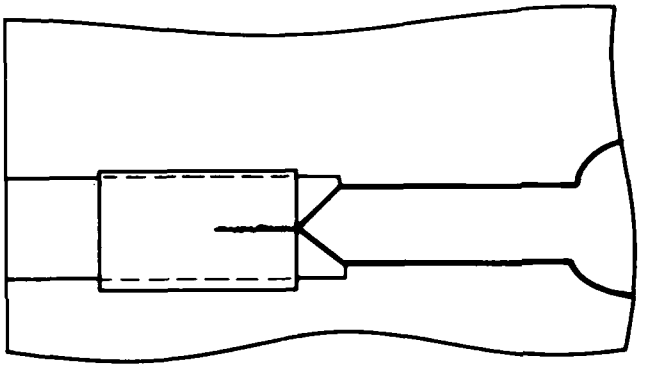

Figure 10d - "Krak" Gage in Wide Groove
(ITT Type KG-A05 and KG-A10)

Figure 10 - Procedures Using Bondable Gages to Detect Crack Propagation

tended to come unbonded due to the high strains occurring where they were located. This unbonding produced the same type of signal as expected for the strain release caused by the extension of the crack. Because of this unbonding, consistently detecting crack initiation was impossible.

The crack propagation gages also suffered from this unbonding problem. These gages are designed to fracture with the crack extension, thus producing a measurable change in gage resistance. The unbonding prevented the gage from following the crack extension in the specimen.

High speed photography and moiré fringes were used briefly with the hope of determining strains in the specimen and crack initiation. Because the event was so fast, the films obtained did not have good resolution. In addition, the overall plasticity due to the hinging of the specimen tended to mask the moiré fringe measurements in the crack tip region. No conclusive strains or indications of extension could be observed in the crack tip region using this technique. The use of side grooved specimens precluded any further use of the moiré fringes, but high speed films were still selectively taken and compared with the load point displacement measurements.

The final method used in the effort to detect the onset of crack extension was direct current potential drop (DCPD or PD). This technique relies upon the increase in electrical resistance of the cross-sectional area of the specimen as the crack grows into the ligament. Considerable work has been done applying this method in the static testing of compact tension specimens. That work was heavily consulted about the intricacies of the electrical probe locations on the specimen,[22] and the difficulties associated with using DCPD during fatigue precracking and on already precracked specimens.[23,24] The attachment points for the input current and potential probes are shown in Figure 11. To verify the system, the potential for various crack depths (determined by compliance) was checked during precracking against calibration work on a saw cut CT specimen like that described in Reference 24. This comparison is described, along with a thorough description of the potential drop method as applied in this experimental program, in the appendix.

Problems arose due to the variable effect that closure of the fatigue precrack had on the specimen potential when the specimen was unloaded. We decided that the problem could be avoided by measuring the final potential under load during precracking and determining crack initiation when that value was exceeded during the test.

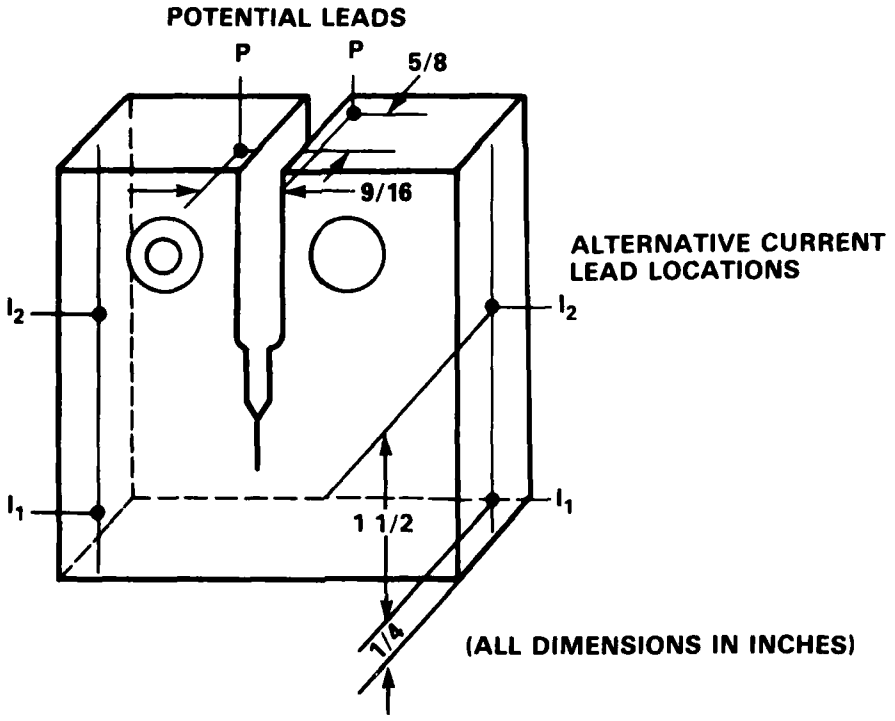

Figure 11 - Potential and Current Lead Attachment Locations

When this procedure was applied during the tests, however, totally unexpected voltage outputs were obtained. The voltage changes were much greater than any of those obtained during the specimen precracking. Apparently, the instrumentation added for the test (the D2' sensor and the common grounding of it) caused these surprising results.

Only two specimens were tested using the DCPD procedure and both produced extreme 2- to 3-V negative to positive potential changes. Although these results were certainly incorrect and possibly caused by an electrical problem in the instrumentation, the DCPD method showed a good deal of promise. Time and cost constraints prevented further examination, however.

Thus, the trial and error testing produced only one measure of crack initiation that would be considered valid: loading to the threshold of crack initiation as determined by breaking open the specimen after the test.

Summary of Instrumentation Design

A viable instrumentation plan was developed where dynamic J-integral tests could be conducted for different load rates. Techniques were developed to obtain all essential measurements for the J-integral except crack initiation. In this effort, various techniques were tried, including a secondary displacement sensor, bondable "Krak" gages, near-crack tip strain gages, and moiré fringe patterns. The potential difference technique also was attempted on two tests, but because of unexplained signals it cannot be relied on at this time. Despite these difficulties, however, values for J_{IC} were obtained by determining the threshold for crack initiation. Table 2 lists the specimens that were tested and identifies the particular technique used to obtain the information desired for determining this toughness criterion.

TEST PROCEDURE AND RESULTS

A precrack had to be placed in each specimen before testing. Each specimen was installed in the fixture in the usual manner and was cyclically loaded in the opening mode using a hydraulic actuator-type machine. The applied load and the corresponding LPD of the specimen were monitored to give the compliance; by combining this with empirical relations in Reference 25, the extent of the crack growth was determined. This operation was terminated when it appeared that a suitable crack length had been obtained. This fatigue procedure was carried out at two discrete load ranges. It conformed to the procedure outlined in Reference 9, which assured

TABLE 2 - INSTRUMENTATION OR TECHNIQUES USED WITH EACH SPECIMEN TO OBTAIN LOAD POINT DISPLACEMENT AND DETECTION OF CRACK INITIATION

Specimen	Displ. Load Pt. ①		Crack Detection ②							Supplemental Data ③		
	EC	FS	LG	NG	CTC	CTS ④	CTK ④	MF	PD	LVDT	S	HS
1	✓		✓		✓							
2	✓		✓									
3	✓		✓									
4	✓		✓					✓				
5	✓		✓									
6	✓			✓								
7	✓			✓				✓				
8	✓			✓								
10	✓			✓								
11	✓			✓								
13	✓			✓				✓				
14	✓			✓				✓				
15	✓			✓				✓				✓
16	✓			✓								
18	✓			✓				✓		✓		
19	✓			✓		1		✓		✓		
20		✓		✓			2			✓	✓	✓
21		✓		✓			2			✓	✓	✓
22		✓		✓			2			✓	✓	
23		✓		✓		1	1			✓	✓	
26		✓		✓		2				✓	✓	
27		✓		✓		2				✓	✓	
29		✓		✓								
31		✓		✓		2			✓		✓	
32		✓		✓		2			✓		✓	
33		✓		✓		2						

① Load Point Displacement
EC - Eddy Current
FS - Fotonic Sensor

② Crack Initiation Detection
LG - Ligament Gage; Eddy-Current Sensor
NG - Notch Gage; Eddy-Current Sensor
CTC - Crack Tip Crack Propagation Gage
CTS - Crack Tip Strain Gage
CTK - Crack Tip "KRAK" Gage
MF - Moiré-Fringes
PD - Potential Drop

③ Supplemental Displacement Data
LVDT - Linear Variable Differential Transformer
HS - High Speed Film
S - Eddy-Current Sensor in Specimen Notch

④ Number of Gages
1 - On One Side
2 - On Both Sides

the formation of a sharp crack tip that would perform in a consistent manner. The cracking sequence finally selected initially called for a 5000-lb cyclical load until the crack reached approximately 60% of the desired growth; then the load was reduced to 2500 lb to complete the growth to about 0.25 in. (a = 1.50 in.). Approximately 35,000 load cycles were required to produce this crack. Figure 12 is a photograph of the setup for this operation.

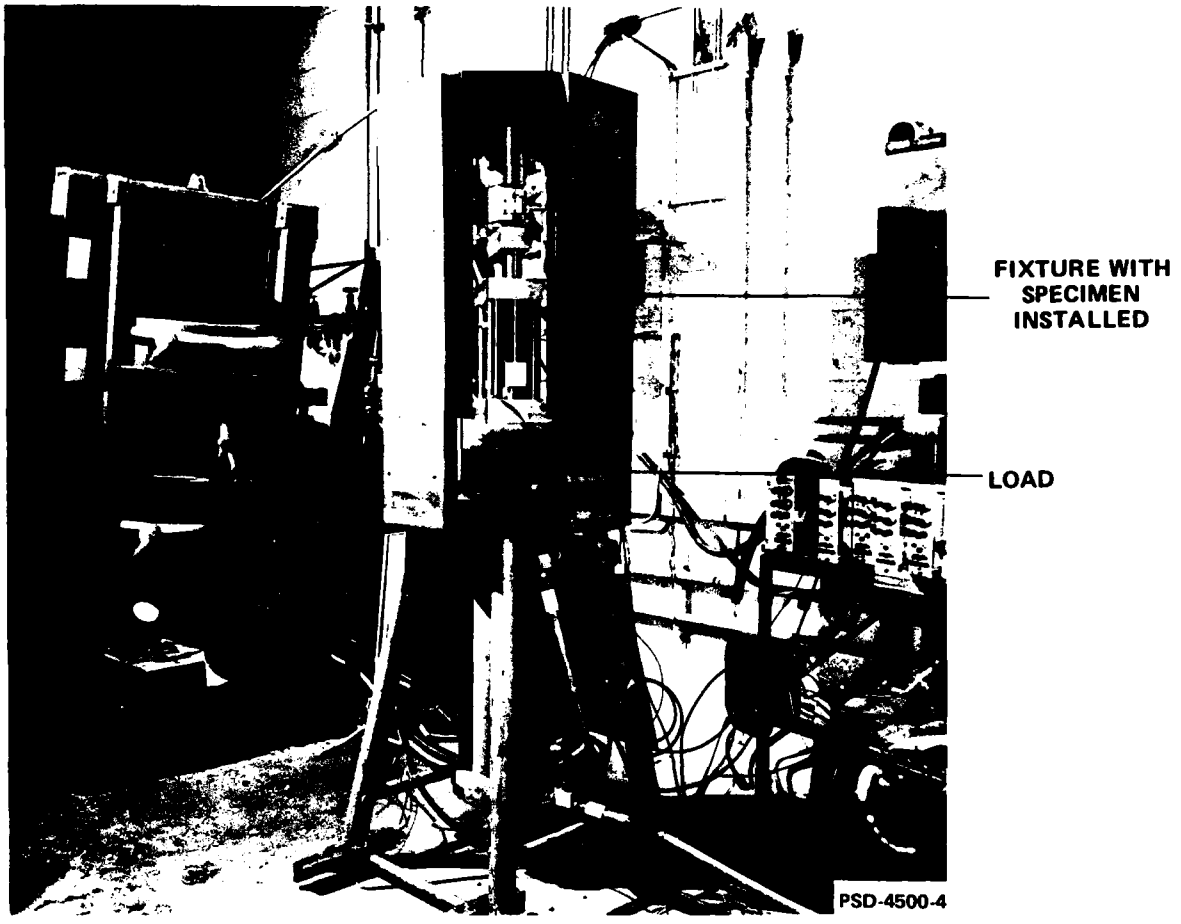

Figure 12 - Set-Up in Cyclic Load Machine for Fatigue Cracking Compact Tension Specimens

Some specimens were precracked at the DTNSRDC Ship Materials Engineering Department. Three discrete peak loads were used, starting with 3500 and ending with 1000 lb and upwards of 100,000 cycles were required to produce the required precrack.

The fatigue crack, rather than propagating at a uniform depth, tends to develop in a convex pattern in the direction of the growth due to the through-thickness variation in the stress state. This depth variation would influence the test results, and to reduce this effect, the side grooves, when used, were machined after precracking. These side grooves were consistently 0.1 in. deep and had the effect of reducing the specimen thickness to 0.8 in. at the test section. Table 3 describes the preparations made to each specimen before testing. It identifies the final crack length a (including machined notch) from the compliance measurement. It also identifies the specimens that contained side grooves.

The setup used in the drop tests is shown in Figure 13. In addition to the measurements that were needed to determine the J-integral for fracture, described earlier, the back face strain (BFS) was also routinely measured, mainly for use in the analytical efforts (see Figure 7). A block diagram of the circuitry used for these basic measurements is shown in Figure 14. Figure 15 presents typical oscillograph data obtained during the test. Peak values from each channel of information were read routinely; on some channels the rise times to peak values along with other pertinent data also were derived. Of course, to obtain the J-integral the applied load and LPD information needed additional analysis, and this was done for most of the tests where the results appeared valid. These channels were usually manually digitized and plots with high resolution were produced with use of the Tektronix™ 4081 Graphics minicomputer. See Figures 16 and 17 for typical plots. Through recent software developments to manipulate arrays and perform integration, plots of

TABLE 3 - SUMMARY OF SPECIMEN PREPARATION

Specimen	Precrack, a (in.)		Side Groove Type[1]	Specimen	Precrack, a (in.)		Side Groove Type[1]
	Compliance	Measured			Compliance	Measured	
1	None			15	1.42	1.49	V
2	1.38	1.45	NA	16[2]		1.50	V
3	1.40	1.47	NA	18	1.57	1.56	NA
4	1.45	1.53	NA	19	1.57	1.54	NA
5	1.40	1.53	NA	20	1.57	1.57	W
6	1.47	1.52	NA	21	1.57	1.56	W
7	1.44	1.48	NA	22	1.57	1.56	W
8	1.47	1.46	V	23	1.57	1.58	W
10	1.43	1.50	V	26	1.42	1.54	W
11	1.46	1.50	V	27	1.48	1.50	W
13	1.41	1.47	V	29	1.55	1.51	W
14	1.42	1.45	V	31	1.49	1.51	W
				32	1.52	1.58	W
				33	1.49	1.49	W

[1] See Figure 9 for details, V - V groove, W - Wide groove, NA - No side grooves.

[2] Specimens 16, 18-23 were precracked by Ship Materials Engineering Department, others by Structures Department.

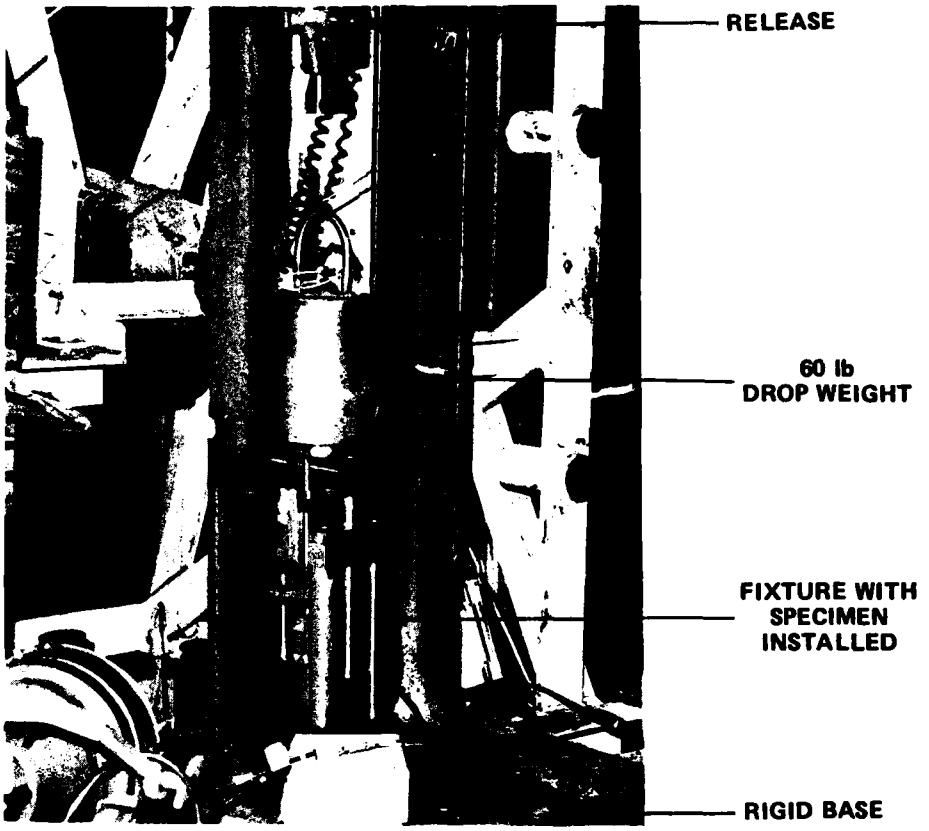

Figure 13 - Drop Test Set-Up

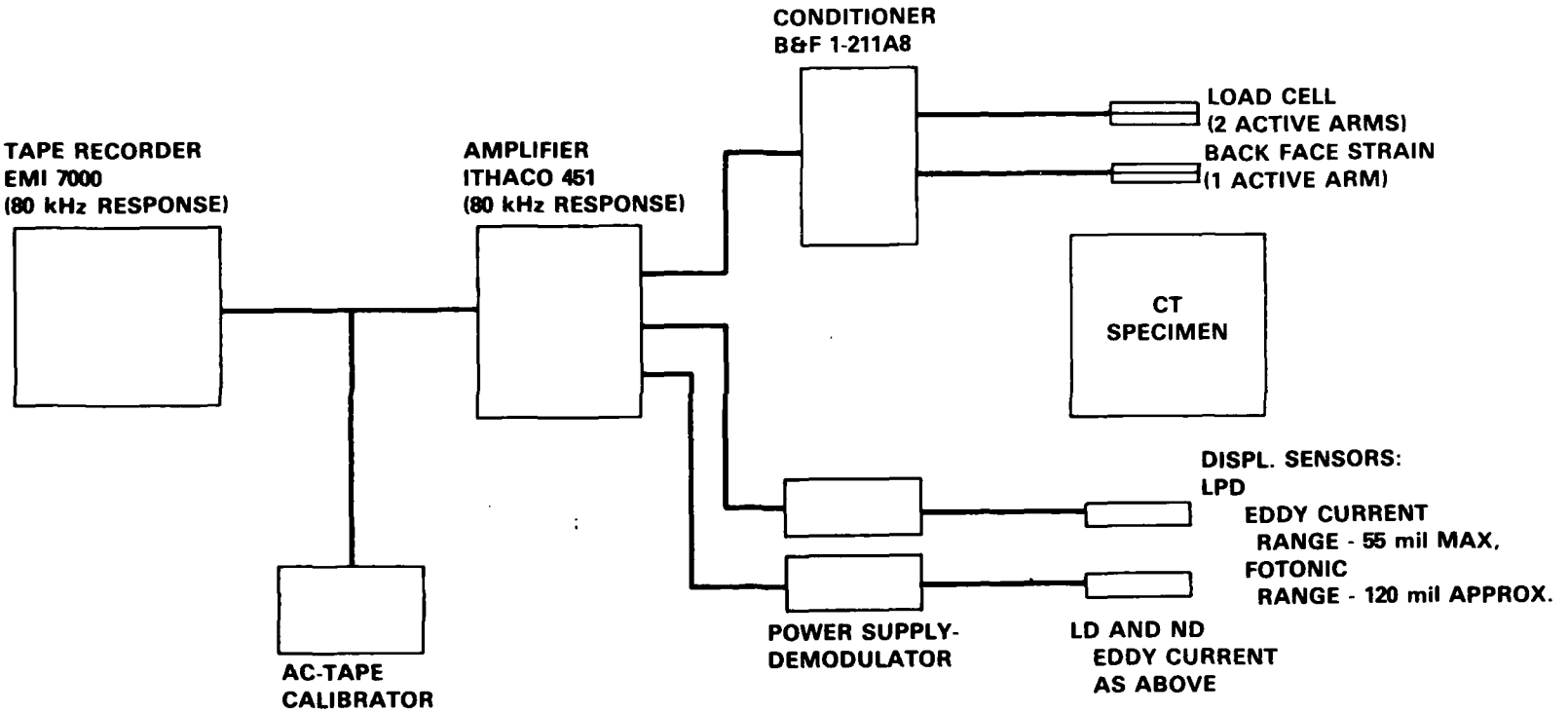

Figure 14 - Instrumentation Diagram for Dynamic J-Integral Tests

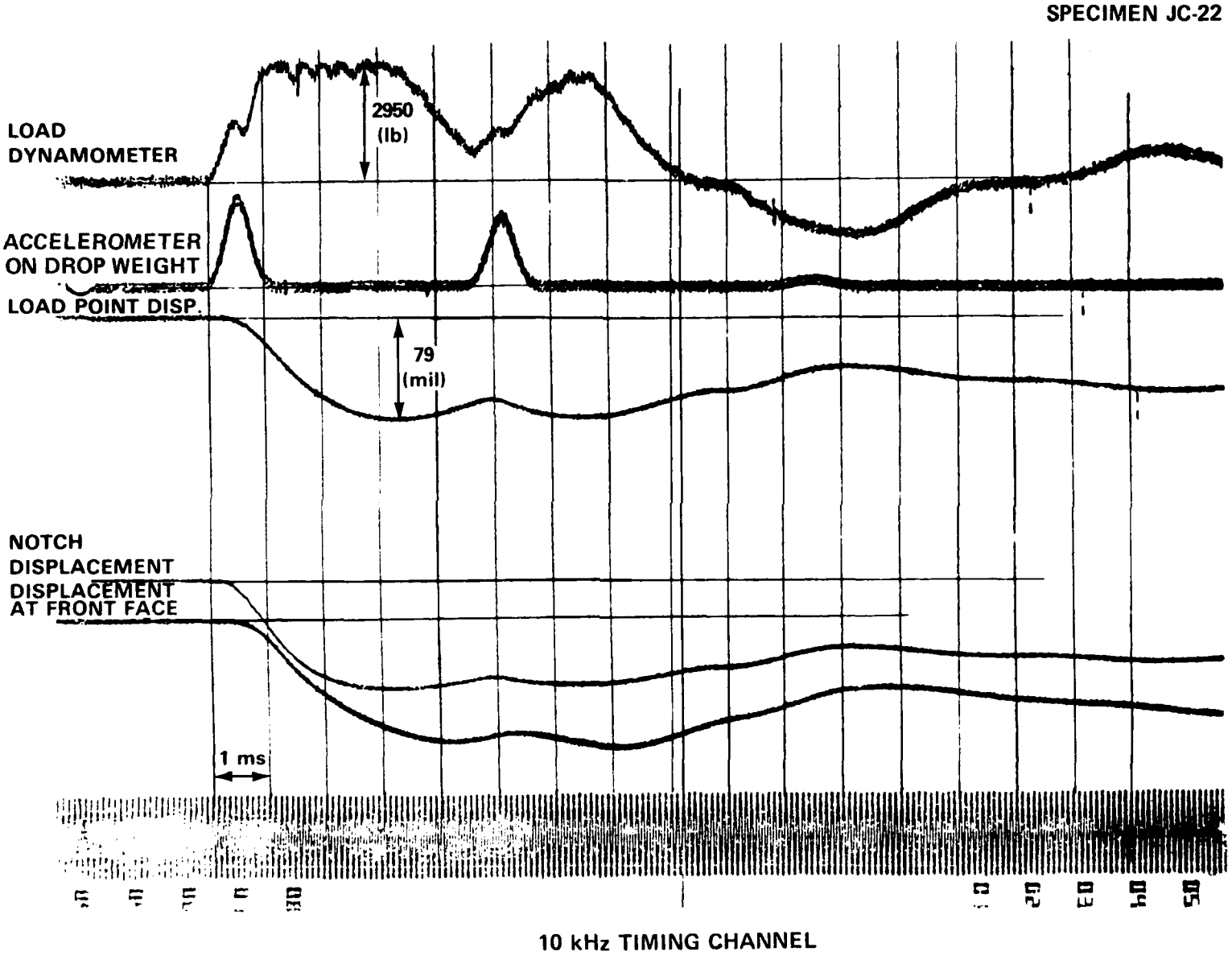

Figure 15 - Typical Oscillograph Record of Dynamic Test Data

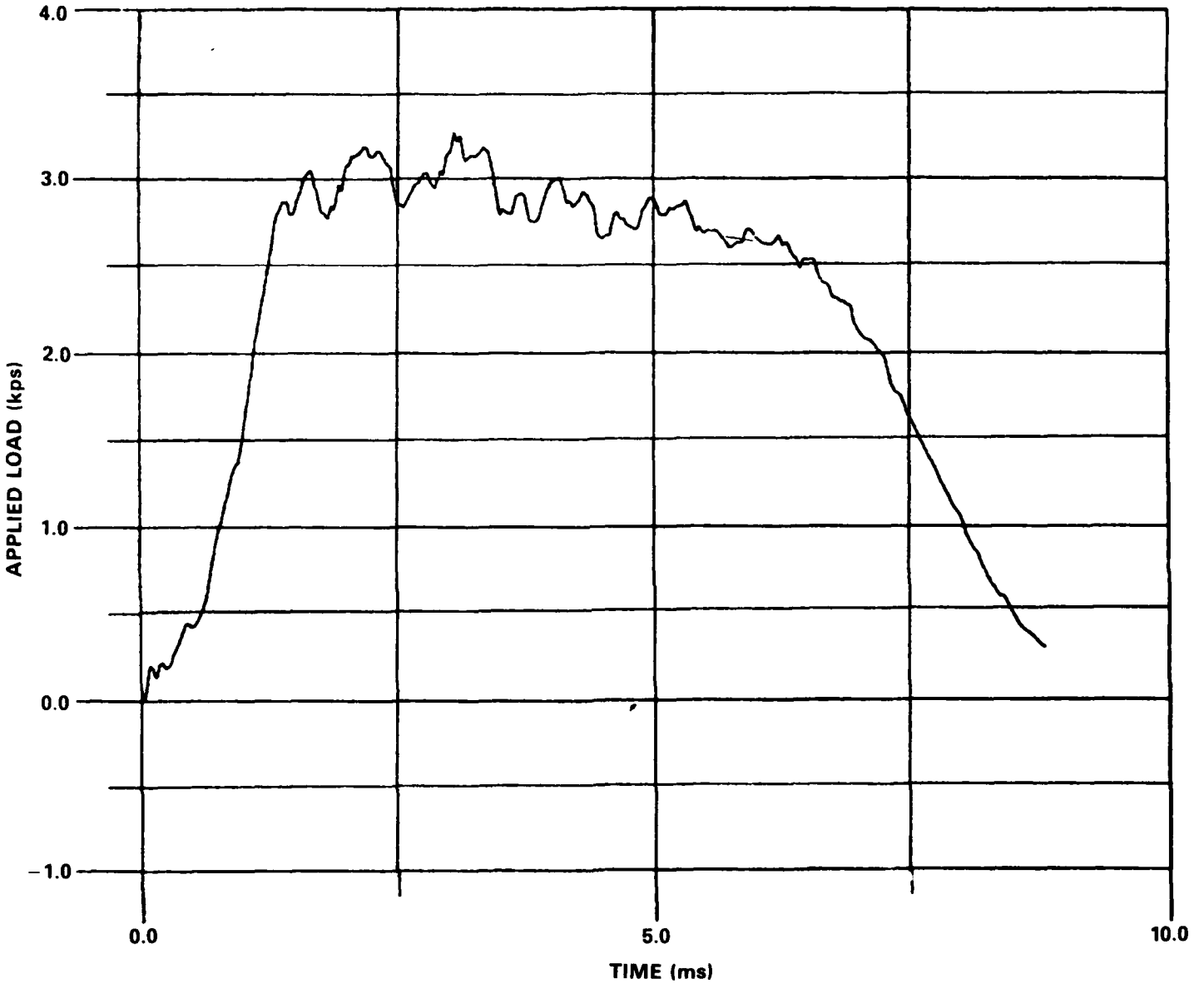

Figure 16 - Digitized Record of Applied Load versus Time for Specimen JC-32

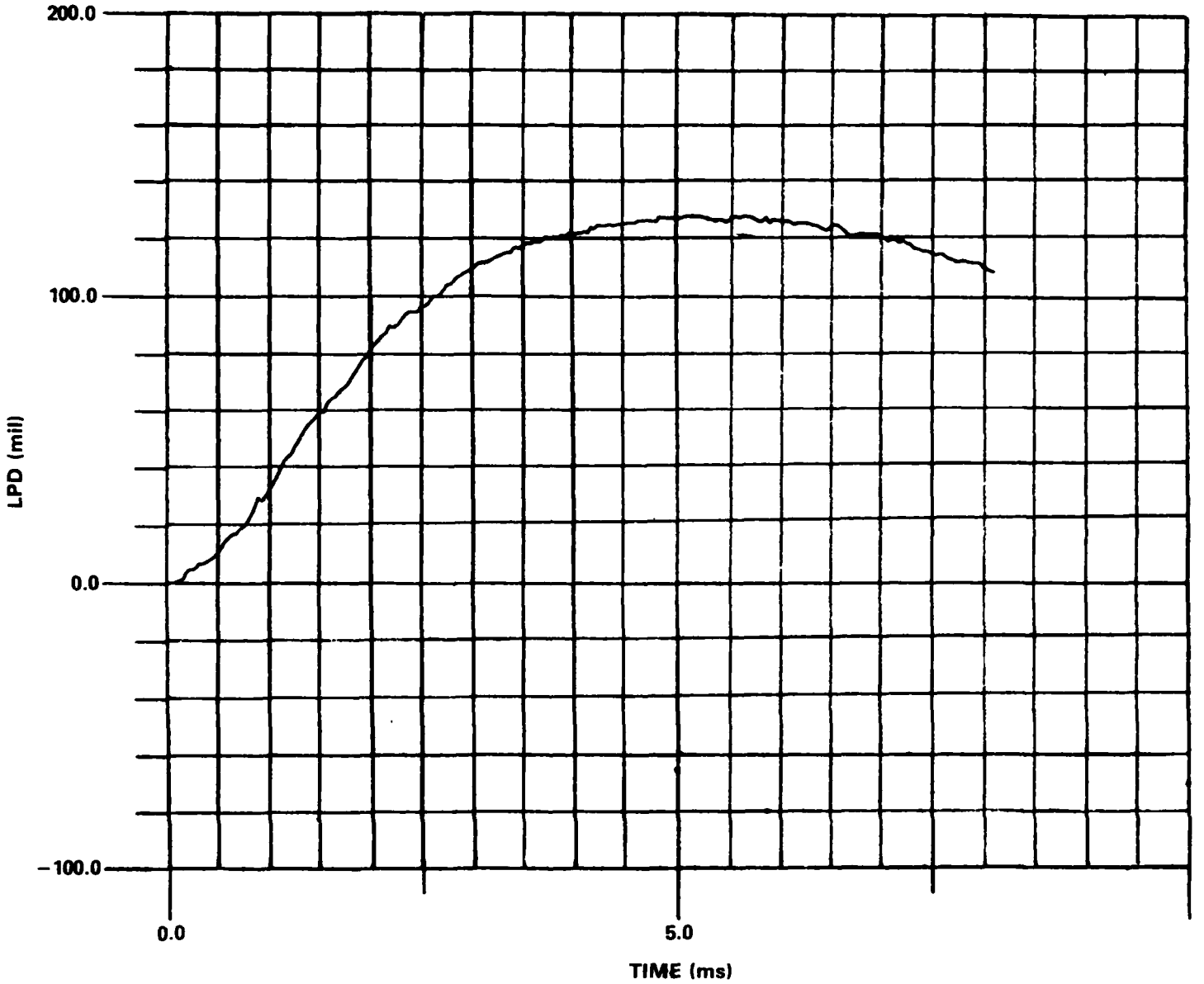

Figure 17 - Digitized Record of Load Point Displacement (LPD) versus Time for Specimen JC-32

load versus LPD, and the J-integral versus time could also be easily generated. (See Figures 18 and 19 for examples.) The advantage of the plot shown in Figure 19 is that the critical value J can be determined immediately if the time for fracture initiation could be identified; also, the time-rate for J ($\dot{J}$) at fracture can be approximated from the slope at fracture. [For justification of determining the J-integral by graphical means, refer to Equation (5) in the background section.]

After the test, each specimen was separated through the ligament section to reveal the crack faces so that the specific fracture regions could be studied. To help delineate these regions the specimen was first heat tinted; this involved placing it in an oven and holding it at a temperature of about 500°F for several hours. This caused oxidation which varied with surface roughness. Thus, for fatigue fracture, which is characterized by a relatively smooth surface, the section would appear lighter than the fractured section caused by a single impact as during the test. To separate the specimen, it was cooled to a brittle state by holding it in a liquid nitrogen bath and then placed over a tapered anvil that was driven into the front of the notch by a free-fall impact weight. Figure 20 is a photograph of the fracture regions in a specimen that had been severely tested. The zones are easily discernable. Each was measured and the results provided essential data for computing the critical J-integral. Then respective areas were measured with a planimeter and, when divided by the specimen thickness, gave the average lengths for each zone (see Figure 21). These measured precrack lengths were also tabulated in Table 3 for comparison with those obtained from the compliance measurements. Table 4 is a summary of the magnitudes for the basic measurements along with the results from analysis of the data and from measurements of the specimen. Repeated tests were run on some specimens and, in those cases, only the results from the initial test are given. Also, for specimens that were tested repeatedly, the crack growth is not meaningful and, therefore, is not listed.

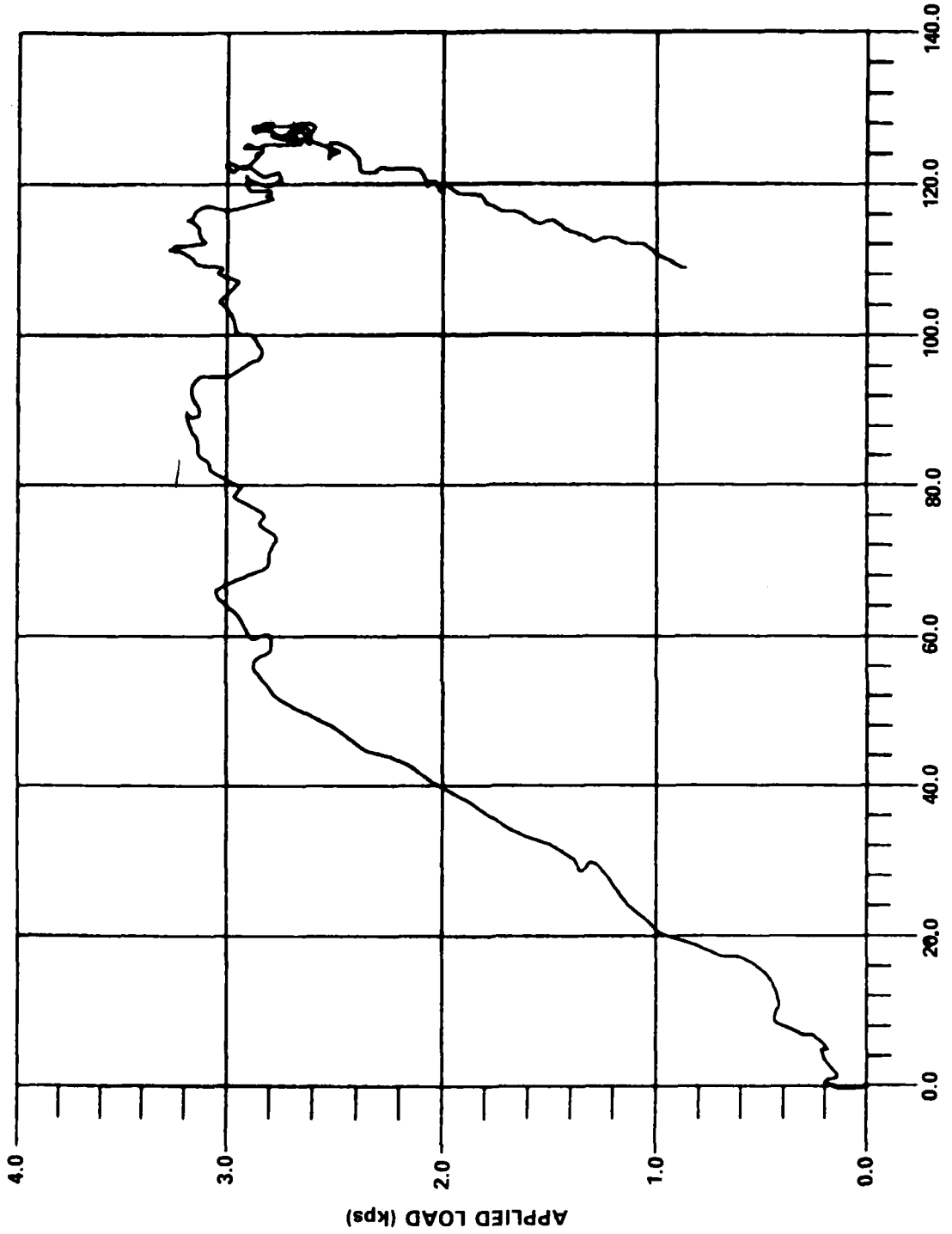

Figure 18 - Load versus Load Point Displacement for Specimen JC-32

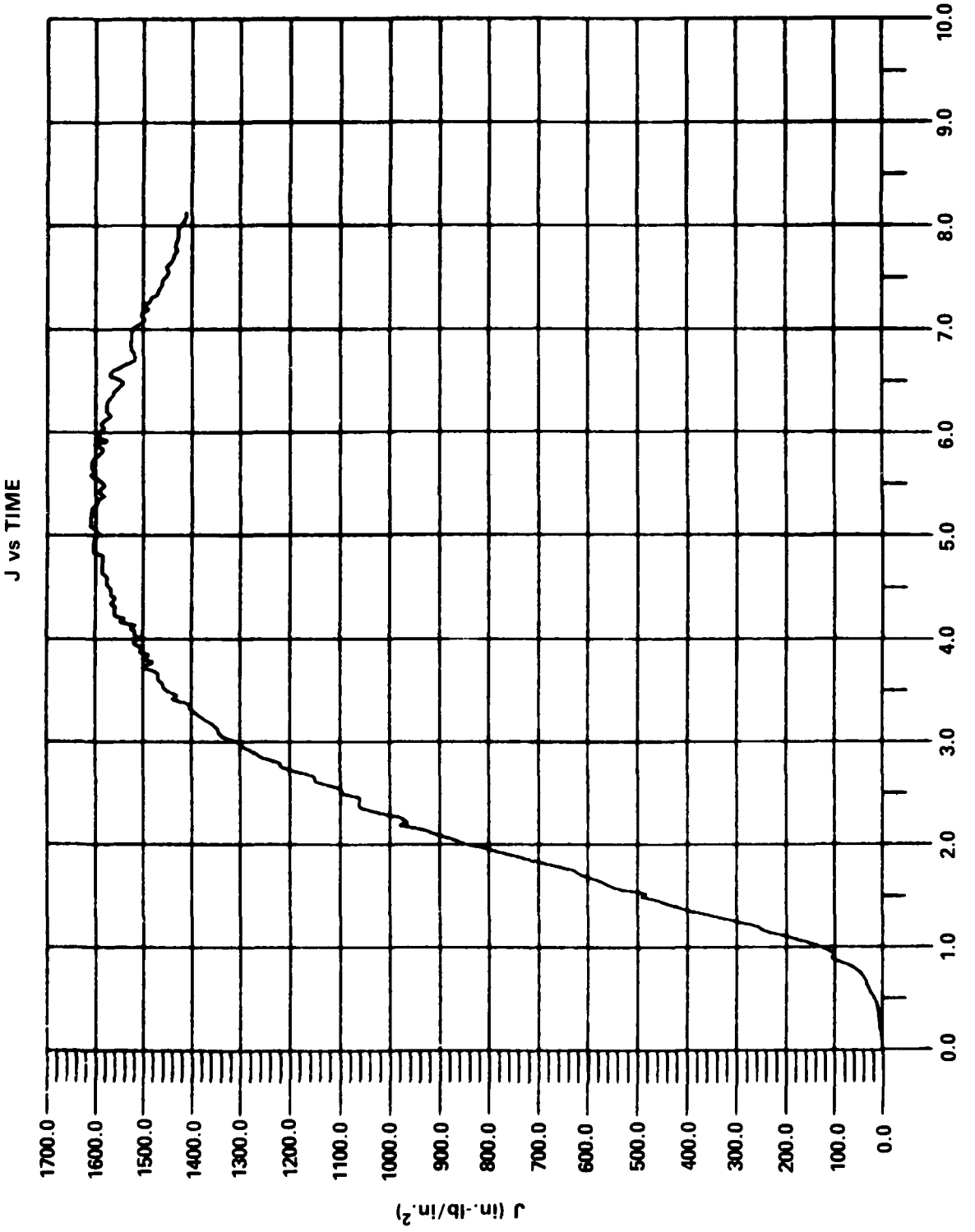

Figure 19 - J-Integral versus Time for Specimen JC-29

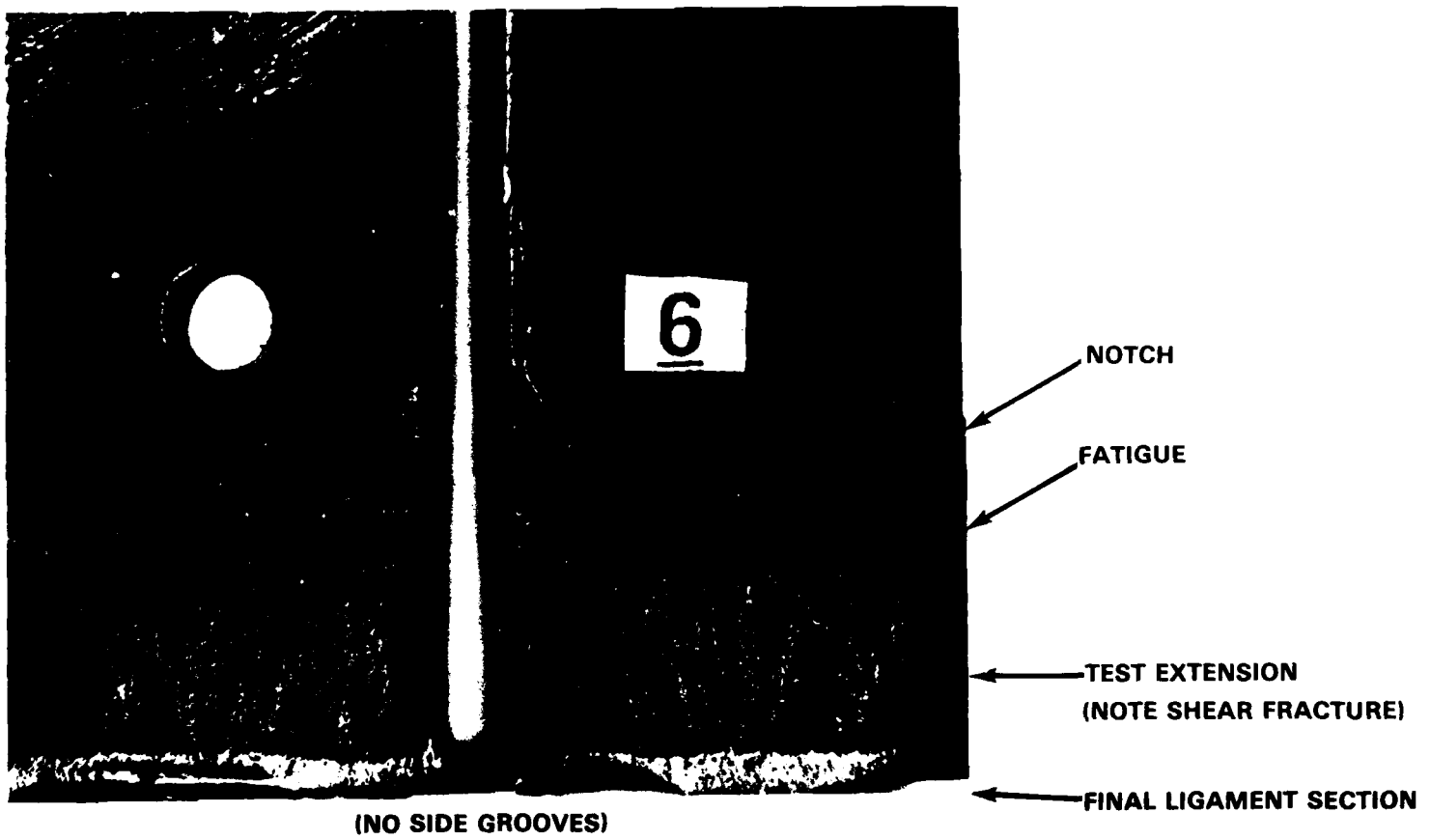

Figure 20 - Details of Fracture Surfaces for a Severely Tested Specimen

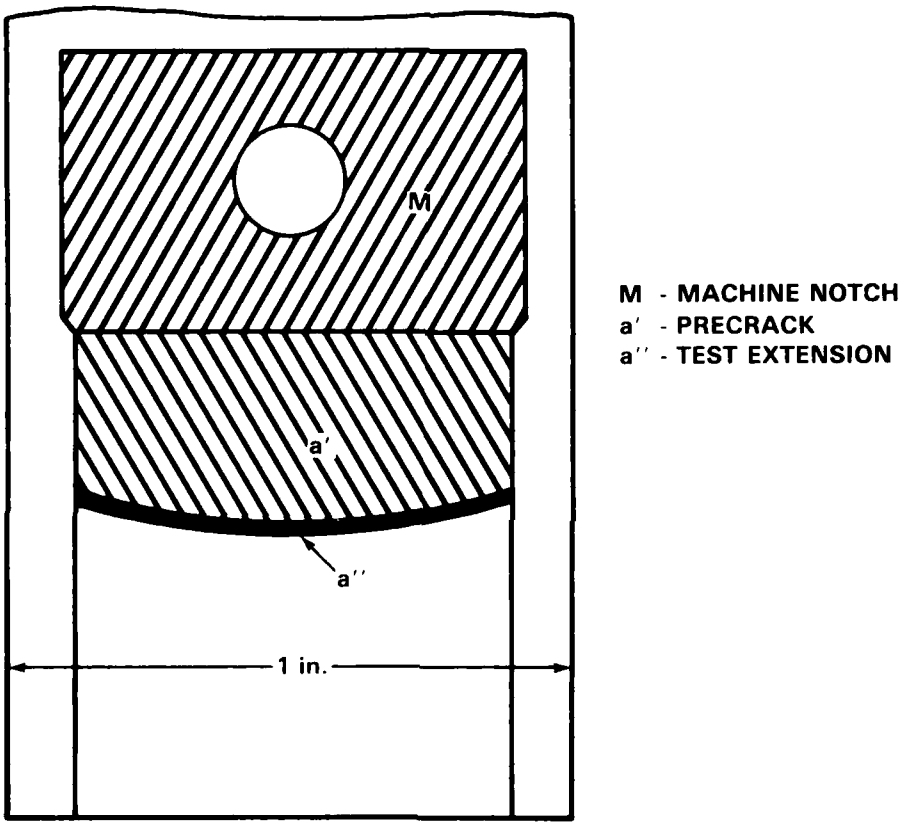

Figure 21 - Measurements Typically Obtained
After Separating Specimen

TABLE 4 - SUMMARY OF TEST RESULTS

Specimen	Test Description			Peak Load lbs	Time To Peak Load msec	At Peak Load			J_I (max) in.-lb/in.^{2}	Time For J_I(max) msec	Crack Extension Measured in.	LPD(max) mils	Time For LPD(max) msec	Load At LPD(max) lbs	Remarks
	Weight lb	Height in.	Element Type ①			LPD mils	BFS in./in. ×10-3	J_I in.-lb/in.^{2}							
JC- 1						MULTIPLE TESTS TO ESTABLISH PROCEDURE									
JC- 2	115	36	8	5430	2.0	40	N.A.②	N.D.③	N.D.	N.D.	0.17	65	3.8	3510	
JC- 3	60	36	8	4820	2.0	42	9.1	N.D.	N.D.	N.D.	0.20	76	5.3	3690	
JC- 4	60	36	8	6920	0.9	N.A.	N.A.	N.A.	N.A.	N.A.	0.24	N.A.	N.A.	N.A.	Exceded Range of LPD
JC- 5	115	36	3	7230	0.6	63	22.9	N.D.	N.D.	N.D.	0.30	N.A.	N.A.	N.A.	Exceded Range of LPD
JC- 6	115	36	3	7600	0.6	61	34.4	N.D.	N.D.	N.D.	0.35	N.A.	N.A.	N.A.	Exceded Range of LPD
JC- 7	115	36	3	6590	0.5	N.A.	8.8	N.A.	N.A.	N.A.	0.37	N.A.	N.A.	N.A.	Exceded Range of LPD
JC- 8	115	6	3	N.A.	N.A.	N.A.	N.A.	N.A.	N.A.	N.A.	None	N.A.	N.A.	N.A.	No Data
JC-10	60	6	3	4410	1.6	59	2.1	555	760	2.1	None	65	1.9	4410	
JC-11	60	5	3	4800	1.9	44	2.5	720	720	2.0	None	45	2.0	4730	
JC-13	60	9	3	5270	1.7	80	N.A.	N.D.	N.D.	N.D.	None	N.A.	N.A.	N.A.	Exceded Range of LPD
JC-14	60	7	3	5325	1.5	46	N.A.	810	1070	2.1	None	56	2.1	5000	
JC-15	60	8	3	4690	1.4	57	13.6	730	1040	1.9	<0.01	64	1.8	4650	
JC-16	60	12	3	4470	1.5	52	33.2	490	510	1.9	0.03	53	1.9	4270	
JC-18	60	3	3	1560	2.4	N.A.	N.A.	N.A.	N.A.	N.A.	N.A.	N.A.	N.A.	N.A.	LPD Channel Saturated
JC-19	60	8	3	4440	1.3	N.A.	N.A.	N.A.	N.A.	N.A.	N.A.	N.A.	N.A.	N.A.	LPD Channel Saturated
JC-20	60	8	3	2940	1.8	67	N.A.	835	1000	2.8	N.A.	80	2.7	2810	
JC-21	60	8	3	2870	1.8	N.A.	N.A.	N.A.	N.A.	N.A.	N.A.	N.A.	N.A.	N.A.	LPD Channel Faulty
JC-22	60	8	3	2950	2.1	70	N.A.	950	1120	3.0	0.02	79	3.1	2800	
JC-23	60	8	18	2400	2.8	54	24.1	550	670	4.5	None	63	4.6	2220	
JC-26	60	12	18	4100	2.2	66	32.6	1130	<1500	3.9	0.02	83	3.9	3900	
JC-27	60	10	18	4080	2.8	62	26.2	820	>960	3.5	None	76	3.5	4000	
JC-29	60	10	18	4200	2.4	58	13.8	540	1040	3.2	0.01	64	3.2	4100	
JC-31	60	10	18	3100	N.A.	N.A.	N.A.	N.A.	N.A.	N.A.	N.A.	78	4.2	N.A.	Load Circuit Faulty
JC-32	60	12	18	3250	3.1	112	42.9	1500	<1650	5.2	0.04	128	5.2	2800	
JC-33	60	11	18	3100	2.8	74	40.5	1140	1380	4.6	0.02	117	4.7	2900	

① See Table 1 For Identification

② N.A. - Not Available

③ N.D. - Not Determined

FINITE ELEMENT ANALYSES

GENERAL

In addition to obtaining sound experimental data, a major goal of this program was to correlate these data with some form of analytical solution. We originally hoped to develope a reciprocating relationship in which experimental data would be obtained, and then compared with data obtained by numerical analysis. The results of this comparison would then be used to guide future testing. This approach would be a prudent and cost effective way of optimizing the experimental and analytical procedures at the same time. However, the synergism of this classical scientific approach did not develop as anticipated. The "short falls" involved both the experiment (the problems with data acquisition described in the previous section) and the newly evolving methods of analysis. A thorough description of these numerical methods, the difficulties encountered with their use, and an evaluation of the results follow.

Several methods are applicable to the analysis of a compact tension fracture specimen. In this case, finite element computer codes were chosen as the primary analytical method. With various finite element computer codes it was possible to analyze both the dynamic and the static nonlinear response of the specimen. This capability was crucial since the goals of this program are to determine the effects of high load rates on inelastic fracture initiation and to examine the applicability of current nonlinear static fracture criteria (such as the J-integral) to cracked specimens under dynamic loading. The flexibility of general purpose finite element programs was desirable. Variations in specimen geometry (crack depth), material, and loading magnitude and rate could all be easily modeled and altered for the many different test cases. Another factor influencing the choice of finite element procedures as the analytical tool for this program was the large amount of ongoing

research in the application of finite elements to fracture problems. This research would provide information and insight for these analyses. Some closed form theoretical solutions were also employed in conjunction with the finite elements. These were used primarily to verify and guide the preliminary static finite element solutions.

REVIEW OF PRELIMINARY ANALYSIS

The first analysis was performed on specimen JC-6. The analysis of this specimen test has been informally reported.* In the interest of clarity and continuity, a summary of that analysis and the insights gained are presented in this section.

As experimental results indicate, JC-6 was among the most severely tested specimens. It sustained a peak load of 7600 lb (which was the highest in the test series) and reached that peak load in a very short time (0.6 ms). With the full test series completed, it is much easier now to look back at the results and see that JC-6 was not a particularly good choice for experimental-analytical comparison. As Table 4 shows, after tests of JC-7, it became apparent that the tests with a 115-lb weight and 36-in. drop height developed extreme loadings. The weight and drop height were subsequently lowered with the aim of imparting just enough load to achieve crack initiation. The primary difficulty caused by the high loading magnitude and rate in JC-6 (and other early series specimens) is decreased accuracy and reliability in the experimental results. The accurate ranges of the load point displacement sensor and possibly other instrumentation were exceeded. The limited results available may be reasonably accurate (if the response of the instrumentation was adequate) but the high loading rates also cast doubt as to the actual material

---

*Rasmussen, E. A., "Experimental and Computational Analyses of a Dynamically Loaded Compact Tension Specimen," Enclosure (1) to DTNSRDC letter 81-1720-59, dated 12 May 1981.

properties to assume for the specimen. Dynamic loads producing high rates of strain can substantially affect yield stress as well as other properties.[26] As will be seen later, the search for an accurate description of material properties is a persistent one.

One of the most important objectives of the comparison was to validate or contradict the experimentally obtained data, in which there was already considerable doubt at the time analysis was begun. For this first analysis, various finite element codes were used to model the specimen. These codes were ADINA,[27] HONDO II,[28] and PAPST.[16] The use of these three codes allowed several different idealizations of the specimen and thorough analysis under both static and dynamic loads. This also served as a means of certifying the analytical results by comparisons among results obtained using various codes, idealizations, and types of elements.

The basic finite element analysis procedure follows. First, the compact tension specimen was modeled using either 4-, 8-, or 12-noded isoparametric elements, depending on which code was in use. The idealization for the 8-noded element ADINA analysis is shown in Figure 22. Two-dimensional plane stress elements were employed in this analysis. Several investigators have used finite element techniques to analyze CT specimens made from various steels that exhibit elastic-plastic or fully plastic fracture. The general outcome of these results is that (two-dimensional) plane stress elements yield displacement results that are reasonably close to those obtained experimentally or by three-dimensional finite element methods.[29,30] No special treatment such as collasped elements or elements with an imbedded singularity function were used in these cases to model the crack tip region. This type of procedure was not performed because the desired result of the analysis was the displacement at the load point. Modeling of the stress singularity at the crack

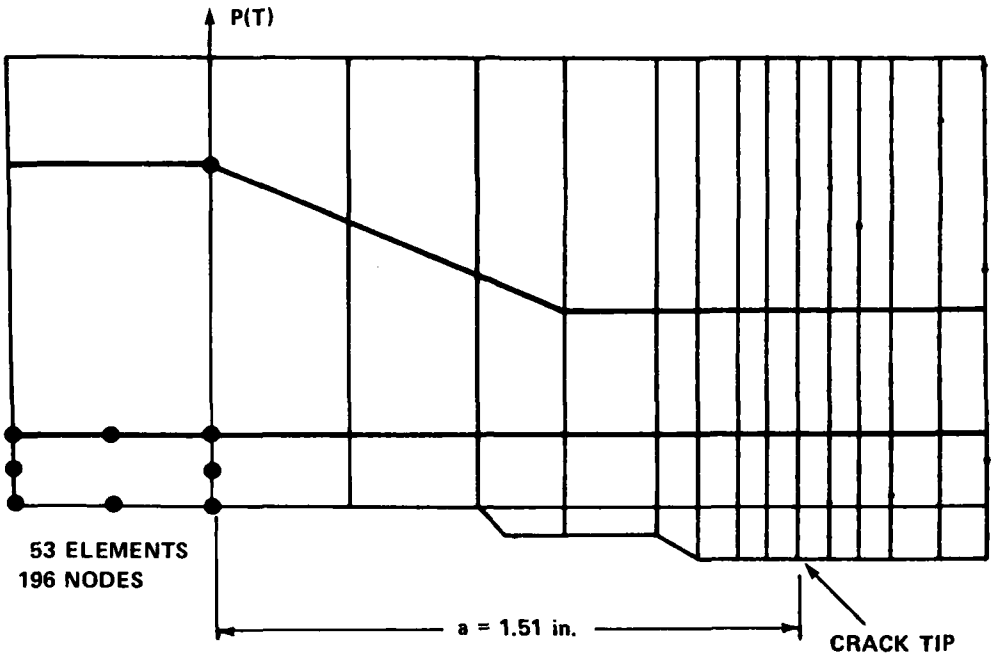

Figure 22 - ADINA Two-Dimensional Finite Element Idealization

tip was assumed to have negligible effect on this displacement. For the static condition, Hilton and Gifford[31] confirmed the assumption by showing that various treatments of the crack-tip singularity yielded essentially the same J-integral value for a finite element model of an edge-notched specimen.

The instrumentation record in which we had the most confidence was the load dynamometer. For this reason, the load was simulated by a multilinear curve and used for input in the finite element solution. The load point displacement was then computed for the various load steps. We hoped that these values would be close to those measured by the load point sensor in the experiment. From these displacement values, load versus load point displacement graphs would be developed so that an analytical value of the J-integral could be found for comparison with the experimentally obtained value. Also, from the analytical solution, stresses and plastic zones could be determined that could perhaps give insight into fracture response of specimens under the dynamic loading.

Another aspect of the analytical solution was the static analysis of the specimen. We were hoping to obtain some understanding of the dynamic effects in the specimen by comparing a dynamic solution to a static one. Also, the numerical solution could be checked to determine its convergence with the theoretically determined plastic limit load of the compact tension specimen. This value was calculated using the Merkle-Corten[17] formula for the fully plastic load in conjunction with the Green and Hundy[32] plastic constraint factor of 1.25. A limit load value of 3788 lb was obtained.

The most positive result of this first attempt at finite element analysis was the close agreement between the various programs used. As can be seen in Figures 23

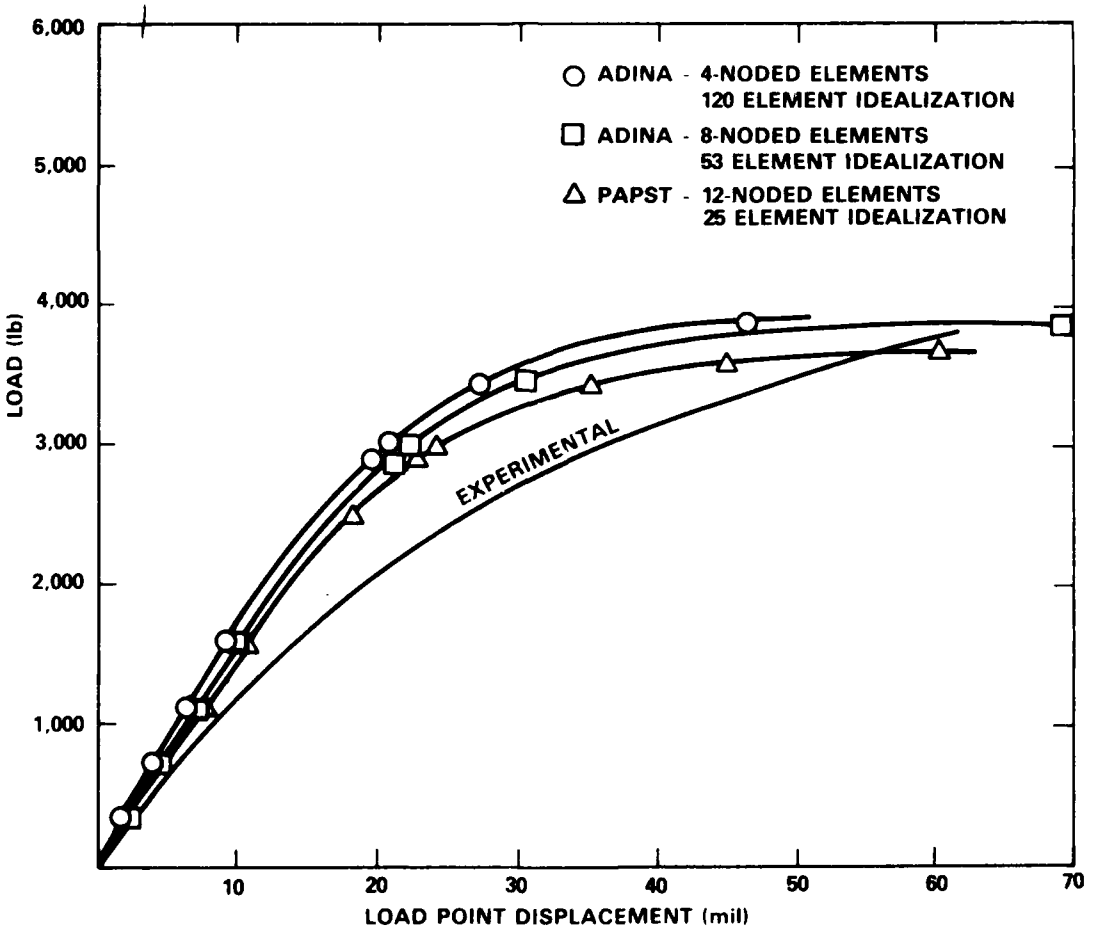

Figure 23 - Specimen JC-6 Load versus Load Point Displacement for Static Finite Element Solutions

and 24, under static and dynamic loading, load versus load point displacement plots for three different combinations of program and element type agree quite well. This agreement also carries over to comparisons of the J-integral and plastic zone sizes

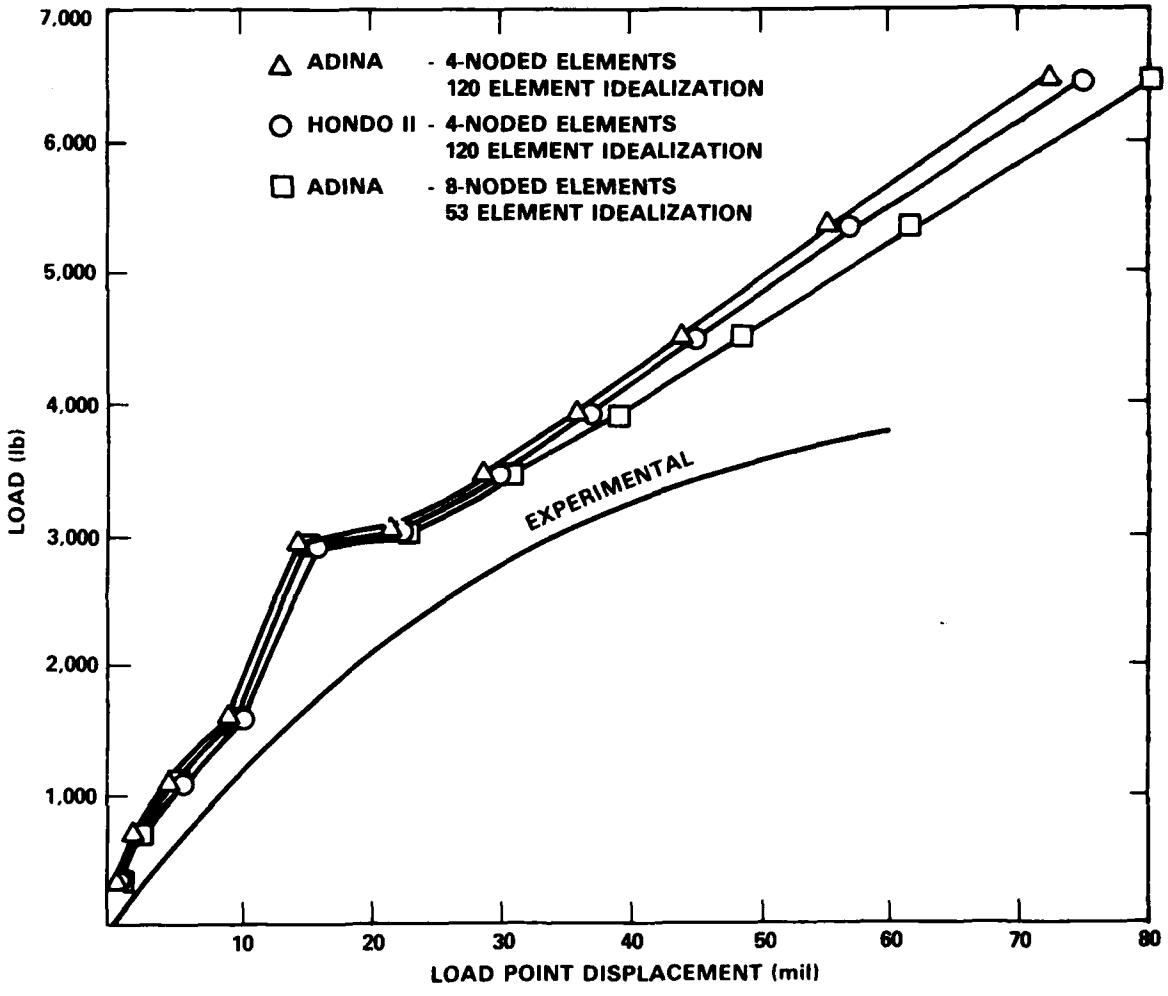

Figure 24 - Specimen JC-6 Load versus Load Point Displacement for Dynamic Finite Element Solutions

as shown in Table 5 and Figure 25. This close agreement instilled confidence that the numerical solutions were reasonably correct. Another good agreement, for the static loading condition, can be seen in Figure 23. The static solutions approach

TABLE 5 - ANALYTICAL J-INTEGRAL VALUES FOR SPECIMEN JC-6

Load (lb)	J-Integrals (in.-lb/in.^{2})			
	HONDO (Dynamic)	ADINA (Dynamic)	ADINA (Static)	PAPST (Static)
500	2.2	2.5	5.0	4.0
1000	10.5	4.5	13.5	14.5
1500	31.5	29.5	30.0	33.3
2000	50.5	55.5	55.5	60.0
2500	66.5	71.0	94.0	101
3000	141	145	154	165
3500	283	309	285	355
4000	388	421	---	---
4500	510	553	---	---

the calculated limit load value quite closely; that is, the deflections tend to become extremely large as this load value is reached. This fact indicates that the static finite element solutions are producing accurate displacements.

As can also be seen in Figures 23 and 24, the finite element and experimental solutions do not agree well at all. While the accuracy of the finite element solutions was not a known quantity, the repeatability of results by the different codes lent some credence to those results. At the same time, there was inconsistency in some of the experimental records (load point displacement being a crucial one). These factors led to a review and modification of some of the instrumentation.

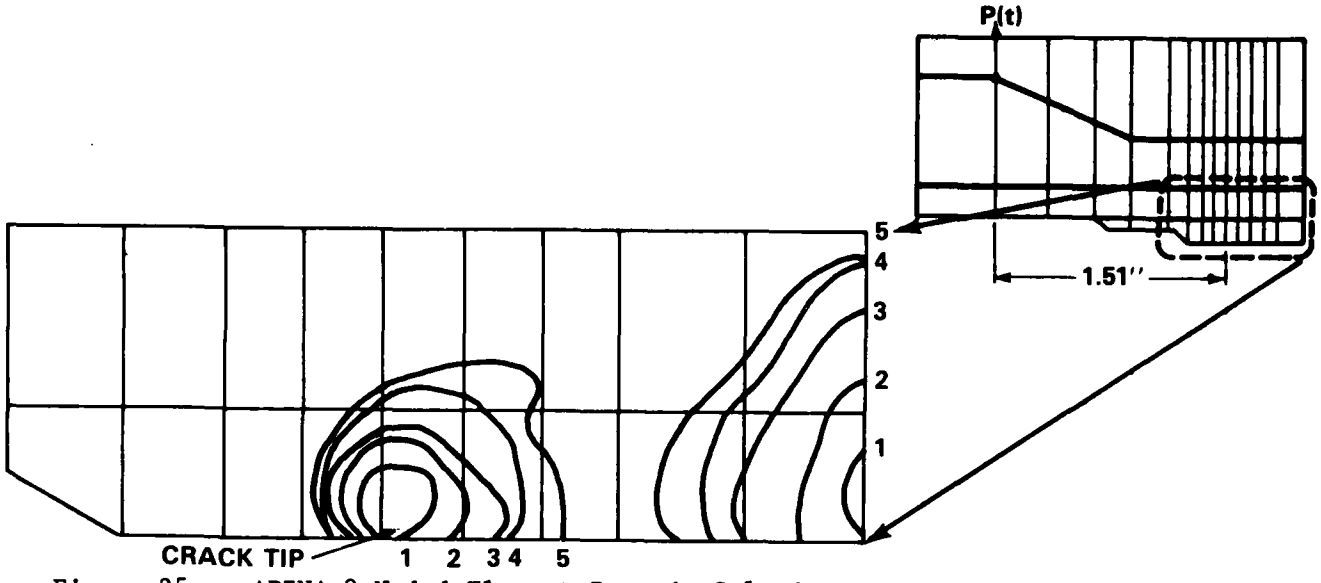

Figure 25a - ADINA 8-Noded Element Dynamic Solution

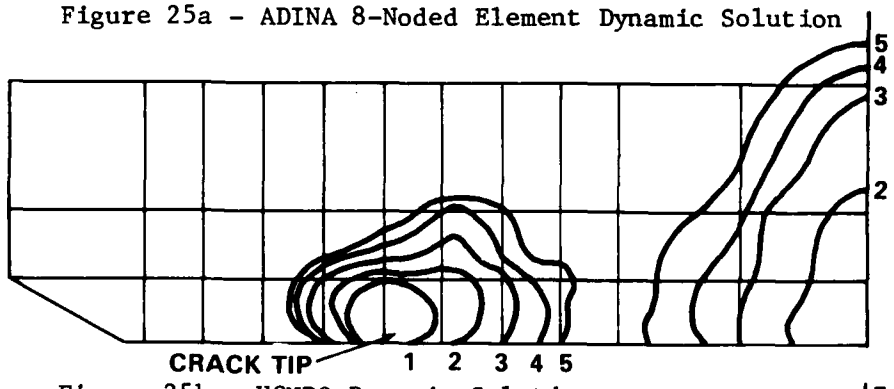

APPLIED LOADS-

1 = 2,923 lb
2 = 3,000 lb
3 = 3,450 lb
4 = 3,900 lb
5 = 4,600 lb

Figure 25b - HONDO Dynamic Solution

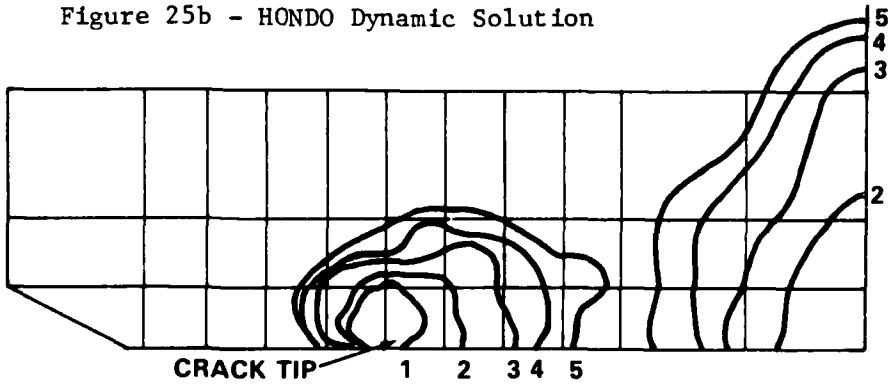

Figure 25c - ADINA 4-Noded Element Dynamic Solution

Figure 25 - Dynamic Finite Element Plastic Zone Growth for Specimen JC-6

SUBSEQUENT STUDIES

Further finite element studies were performed after most of the specimen tests had been completed. At this time, we had more confidence in the instrumentation, which had been fine tuned and debugged over the course of the tests. Most important, the load point displacement measurements obtained by the fiber optic sensor were more consistent and reasonable than those obtained by eddy current sensor. Thus further finite element analysis was desirable at this time. Now that the instrumentation had been refined, we hoped that further analyses would better indicate the ability of these methods to predict specimen response under dynamic loading.

Using the same general procedure used in the preliminary analyses, four more specimens were analyzed. The specimens had markedly different crack depths and load histories. Figure 26 shows the specimen numbers and crack depths along with the respective load histories of the specimens used in this second set of finite element analyses. The load histories shown are the actual input data for the computer solutions. For this reason, the curves are represented in a piece-wise linear fashion. These idealized load curves were taken directly from the experimental load records but with an effort to generally smooth the curves and disregard extraneous spikes. The slower, lower magnitude loading had fewer spikes and required less smoothing. The load history for JC-6, analyzed previously, is also provided in Figure 26 for comparison. As can be seen, the histories of the four later tests exhibit loads of lower magnitude and much longer duration. This change in load-history character is due to the lighter drop weight, lower drop height and, for specimens JC-23 and JC-27, a different load programmer. The slower rate of these curves made the finite element analysis somewhat easier to perform, particularly the choice of time steps (increment between solutions) and the providing of more complete solutions.

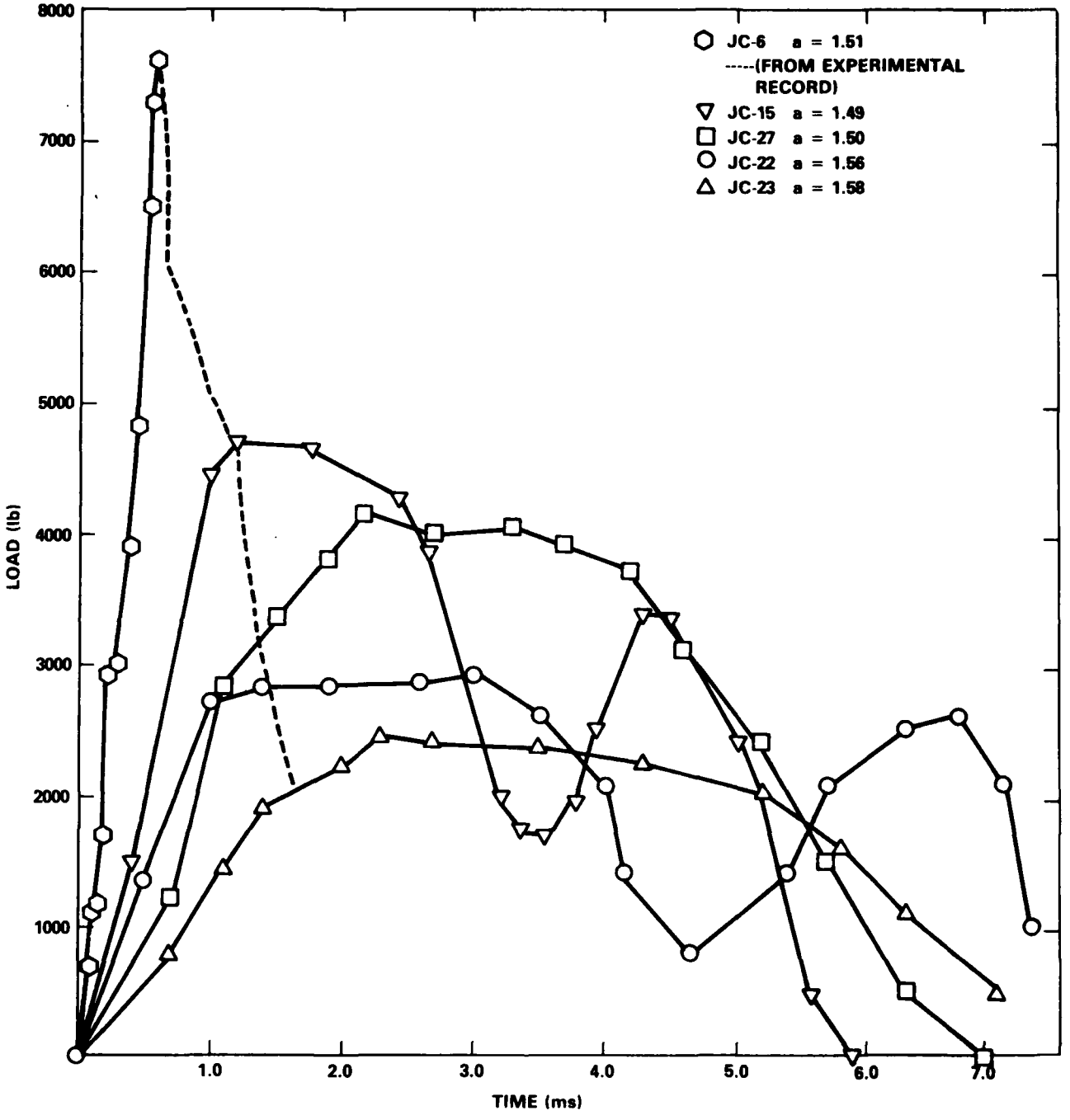

Figure 26 - Input Load Histories for Finite Element Analyses

The ADINA program and the idealization shown in Figure 22 were used exclusively for this series of analyses. This combination had yielded the best results in the previous analysis of specimen JC-6 dynamic loading.

There were some modeling difficulties in the second series of analyses due to the side grooves on the actual specimens; the grooves reduced the thickness from 1 to 0.8 in. in the area of the crack and uncracked ligament. These side grooves were of two types, either 1/8-in. radius curves or V-notches. Modeling this variable thickness in the specimen (without using an expensive three-dimensional dynamic solution) required some manipulation of the previously used finite element model. The side grooves were modeled by reducing the thickness of the bottom row of elements in the idealization (Figure 22) from 1 to 0.8 in. This change was important because, for two-dimensional plane stress elements, the element thickness is a component of the stiffness. The actual and idealized specimens are shown in Figure 27. For specimens with wide grooves, about the same volume was removed in the side grooved region in both cases. Maintaining this equivalence of volume was considered important so that about the same mass would be present in the region of the crack tip.

The load pin hole was not modeled. Unlike a static compact tension test, which uses a loosely fitting pin to apply load, the hole was almost completely filled with a tightly fitted bolt. Leaving the idealized specimen without a pin hole models the mass effect of this bolt-specimen interface reasonably well. Consideration of the load pin and hole led to another, perhaps more pertinent question: Is it necessary to model the stiffness and mass of the bottom loading clevis, since the applied load is measured at the end of the clevis opposite the specimen? There was a consistent lag in displacement response behind load response in the experimental records. The exact cause of this time lag was not clear, but we decided that the experimental displacement response curves, shifted to eliminate this lag, were the most appropriate

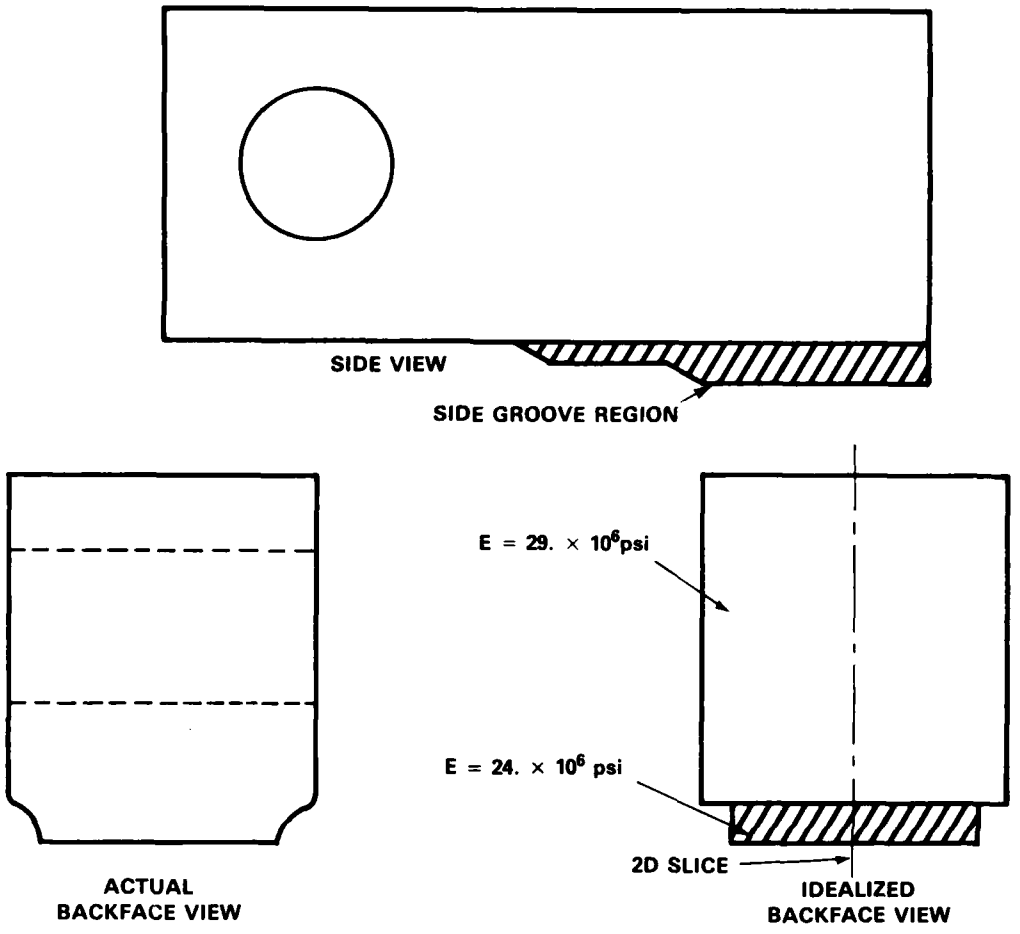

Figure 27 - Actual and Idealized Side Groove Geometry

goals for the finite element analyses. If agreement with these was achieved, then the relative effect of the clevis could be further quantified. This will be addressed later in this section.

A method of verification was needed to determine the validity of the side grooved specimen model. A comparison of the static, linear elastic finite element solution to that obtained by a compliance equation would provide this verification in the elastic range. Compliance is defined in the linear elastic case as the load point displacement per unit load. The equation chosen was developed by Holsberg.[25] It relates the compliance to the crack depth (a) and total specimen width (W):

$$C = \frac{(1-\nu^2)}{2BE}\left[41+\frac{\left(5+\frac{3a}{W}\right)^2}{2\left(1-\frac{a}{W}\right)^2}-\frac{3\left(5+\frac{3a}{W}\right)}{\left(1-\frac{a}{W}\right)}-9\log_{10}\left(1-\frac{a}{W}\right)\right]$$

where C = Compliance = load point displacement/load

ν = Poisson's ratio = 0.3

E = Young's modulus = 29.0×10^6 psi

B = Specimen thickness = 0.8 in. (with side grooves)
1.0 in. (without side grooves)

a = Crack depth = 1.51 in.

W = 2.0 in.

For the side grooved specimen (B = 0.8 in.) the equation yields:

$C = 7.791 \times 10^{-6}$ in./lb

and for a similar specimen without side grooves (B = 1.0 in.);

$C = 6.232 \times 10^{-6}$ in./lb

Two finite element analyses were performed: one on a specimen with the side grooves and one without side grooves. For linear elastic behavior, the results are shown compared to those obtained by the compliance equation in Table 6. As can be

TABLE 6 - LOAD POINT DISPLACEMENTS BY COMPLIANCE AND FINITE ELEMENT METHODS FOR SIDE GROOVED AND FULL THICKNESS SPECIMENS

Effective Specimen Width (in.)	Load Point Displacement Under Static 1000-lb Load (in.)	
	Finite Element	Compliance Equation
1.0	0.00646	0.00623
0.8 (Side Groove)	0.00710	0.00779

seen, the results for the 1.0-in.-thick specimen agree quite well with the finite element solution. The results for the 0.8-in.-thick side grooved solution show that the finite element solution is considerably stiffer (10%) than that obtained by the compliance equation. It is not clear whether this discrepancy is due to inaccuracies in the finite element model or the assumption of 0.8 in. for the specimen thickness in the equation producing an overestimation of specimen compliance. It was felt that for the wide side grooved specimen, the compliance should be close to that of a 0.8 in. constant thickness specimen. Obtaining this agreement would require a reduction in stiffness of the 0.8-in.-thick elements.

The most obvious way to reduce the stiffness is to further decrease the thickness of the elements to less than 0.8 in. This was undesirable because it would produce a modeled crack width smaller than that of the actual specimen. This would lead to an overprediction of displacements for loads producing plasticity in the crack region. A better possibility was to reduce the Young's modulus (E) of the thinner elements. The only problem caused by changing the Young's modulus would be a variation in the amount of elastic strain occurring before the onset of plasticity. If the new, smaller Young's modulus is close to the old value, there would be a very minor difference with plasticity occurring at perhaps 0.1% higher elastic strain. With displacements of the specimen being the primary results, and considering finite element accuracy, this slight error was thought to be insignificant.

Having decided that reducing the Young's modulus of the thinner element was the preferred method to match the compliance solution, we had to determine what reduced value was best. Using the same linear-elastic analysis as before, various values for Young's modulus were substituted into the finite element solution. The results are shown in Table 7 and are compared to the compliance equation results.

TABLE 7 - LOAD POINT DISPLACEMENT BY COMPLIANCE AND FINITE ELEMENT METHODS FOR A SIDE GROOVED SPECIMEN VARYING YOUNG'S MODULUS

Load Point Displacement Under Static 1000-lb Load (in.)			
Compliance Equation $E=29 \times 10^6$ psi	Finite Element Method		
	$E=27 \times 10^6$ psi	$E=26.1 \times 10^6$ psi	$E=24 \times 10^6$ psi
0.00779	0.00732	0.00746	0.00777

An elastic modulus of 24×10^6 psi produced load point displacements closely matching those predicted by the compliance method.

After developing a suitable model for the side-grooved compact tension specimen, the next step was to conduct dynamic analyses using the experimental load versus time histories as input. Specimen JC-27 was analyzed first. As can be seen in Figure 26, the load history for JC-27 was smoothly shaped and of relatively long duration. Peak magnitude was 4150 lb at a time of approximately 2.0 ms (these may differ slightly from actual experimental values due to piecewise linear approximation of load histories).

Choosing accurate material properties for the dynamic analyses caused some difficulty. Only one static coupon test had been performed on the HY-80 plate from which all the specimens were machined. This test produced a 0.2% offset yield stress of 88,380 psi and an engineering ultimate stress of 105,300 psi at approximately 6% strain. The ADINA finite element program is designed so that, for an elastic-plastic, isotropic hardening material, only a bilinear stress strain curve may be

specified. The required input parameters are Young's modulus, Poisson's ratio, yield stress, and strain hardening modulus. These requirements limit the accurate modeling of the nonlinear material. Choosing an accurate strain hardening modulus to best represent the nonlinear behavior of the material is particularly difficult. Hammel et al.[29] addressed this problem for a statically loaded steel compact tension specimen, and their best results were obtained using a strain hardening value tangent to the early, steeper portion of the hardening curve.

After considering that work and the error induced by having only one material property test, we decided to input the 88,380 psi value as yield stress and to use a hardening modulus of 300,000 psi, which is indicative of the slope of the true stress/true strain curve between the values obtained from the coupon test. The Young's modulus (for other than the side-grooved region) and Poisson's ratio were 29.0×10^6 psi and 0.3 respectively. The idealized stress-strain curve is shown in Figure 28.

Specimen JC-27 was analyzed under plane stress conditions. The primary desired outcome from this and subsequent analyses was agreement with the experimental load point displacement response. If good agreement occurred between these displacements, other calculated values, such as the J-integral would also be in close agreement because the experimental load history is used as input for the finite element analyses. For this first case, the analytically obtained displacments were much larger than those from the experimental record. It was determined that these large displacements could be at least partly due to the use of static material properties in the dynamic solution. The decision was made to modify the material properties in order to obtain a solution in agreement with the experimental results. Yield stress was the most obvious choice because there are a limited number of references available

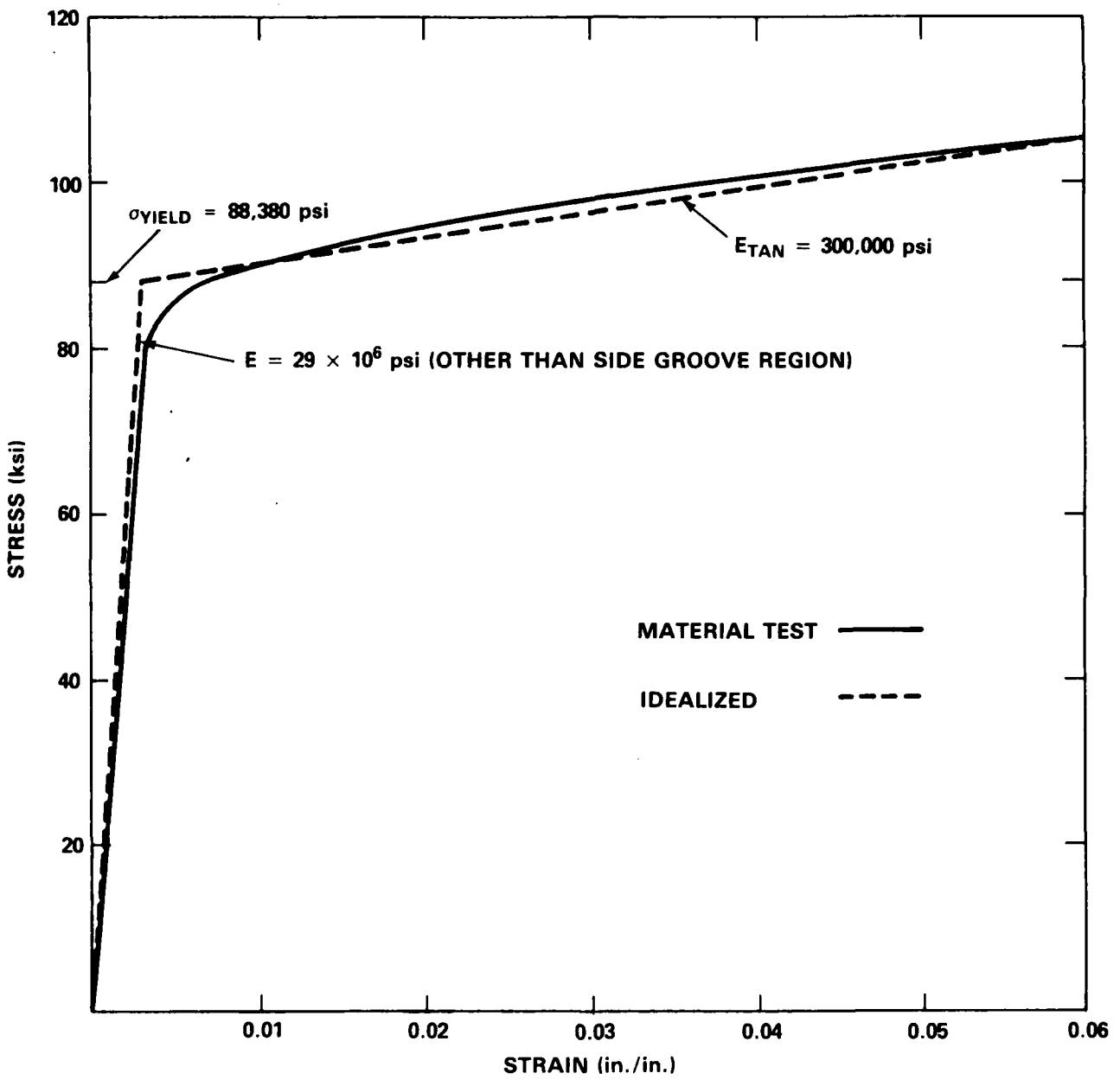

Figure 28 - Actual and Idealized Material Stress/Strain Relations

documenting measured increases in HY-80 yield stress with increasing strain rate.[26,33] The effect of strain rate on other material properties of HY-80 could not be found in the available literature.

Various increases in yield stress were then used in an effort to decrease the deformation of the idealized specimen. As shown in Figure 29, calculated displacements were nearly inversely proportional to yield stress. A value of 110,480 psi (a 25% increase over 88,380 psi) produced displacement results very close to those obtained from the experiment. This yield stress value seemed quite large even with the relatively high strain rates present. The measured back face strain rate for this test was on the order of 12 s^{-1}. According to References 26 and 33, tests conducted on HY-80 at approximately these strain rates indicated the yield stress increase would be more on the order of 5 to 10%. The back face strain rate is not representative of the strain rate near the crack tip, but much of the plasticity present in the specimen does occur at the back face so the strain rate measured there is important in terms of contribution to overall specimen deformation. It seems likely that it is not only the material properties, but also the finite element model contributing to the overly flexible analytical response. In an effort to resolve this material property question, more analyses were performed using other experimental records.

The JC-23 specimen test was particularly suitable for finite element analysis because the load was of relatively small magnitude and was applied over quite a long duration (Figure 26). An extensive analysis was performed on this specimen in hopes of resolving the yield stress question. In addition, we investigated other methods of modeling the geometry and loading of the specimen to better simulate the experimental case. The first analyses were done using a constant hardening modulus of 300,000 psi. The yield stress was varied to obtain displacement results matching

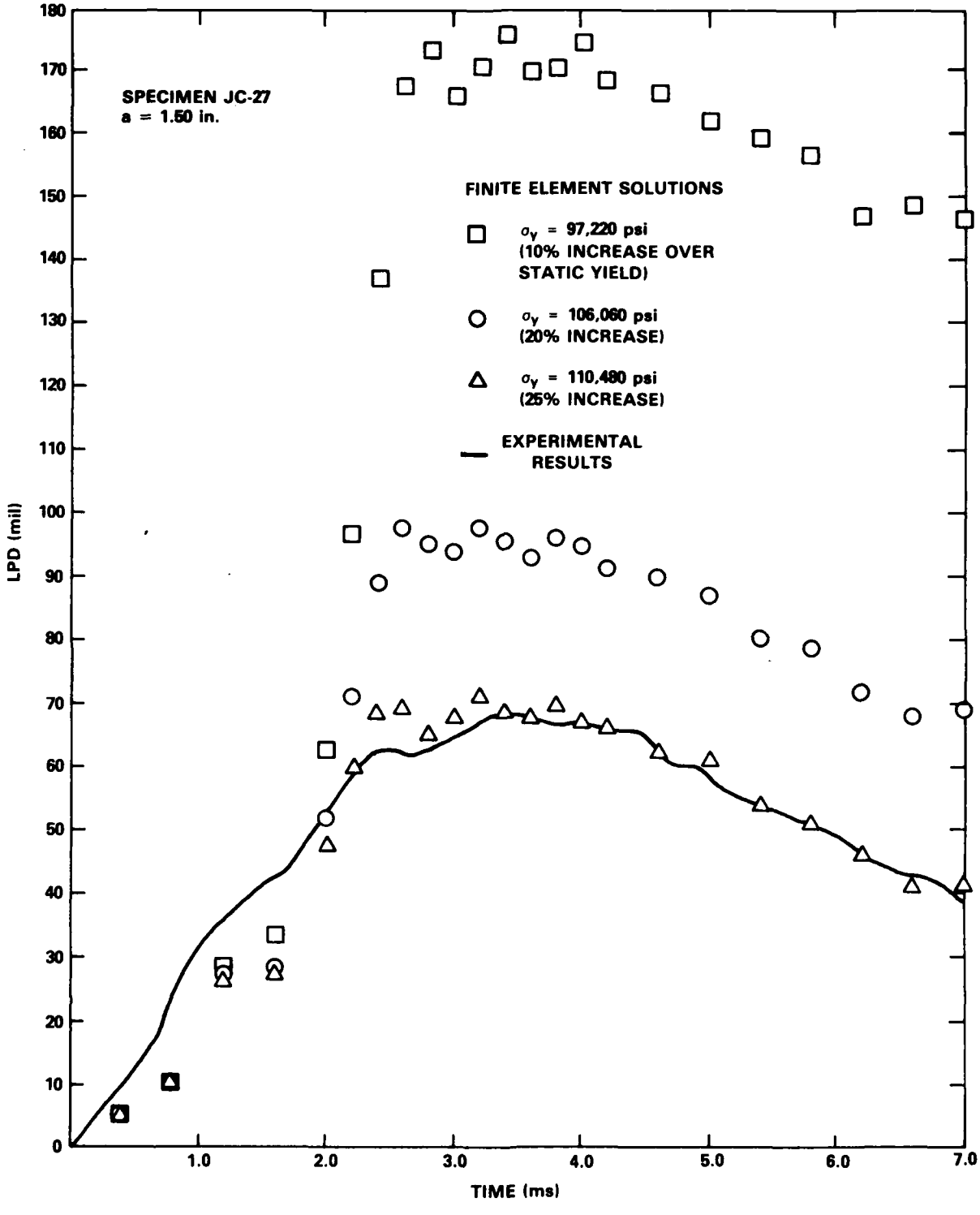

Figure 29 - Experimental and Finite Element Load Point Displacement versus Time Results for Specimen JC-27

those from the experimental record (the procedure was similar to that used in the JC-27 analysis). The results of this investigation are shown in Figure 30. The displacements for a yield stress of 92,800 psi, a 5% increase over the static measured yield, are quite close to the experimental deflection curve. This figure is also a good example of the sensitivity of the finite element displacements to yield

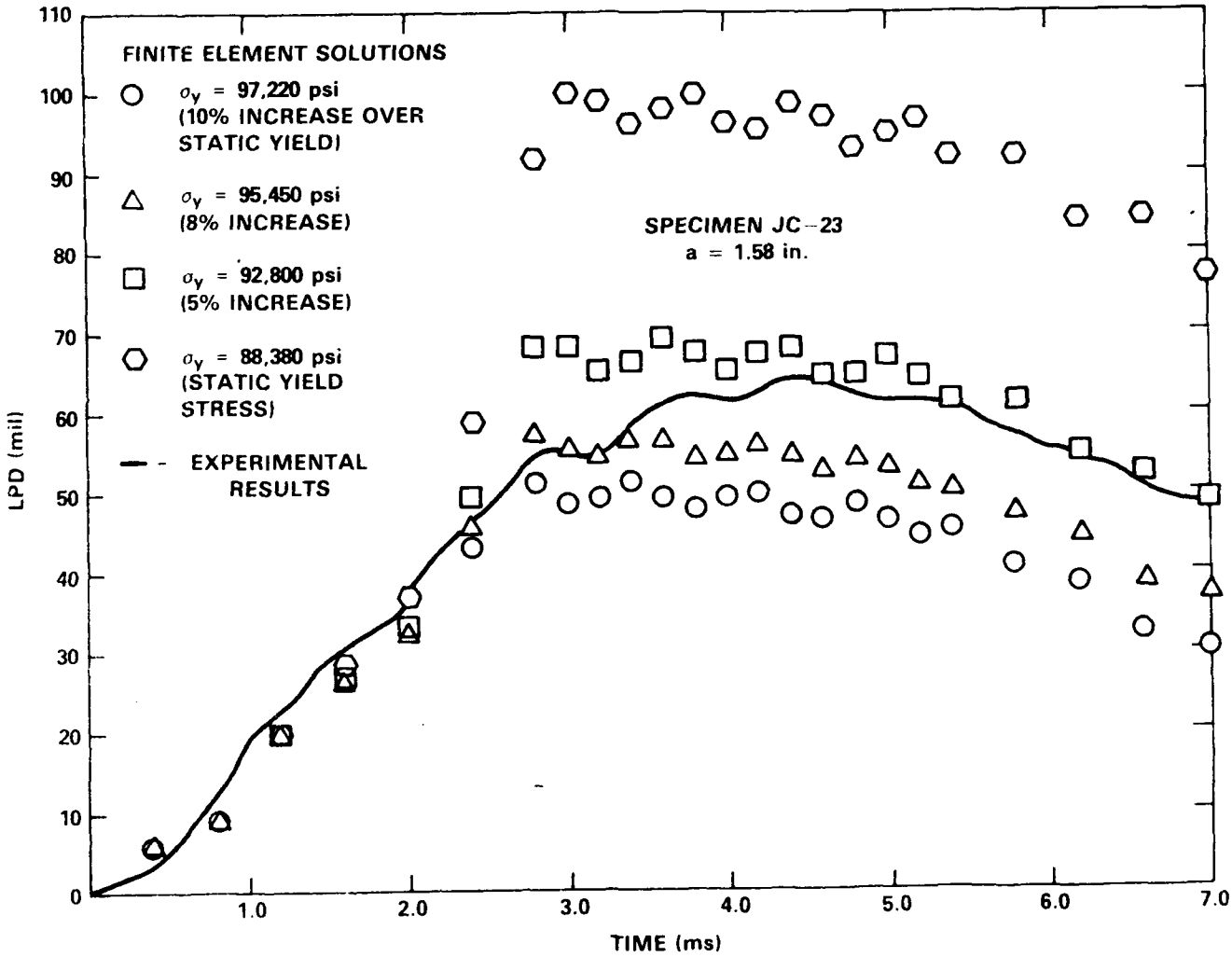

Figure 30 - Experimental and Finite Element Load Point Displacement versus Time Results for Specimen JC-23

stress change. As shown, load point displacement differed as much as 40% with a yield stress change of only 5% (88,380 to 92,800 psi). This important result indicates that accurate measurement of the material's yield stress is crucial for this type of testing. In this program, for which only one coupon test was performed, the measured yield stress is surely accurate to within 5% at best. These results show clearly that this accuracy is inadequate. As with JC-27, JC-23 undoubtedly experienced some strain rate effects. Figure 26 shows, however, that the loading rate for JC-23 was less than that for JC-27. Also, from the experimental records, the backface strain rate was 8.0 s^{-1} which is less than that measured for JC-27. Yield stress increases for HY-80 under strain rates of this magnitude should be only on the order of 3 to 5%.[26,33] Thus for this test (and probably for the lower load rates in general), pinpointing the amount of yield stress increase is not as important as obtaining an accurate static yield stress for the material.

Perhaps the most important result of these analyses thus far is that once the correction of material properties is performed, the finite element results model the experimentally obtained displacements quite well. A predictive capability, therefore, is certainly obtainable. Also, the idealization chosen is probably adequate for this analysis.

To further verify these results, an effort was made to fine-tune the idealization by modeling the contribution of the lower loading clevis. As mentioned earlier, the effect of the stiffness and mass of the clevis on the specimen was unknown. Since the applied load is measured at the necked-down area of the lower clevis, the clevis should be modeled as an extension of the specimen. The mass and stiffness were modeled by means of a linear elastic truss element and a concentrated nodal mass. The neck of the clevis, the flexibility of which was thought to be a possible cause of the consistent lag of experimental displacement measurements behind the load

record, was modeled by a truss element having the same length and stiffness. The rest of the clevis was assumed to be rigid and was treated as a concentrated mass at the specimen load point as shown in Figure 31. Most likely, this model would accurately reproduce any deformational and inertial effects of the actual clevis on the measured load-point displacement. This idealization was run using the same JC-23 input values that produced the best results shown in Figure 30. The load point displacement obtained from this analysis is shown in Figure 32; the experimental

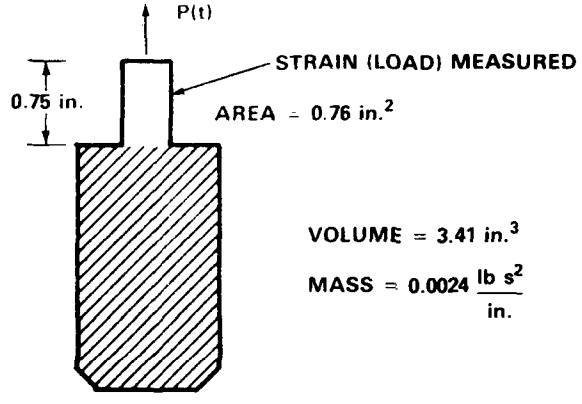

ACTUAL CLEVIS GEOMETRY

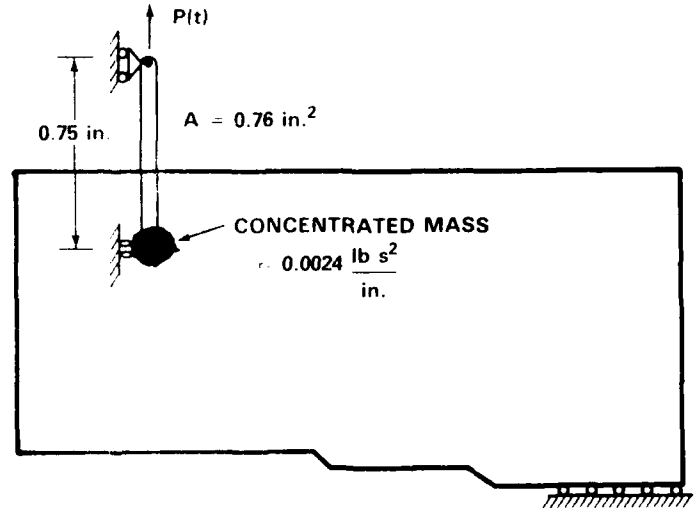

IDEALIZED MODEL OF CLEVIS INCLUDED IN IDEALIZATION OF SPECIMEN

Figure 31 - Finite Element Model of Loading Clevis

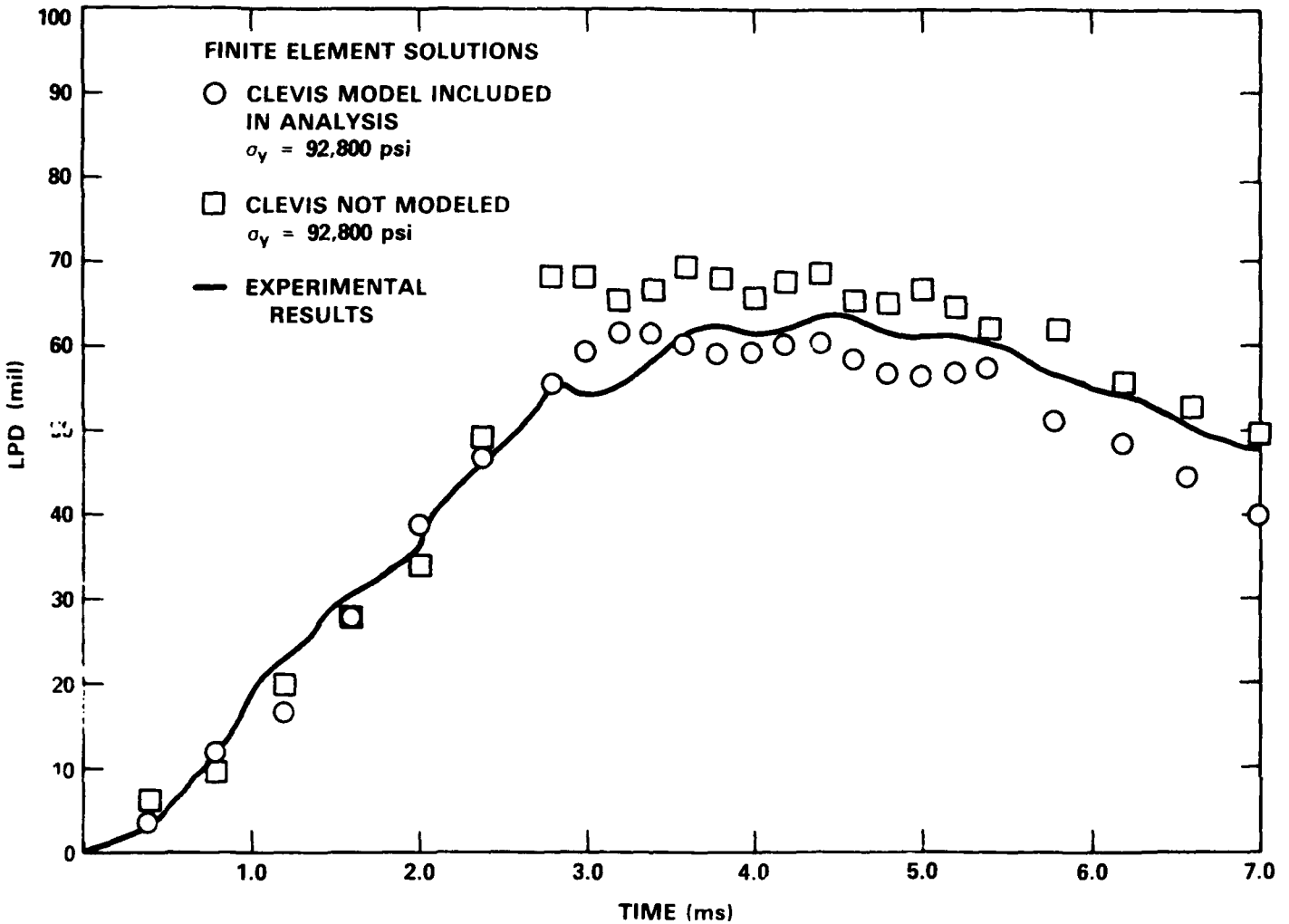

Figure 32 - Effect of Clevis on Finite Element Load Point Displacement Response for Specimen JC-23

value and the best result without modeling the clevis are both included. As shown in the figure, the clevis model had a slight damping effect and reduced the displacement a small amount. No significant time lag was evident, but the first computer displacement output was probably too late for this to be a conclusive result. A second attempt was made, this time including the approximate stiffness of the body of the clevis (not just the neck) in the truss element. This more detailed clevis model was used in conjunction with the JC-27 idealization and loading input. Specimen JC-27 exhibited a displacement lag of about 0.3 ms behind the load record when tested. We hoped that the more accurate model of the clevis and an additional finite element displacement output at 0.2 ms would show evidence of this lag. The results of the JC-27 analysis are presented in Figure 33. Shown are the displacement history obtained without modeling the clevis and the displacements for the case with the accurately modeled clevis. Close examination of the results for a time of 0.2 ms reveals that only a very small displacement (perhaps not discernable on the experimental records), had occured up to this time. This delay caused by the clevis flexibility could be a major component of the experimental time lag. In this case, the analysis did not clearly show the full 0.3 ms delay of the experimental displacements, but it must also be remembered that no flexibility in the load bolt connection was included.

The fact that the experimental time lag appears to be largely due to the flexibility of the loading clevis (more correctly, due to the load measurement taking place on the clevis and not at the load pin) is an important finding. It means there were no large losses in the system, only a delay of the force acting on the specimen itself. Although the mass of the clevis does appear to play a slight role in determining magnitude of load point displacement in the two analyses performed (Figures 32 and 33), there does not appear to be a specific trend. Considering the

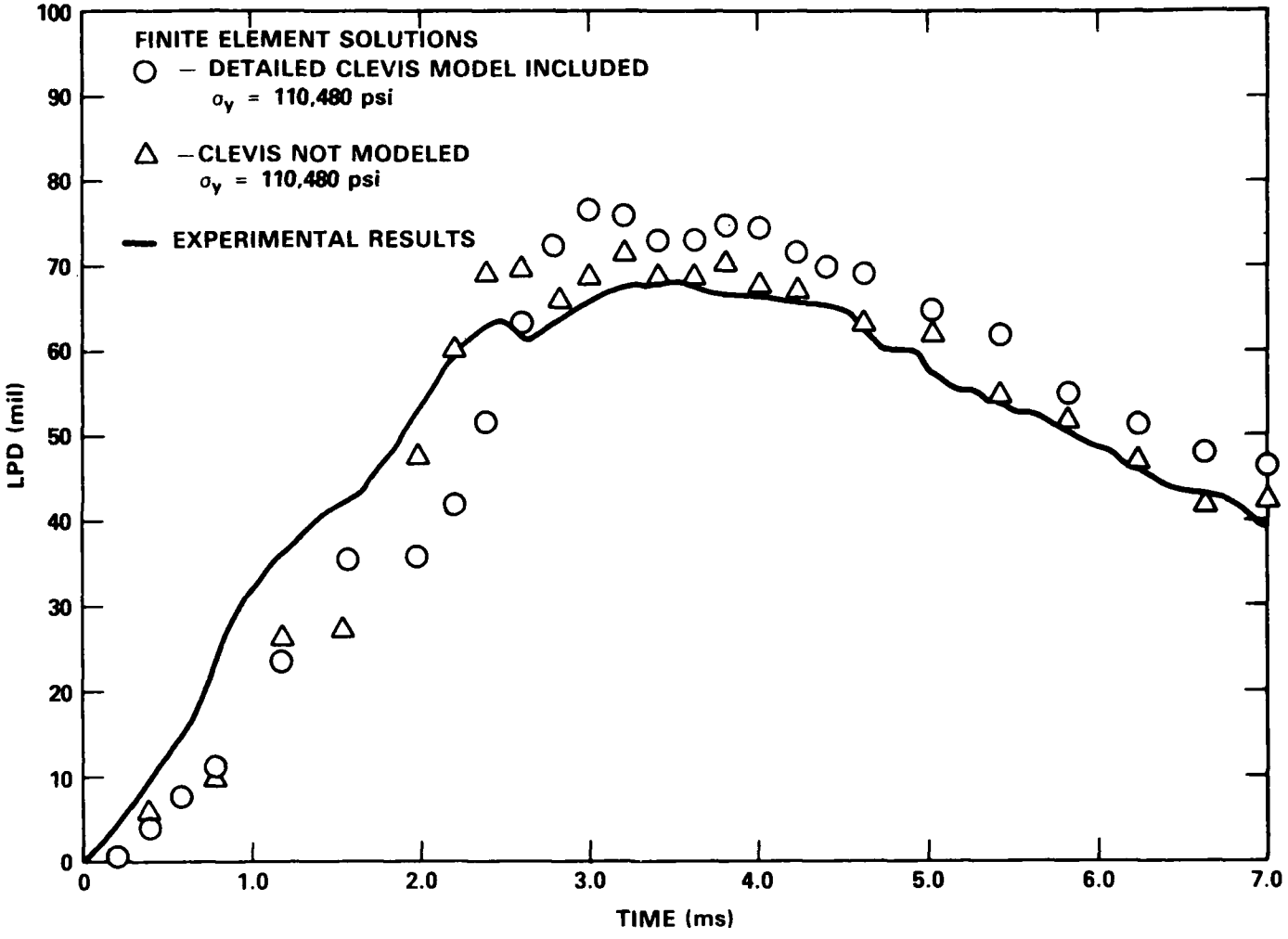

Figure 33 - Effect of Clevis on Finite Element Load Point Displacement Response for Specimen JC-27

number of other uncertainties and observing that the inertial effect of this mass tends to be small, it appears reasonable to ignore the inertial contribution of the clevis.

These findings justify the shifting of the experimental displacement curves so that displacement coincides with load increase. Unless the experimental displacement curve is shifted, the results obtained for the load versus load point displacement curve and, subsequently, the J-integral will be incorrect. The specimen will appear considerably stiffer than it actually is because of the apparent lack of displacement during the early time loading. The finite element results indicate that this lack of displacement is caused primarily by the flexibility of the clevis so that it is reasonable to remove the clevis, in effect, and apply the load directly to the specimen. Shifting the experimental displacement curve suggests that there is no clevis and that the only response is the response of the specimen. These conclusions indicate that the best method for reproducing shifted displacement response of the specimen is applying the load directly to the idealized specimen and not modeling the clevis at all. This, of course, is true only if the inertial effects of the clevis are small (as they appear to be). Thus, we apparently had completed a full circle. The first analyses were performed on JC-27 and JC-23 without modeling of the load clevis. It now appears that this type of analysis is most appropriate for reproducing the shifted experimental displacement curves.

Having determined the most appropriate idealization geometry, we decided to continue finite element specimen analysis to further investigate the material property questions raised earlier. Two more specimen tests were investigated. Specimens JC-15 and JC-22 were chosen because they were subjected to loading that was basically different from the loading of the previously analyzed specimens. Their load

histories are shown in Figure 26 along with the load histories of the other analyzed specimen tests. The loading rates for JC-15 and JC-22 were somewhat higher at the beginning of the load history curve, then peaked quickly, and the load value oscillated once before declining again. This shape resulted from the properties of the load programmer used for these tests--a nylon plug, which produced load characteristics considerably different from those of the 1/8-in.thick lead pad used in tests of the previously analyzed specimens. Specimens JC-15 and JC-22 also underwent a slight amount of crack extension, indicating that a critical value of the J-integral (J_{IC}) was reached in these tests, although hopefully not exceeded by too large an amount. We wanted to analyze specimens in which crack growth had occurred to find any noticable differences between the experimental displacement curve and the finite element results due to the crack extension that would not be accounted for in the analysis.

First, JC-22 was analyzed using the same basic procedure described earlier. Because of the load rate and magnitude, the JC-22 specimen behavior ought to be similar to that of the JC-23 specimen. As with the previous analyses, material yield stress had to be varied to produce finite element load point displacements approximating those measured in the experiment. As shown in Figure 34, a yield stress of 98,990 psi produced finite element displacements reasonably close to the experimental results. This value was 12% above the static yield as compared to the 5 and 25%, respectively, required to achieve reasonably close solutions in specimens JC-23 and JC-27. Because the back face strain rate for this test was not obtained, no strain rate comparison was available. Figure 26 shows that the initial load rate is somewhat higher than for JC-23 and about the same as for JC-27. From the results

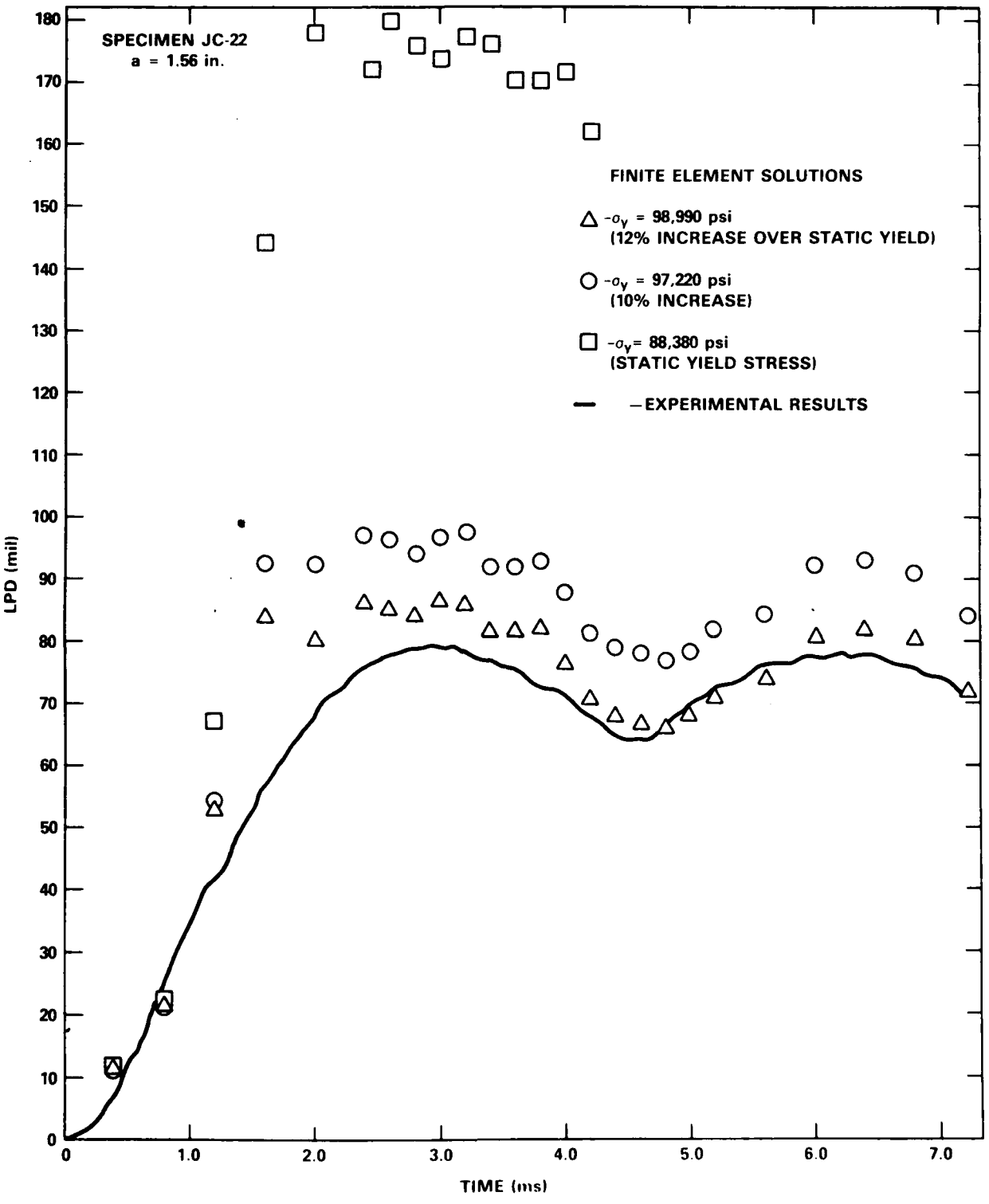

Figure 34 - Experimental and Finite Element Load Point Displacement versus Time Results for Specimen JC-22

of the three analyses performed thus far, it appears that the smaller experimental displacement, accounted for in the analysis by increased yield stress, is load rate (strain rate) dependent.

A pleasing product of the JC-22 solution was the manner in which the finite element solution followed the oscillation of the experimental displacement curve. This agreement indicates that the effect of the lower Young's modulus in the side groove region seems to be minimal, since the displacement during the unloading and reloading agrees with the experimental results quite well. The nagging question of why the large increase in yield stress is necessary to obtain an analytical solution approximating the experiment remains. As was discussed previously, strain rate effects are a possible explanation especially as they may affect the hardening modulus. In the case of JC-22, if the strain rates are on the order of those found in JC-27, this could explain nearly all of the required yield stress increase. However, considerable doubt remains.

Specimen JC-15 was the most severely tested specimen in this set of four analyses. It was also the only specimen of the four having narrow V-shaped side grooves. As shown in Figure 26, the initial load rate and peak load were quite high. From the previous cases, one would expect at least a 25% increase in yield stress to be required to obtain displacements near those measured in the experiment. The plots of load point displacement versus time obtained from the experiment and from the analytical solutions are compared in Figure 35. In this case, a 40% yield stress increase was needed to obtain displacements relatively near the experimental values. The back face strain record for this test indicated a strain rate of approximately 20 s^{-1}. This strain rate could cause up to a 10% increase in the yield stress for HY-80[33] but certainly not the 40 or even 50% increase required to match the experimental displacements.

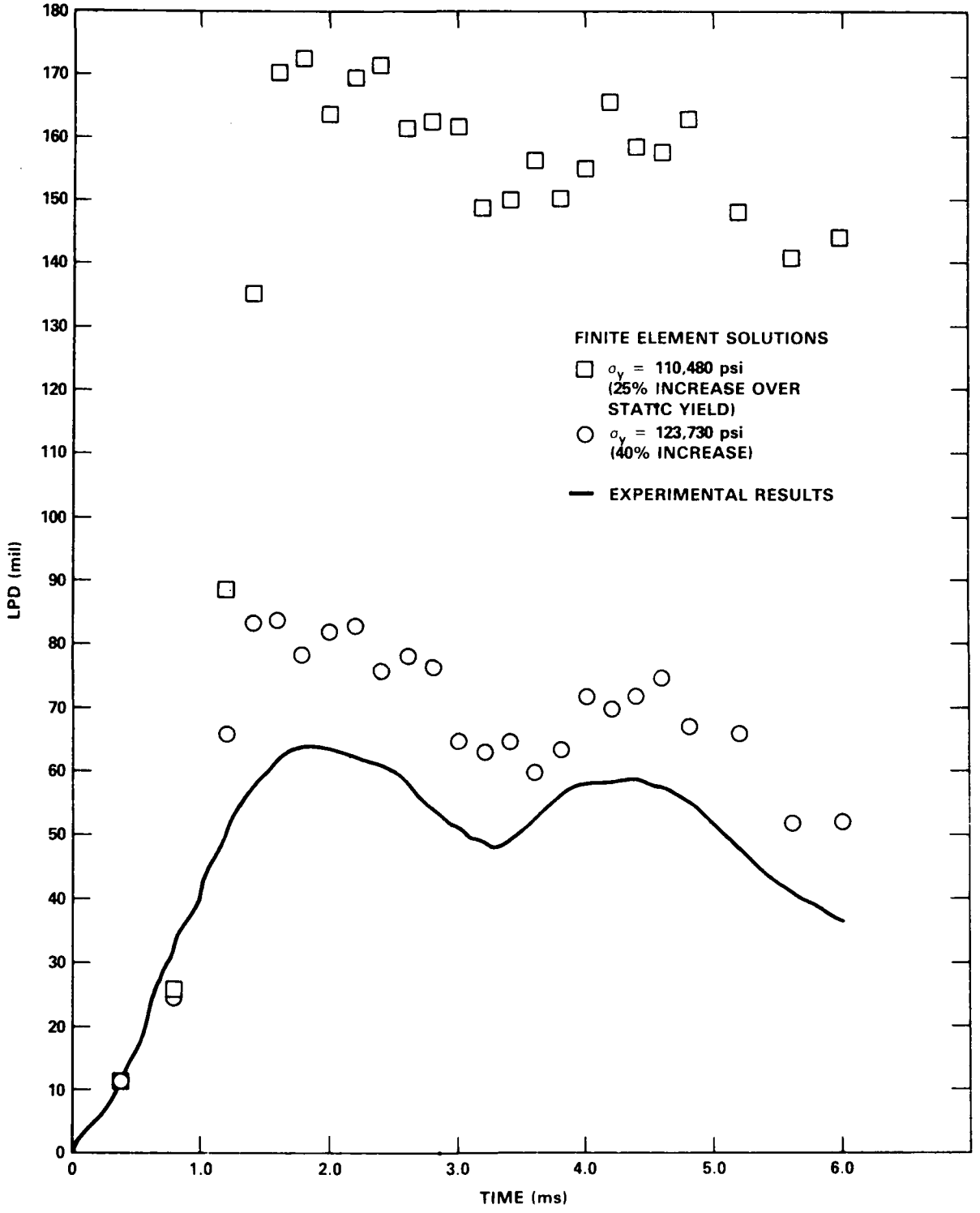

Figure 35 - Experimental and Finite Element Load Point Displacement versus Time Results for Specimen JC-15

The finite element solution for JC-15 indicates that the idealization used, specifically the method in which the side grooves were modeled, was inappropriate for this analysis. Intuitively, one would expect the specimen with the V-shaped grooves to be somewhat less compliant elastically than the finite element model used. Apparently, it is also considerably less plastically compliant than the finite element idealization. The finite element model overpredicts the actual displacements because the reduced thickness section of the model, which was developed to represent the wide side grooves, does not accurately represent the V-shaped grooves present in specimen JC-15 (see Figures 9 and 27). In effect, the plastic zones at the crack tip and back face in the reduced thickness region of the model expand further under a given load than is appropriate. This is also a possible explanation for the overprediction of displacements that occurred in the analysis of specimen JC-27. As shown in Table 8, which gives pertinent experimental and finite element data for the four specimens analyzed, JC-27 sustained the highest load of the wide side grooved specimens. At higher loads, possibly producing larger plastic zones, the side groove model becomes increasingly inaccurate because the gradual increase in thickness of the actual specimen is not modeled. This means that the plastic zones will be larger in the finite element analysis than in the actual specimen causing an overprediction of displacements. The smaller magnitude of the loads on specimens JC-22 and JC-23 may have reduced this effect to the point that accurate answers could be obtained using reasonable dynamic yield stresses.

DISCUSSION

Over the course of the experimental program, an accurate method for testing compact tension specimens under dynamic loading was developed. This capability raises questions of how the data obtained by this method should be applied. As a means of comparison, the J-integral was routinely determined from the specimen test

TABLE 8 - SUMMARY OF FINITE ELEMENT ANALYSES

Specimen	Peak Load (lb)	Approximate Initial Load Rate (lb/ms)	Experimental Back Face Strain Rate (s^{-1})	Experimental Peak Displacement (10^{-3} in.)	Expected Yield Stress Increase (Ref. 26,33) Based on Strain Rate (%)	Required Yield Stress Increase in Finite Element Analysis (%)
JC-15	4700	4450	20.0	84.0	7	>40
JC-22	2900	2700	N.A.*	79.0	----	12
JC-23	2450	1355	8.0	64.0	4 - 5	5
JC-27	4150	2230	12.0	69.0	6 - 10	25

*Not Available; no back face strain record was obtained for this test.

load and load point displacement data. These values were then used as a measure of the material J_{IC} by determining which calculated value of J best corresponded to crack initiation. One must question the application of standard static-test methods of determining the J-integral in light of (1) the inertial effects caused by the dynamic loading and (2) the associated vibratory loading and unloading of the specimen. The actual significance of these effects cannot easily be quantified. It is possible that, for these specimens, inertial effects are not that large, considering the damping caused by the programmers and load line velocities of 10 to 50 in./s. The relatively smooth load histories obtained in the test data seem to support this contention. Also, the J-integral was the only readily available measure of material toughness that could be easily applied to these tests. Thus the J and J_{IC} values were used for comparisons, although doubt about their ultimate validity has not been resolved.

The J-integrals obtained for specimen tests where the instrumentation seemed to be accurate are presented in Table 9. This table is separated into two sections: specimens tested at load rates produced using a nylon load programmer and those tested using a lead load programmer. The J-integrals were calculated by determining the maximum area under the load versus LPD curve and applying the Merkle-Corten equation.[17] No provision was made to account for crack extension, so that the calculated J_{max} may be incorrect for specimens having undergone substantial crack growth. Considering the instrumentation problems incurred in this program, it is especially pleasing to observe how well these test results appear to bracket a critical J_I value of approximately 1000 in.-lb/in.^{2} for both loading situations. This is slightly lower than the 1110 in.-lb/in.^{2} value obtained from three static J_{IC} tests on the same plate, although with the relatively few available data points,

TABLE 9 - SUMMARY OF EXPERIMENTAL J_{IC} RESULTS

Specimen	Drop Height (in.)	Peak Load (lb)	Max J_I (in.-lb/in.^{2})	Crack Extension (in.)
Nylon Programmer				
JC-10	6	4410	760	None
JC-11	5	4800	720	None
JC-14	7	5325	1070	None
JC-15	8	4690	1040	<0.01
JC-20	8	2940	1000	*
JC-22	8	2950	1120	0.02
Lead Programmer				
JC-23	12	2400	670	None
JC-26	12	4100	1500	0.02
JC-27	10	4080	960	None
JC-29	10	4200	1040	0.01
JC-32	12	3250	1650	0.04
JC-33	11	3100	1380	0.02

*Specimen was tested twice; visible extension observed after it was broken open.

the difference is probably not significant. Hasson and Joyce[12] reported a similar result for compact specimens loaded in a servohydraulic test machine. In their work, J_{IC} for HY-80 steel, as determined by the Merkle-Corten formula, was comparable (at room temperature) for load point rates of 5.1 in./s and 1.6×10^{-4} in./s. At lower than room temperature, the rapidly loaded specimens produced J_{IC} values lower than those found under static conditions.

The experimental results obtained after much alteration and fine tuning of instrumentation seem to be reasonably believable and accurate. Questions remain as to what fracture toughness assessment is most applicable in this case considering the apparent shortcomings of the J-integral. New toughness parameters, such as J' and ΔT, which are valid in the dynamic and nonproportional loading cases, are being investigated.[34,35] Though not readily available at this writing, these or other parameters may allow an ultimate assessment of this work.

The finite element analyses, we had hoped, would play a role in the characterization of the material toughness. The problems encountered in matching the load point displacement histories of the experiment diminished that hope. The large yield stresses required to retard the finite element load point displacements require more investigation. There are several possible explanations for the discrepancies between the finite element results. The first explanation presumes inaccuracies remain in the load point displacement measurement. This appears unlikely in tests where the fiber optic Fotonic sensor was used for displacement measurement. Much "double checking" was done with this sensor including measurement of set displacements with the sensor and feeler gages. Results of this verification indicated that the load point sensor is probably accurate to within 10%.

A second possible explanation is that the finite element solution was dependent on a poor model of the material properties. A bilinear stress-strain model is not as accurate as power hardening or multilinear types of representation. More important, the simple bilinear model includes no accurate account of the strain rate effect on the material properties. We investigated this possibility somewhat by increasing the yield stress until finite element displacements agreed with the experimentally measured values. In some cases, the required amount of yield stress increase seemed reasonable. However, the bilinear nature of the stress-strain curve and lack of strain rate alteration in the hardening portion remain questionable areas. The effect of strain rate on the hardening modulus could be just as significant as yield stress in predicting displacement when plastic zones become large. If the hardening modulus is increased only slightly, a disproportionate decrease in displacement could occur. Investigation of this phenomenon is worthy of future study, particularly when the material is better characterized.

A sizable amount of current research is concerned with development of accurate finite element constitutive relationships. The finite element code ABAQUS offers much promise in this area; it has both exponential hardening material description and Malvern strain rate sensitivity capabilities built in.[36] Had this code been available at the start of our work, it might have been used for the analyses. At this writing, consideration is being given to reanalyzing some of the specimens in this test program using ABAQUS and a presumably better material description that includes rate effects. The overall lack of material property data available for HY-80 steel tested at high strain rates would be a hindrance, however. This lack of data makes the validity of the derived property constants that are required questionable. Therefore, one can only presume that having this strain rate capability is truly advantageous. This question points out the need for a large scale material

characterization program for the naval HY steels much like that already performed by the nuclear industry on A533B reactor pressure vessel steel.

A third possible explanation for the discrepancies between the finite element results and the measured test results is inaccuracy in the finite element idealization. As mentioned in the last section, inadequacies in the side groove model appear to be a possible cause for the large overprediction of displacements that occurred in the analyses of the more severely loaded specimens, and particularly for the specimen having V-shaped side grooves. Another possible inaccuracy in the finite element model is the manner of load application at the bolt connection. As modeled in the finite element idealization (Figure 22), the load history is applied as a concentrated load at one point in the specimen. This situation would correspond to a static compact specimen test with undersized load pins. For this dynamic test situation, tightly fitting bolts were used to transfer the load in order to remove as much of the "slack" in the system as possible. Considerable effort was made to allow the specimen to rotate freely about these bolts. The bolts were lubricated where they interfaced with the specimen and were tightened to the point where they could still spin freely. Despite these precautions, there may have been some applied moment at the load holes, and the point load used in the finite element analysis may not have been a good representation of the distributed loading applied by the snugly fitting bolts. This is another area for future investigation. Idealization changes in the load pin region and the use of distributed or multiple point loads may cause unexpectedly large changes in the displacement response of the specimen.

The finite element analyses were extremely sensitive to crack length. This was among the most enlightening results of the various finite element analyses and was in fact stumbled upon quite accidently. During the analysis of specimen JC-27, the crack length was input as 1.51 in. instead of the actual measured value of 1.50 in.

When this was corrected, and the analysis rerun with a crack depth of 1.50 in., the result was a 40% smaller peak load point displacement. The load point displacement histories for the two analyses are shown along with the measured experimental value in Figure 36. Both analyses were conducted using a yield stress 20% above the static value and the same elastic and hardening moduli. The extent of the change in displacement response was quite surprising. To further investigate this effect, another specimen analysis was performed.

Specimen JC-23 was more deeply cracked, and had been less severely loaded, than specimen JC-27. We chose to analyze it with different crack depths to see if a change in the load point displacement as large as that found in specimen JC-27 would occur in this case. Shown in Figure 37 are the LPD histories obtained for crack depths of 1.58 in. and 1.59 in. As in specimen JC-27, this small change in crack depth resulted in roughly a 40% difference in peak displacement. This similar result for a substantially different test seems to indicate that the deeply cracked nature of the specimens in this test program (a/W from 0.725 to 0.79) is the major contributing factor to the crack depth sensitivity.

A question remains as to whether this crack depth sensitivity occurs in the actual specimen to the degree in which it occurs in the finite element analyses. The elastic compliance[25] versus the crack depth for the side grooved specimens is plotted in Figure 38. As shown in this figure, the a/W values for the specimens used in this program fall in a very rapidly changing section of the curve. Despite this, even in the most deeply precracked specimens, the elastic displacement response would only vary about 5% for a crack depth change of 0.01 in. The rest of the change in displacement must be due to the large amount of plasticity occurring in the relatively small remaining ligament section. As shown in the two test cases, the relative effect due to change in crack depth appears to be essentially independent of

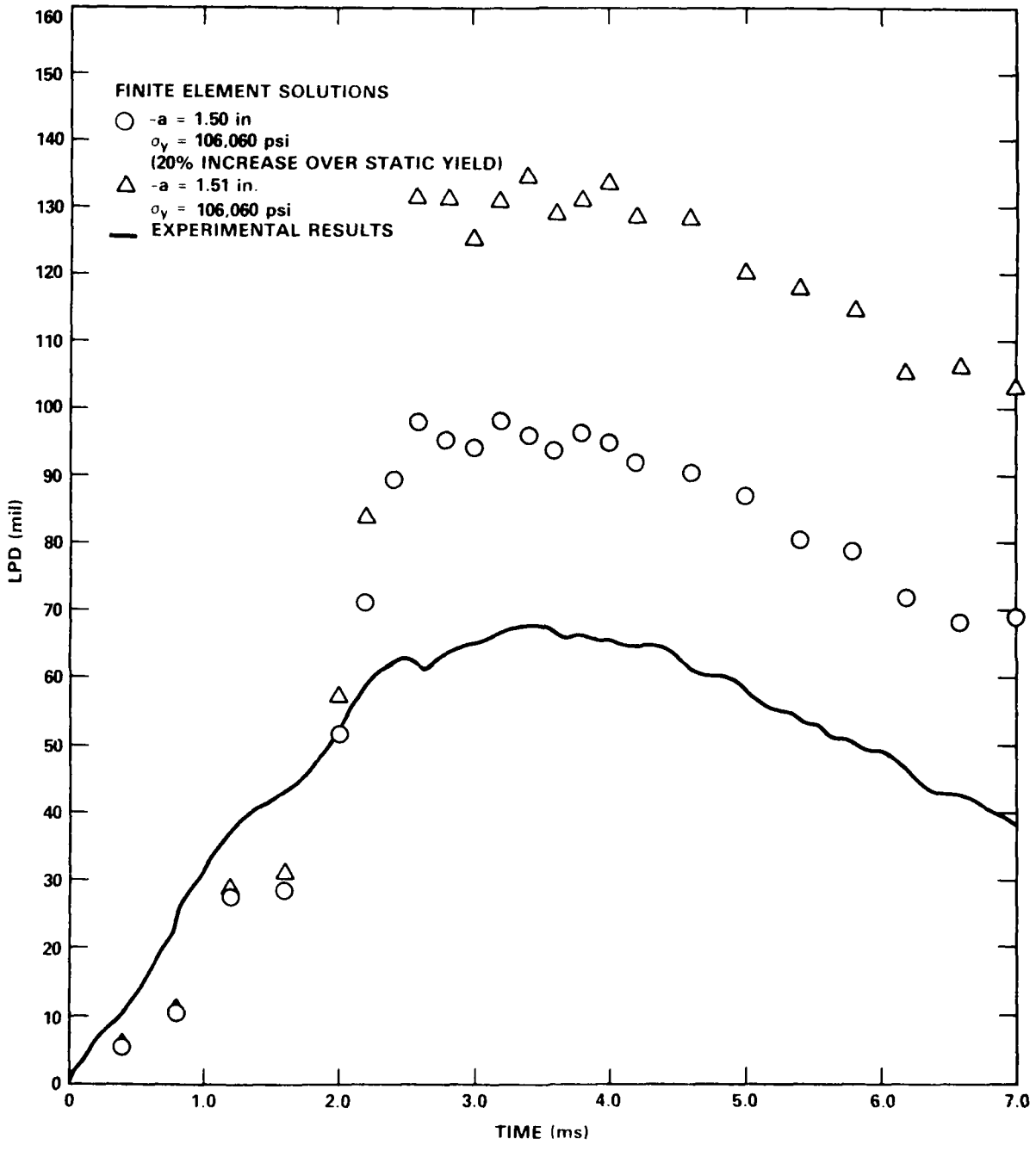

Figure 36 - Effect of Crack Depth on Specimen JC-27 Load Point Displacement Response

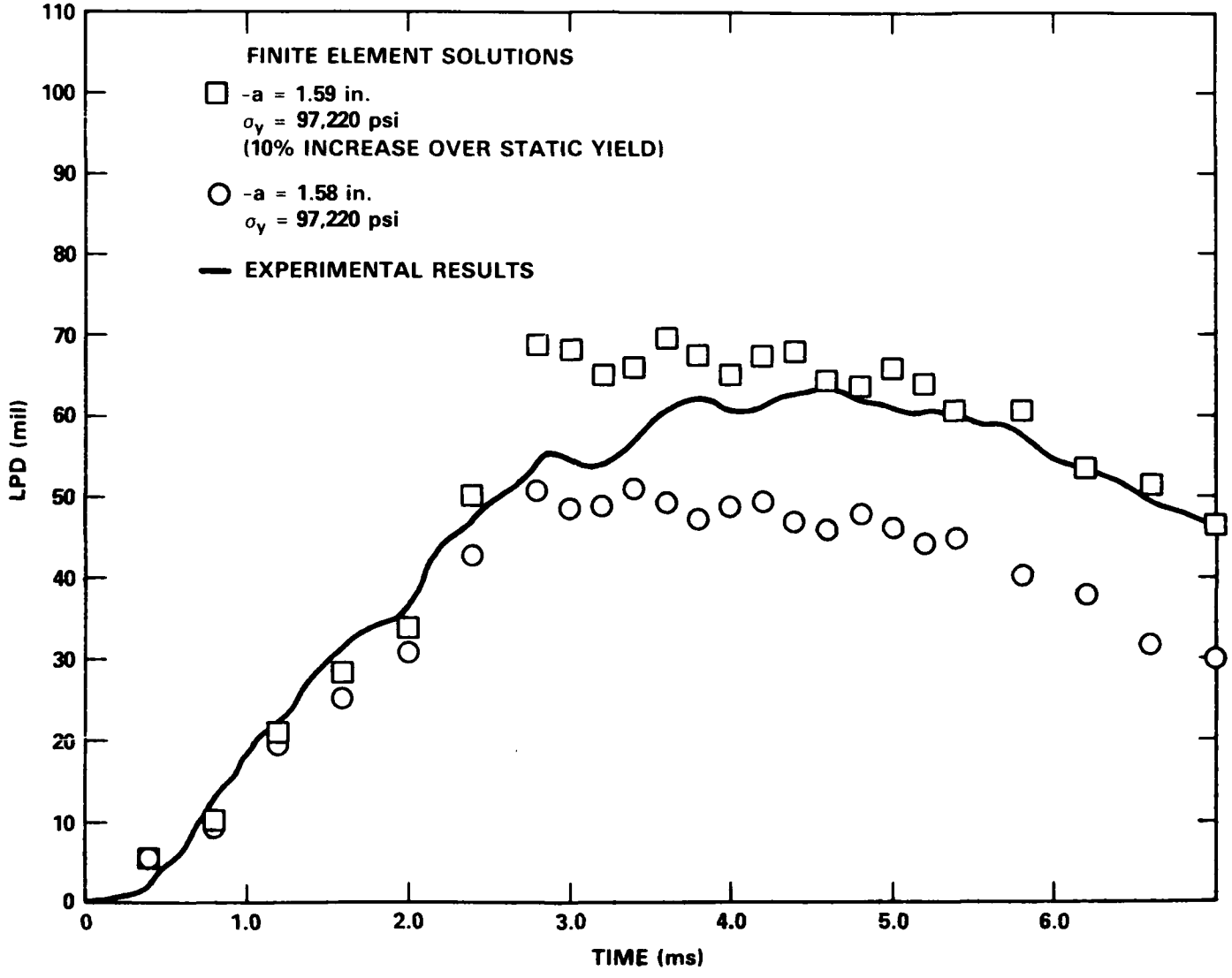

Figure 37 - Effect of Crack Depth on Specimen JC-23 Load Point Displacement Response

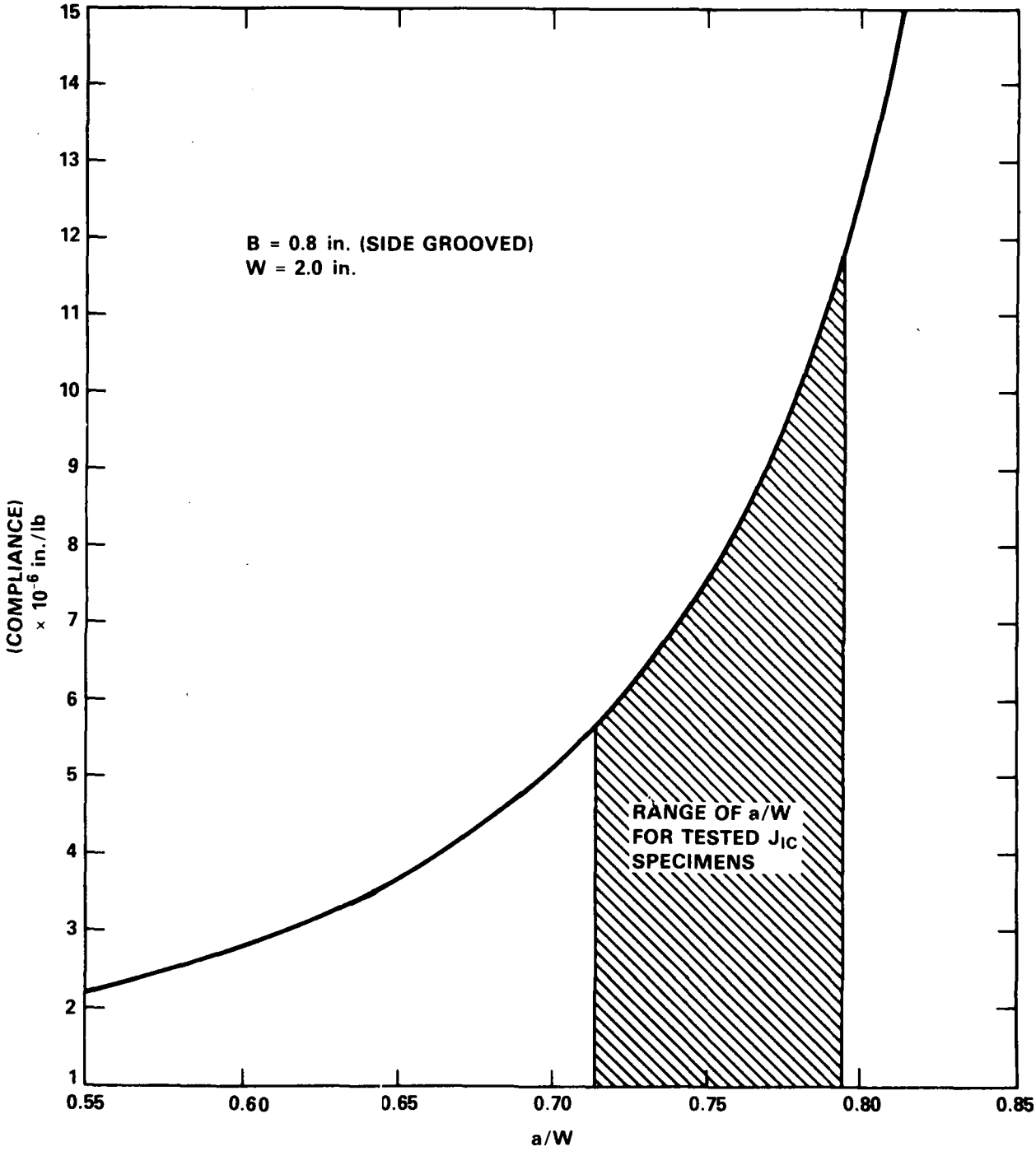

Figure 38 - Crack Depth versus Compliance for a Side Grooved Compact Tension Specimen

yield stress. The effect of variation in hardening in the material models has not been investigated and remains a questionable area.

The ramifications of this crack depth sensitivity could be significant. One must question the finite element solution for any very deeply cracked specimen for which the measured crack depth is averaged to the nearest 0.01 in. and input in the analysis. These results indicate that more accurate crack depth measurement is needed. The effect of curved crack fronts also appears to be a potential source of large error when idealized as a planar crack front in a two-dimensional analysis. This crack sensitivity could have been a contributing factor to the discrepancies between the experimental and finite element results presented earlier. A slight difference between the actual and idealized crack depths could fully explain the overly flexible finite element solutions obtained using what are considered more reasonable yield stress values. Obviously, this topic deserves more thorough investigation. The effect of static versus dynamic loading on this crack depth sensitivity was not investigated. More complete analyses of material property effects are also required. A great deal of finite element work has been performed on the analysis of compact tension specimens (primarily under static load) and good agreement between experiment and analysis has often been obtained. Why then, is this extreme crack tip sensitivity observed in the dynamic analyses performed for this work? Possibly, it results from the various circumstances involved such as dynamic load, deeply precracked specimens, type of analysis, finite element idealization, and material properties. Or, possibly, this phenomenon could be a less obvious source of error in other work involving less deeply cracked and statically loaded specimens having large scale plasticity.

SUMMARY AND CONCLUSIONS

A combined experimental and analytical research program has been described that was aimed at extending a static nonlinear fracture criterion, the J-integral, to inelastic dynamic fracture. Within this program, an experimental technique was developed by which standard compact tension J_{IC} specimens could be tested dynamically, and instrumentation techniques were developed which permitted measurement of fracture events that occurred within only milliseconds. Concurrently, nonlinear, dynamic finite element analyses were used in guiding the experimental work and in interpreting the experimental results. The work described was a pioneering effort spanning 4 years. We encountered many problems, particularly during the experimental phase, and our methods of dealing with these problems have been documented in detail.

The material chosen for the experimental program was 1-in.-thick HY-80 baseplate because of its known toughness and widespread use. Machined, precracked compact tension specimens were dynamically loaded by a weight dropped onto a special test fixture designed to load in the opening mode. A total of 26 steel specimens were dynamically tested (some repeatedly) to develop and prove required instrumentation and to measure an apparent critical value of the J-integral. Time to fracture was of the order of 1 ms or more. Three additional specimens were tested under standard conditions to establish the static value of J_{IC}.

The experimental program required that load and load point displacement (LPD) be measured on the specimens as a function of time. Due to the rapidity of the loading and deformation, load point displacement was particularly difficult to measure. The best system devised consisted of a transmitting-receiving photo-optic displacement sensor specially calibrated to account for rotation of the specimen about its apparent hinge point. This gave an LPD accuracy to within 10%. Load was more easily measured using conventional strain gages mounted on the loading clevis.

To determine the critical value of the J-integral, it was also necessary to observe the time, load, or LPD at which fracture initiation occurred. Various techniques were tried, but even the most promising (DC potential drop) could not be calibrated to reliably indicate fracture initiation. Because of the large plastic strains that develop near the crack tip before fracture, strain gages and "Krak" gages were also ineffective; they came unbonded from the specimen surface before the start of crack growth. As a result, a multiple specimen approach was adopted in which specimens were incrementally loaded up to and just beyond the point of fracture initiation. This yielded an "apparent J_{IC}" value, as calculated by conventional static formulas, of about 1000 in.-lb/in.^{2} for the HY-80 material under test. This compares to an average static value of 1110 in.-lb/in.^{2}.

The term "apparent J_{IC}" is used above for good reason. Plots of load versus LPD will differ, at a given value of load or displacement, under static and dynamic conditions. The additional load on a dynamically tested specimen at the same value of static displacement will depend on the rate of loading, and this will influence the value of the J-integral calculated from the experimental record. Nonetheless, direct use of the dynamic records has been adopted in the past[11,37] and is adopted here. As a consequence, the exact meaning of the fracture parameters calculated herein is presently unknown. This question is currently under active investigation by a number of well-known researchers.[34,35] Despite the uncertainty, however, the comparative fracture performance of different materials can be evaluated with the present experimental setup.

The finite element computations were an important part of this work, and led us to correctly question the accuracy of some of the early experimental data. Another motive for undertaking these calculations resulted from the experimental difficulty

AD-A155 472 DUCTILE FRACTURE OF DYNAMICALLY LOADED NAVAL STRUCTURES-COMPACT TENSION S..(U) DAVID W TAYLOR NAVAL SHIP RESEARCH AND DEVELOPMENT CENTER BET.. 2/2

UNCLASSIFIED E A RASMUSSEN ET AL. FEB 85 DTNSRDC/84/071 F/G 20/11 NL

END

FILMED

DTIC

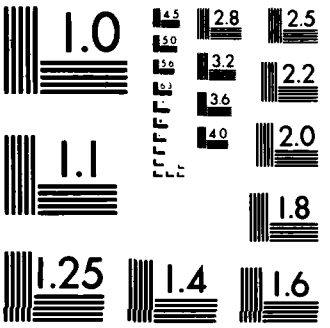

of detecting crack initiation. The thinking was that if one can closely model the experiment numerically, then any deviation between the experiment and the numerical model is due to crack extension, thus pinning down that event.

A complicating factor in the two-dimensional analysis of these specimens was the presence of side grooves designed to suppress the formation of shear lips. These were modeled by reducing the thickness of the elements in the side groove region and by reducing Young's modulus in this region in order to bring the finite element static-elastic compliance into agreement with accepted calibration formulas. The suitability of this model in the dynamic, elastic-plastic range, however, can be established only by comparison with fully three-dimensional solutions. The expense of such solutions precluded this check.

Another complicating question is whether a model of plane stress or plane strain is most appropriate for what is, in reality, a fully three-dimensional problem. Near the crack tip, plane strain is probably more appropriate, with plane stress preferred elsewhere. Neither assumption is exactly correct, but a plane stress model was assumed for all computations in this study.

Finally, it is very important to note that the accuracy of the finite element models was quite sensitive to assumptions for the stress-strain curve and the initial crack depth. We found that a 5% increase in assumed yield stress could decrease the maximum load point displacement by about 40%. This indicates that the effect of strain rate on yield stress should be incorporated into the analysis. We also found that, for these deeply cracked specimens, an error in the crack depth of less than 1% (i.e., an error of 0.01 in.) also could change the peak load point displacement by 40%. These unwanted sensitivities arise because of the extensive plasticity that develops in the specimens and because of the rapid change in (nonlinear) specimen compliance for small changes in crack depth. Because the crack front is rarely

perfectly straight, measuring crack depth precisely is difficult, which makes the sensitivity of peak displacement to this parameter particularly disturbing. This result implies that deeply cracked, highly nonlinear compact tension specimens are not the best choice for characterizing inelastic dynamic fracture in very ductile metals.

The purpose of this work was not to characterize materials, however, although the experimental techniques and analysis methods are certain to be of future use. Instead, we sought to determine if the fracture response of HY steels is significantly different under static and dynamic conditions. If so, the difference would have to be accounted for in the inelastic fracture analysis of full scale structures. This work gives the preliminary indication that at nominal strain rates of interest, the difference is not great enough to be significant. However, this conclusion must be qualified by noting that it is based on the assumption that the J-like fracture criterion derived here has roughly the same meaning as the *J-integral* under static conditions.

ACKNOWLEDGMENTS

A project such as this one, involving many innovative and critical experimental techniques, requires much support. The authors wish to acknowledge the contributions of some of the DTNSRDC personnel who were essential to the performance of this work. Thanks are due to Mr. E. Speaks, who dealt with many of the testing details, Mr. A. Chalk who handled the instrumentation and recording of test data, and to Mr. J. Sikora who performed the moirê fringe studies. For the analytical portion of this task, the ideas and comments of Ms. J. Carlberg were most helpful. Mr. John Gudas, of the DTNSRDC Ship Materials Engineering Department, provided the static J_{IC} values for the HY-80 plate used in this test program. We also wish to thank Mr. A. Wiggs for providing overall guidance during the course of this program.

APPENDIX

FURTHER INSTRUMENTATION DETAILS

MEASUREMENT OF LOAD POINT DISPLACEMENT

The sensor initially selected was a displacement measuring system series KD-2310 manufactured by Kaman Sciences. Its body was 1 1/8-in. long × 1/4-in. diameter and was mounted on the end of a small diameter cable. It was complete with a control module having provisions for adjusting the gain and linearity. According to specification, it had a frequency response from 0 to 50 kHz and a linear response to 55 mil (1 mil = 0.001 in.). It was a noncontact type transducer that operated on the eddy-current loss principal and could be used with any conducting material. Another advantage was that it indicated the average gap over the face of the probe. Thus, providing and maintaining a true parallel target surface was not essential.

One disadvantage of this sensor was that metal located to the side and rear of its face could influence the sensitivity. To reduce this effect, the sensor type having a stainless steel jacket was selected and calibrated in a mounting configuration similar to that used in the test, as recommended by the manufacturer. A micrometer fixture was used for calibrations.

The sensor was threaded through the top half of the specimen and targeted on the lower half; initially a spacer was bonded in the notch and the sensor was located flush with the bottom of the hole. This would protect the sensor if the notch closed during latter phases of the test. However, this problem did not develop, so the spacer was eliminated. Then the sensor was referenced directly on the bottom face of the notch. This alternate procedure helped eliminate the influence of surrounding metal, which we believed was causing sensitivity shifts.

After some actual tests, certain problems with the initially selected sensor began to emerge. The major problem was that, at fracture initiation, the specimen appeared to open more than anticipated, exceeding the linear travel of the sensor. As the testing progressed, this was confirmed by comparison with other instrumentation, and also by physical measurements taken after the test. In addition, the system seemed sensitive to movements of the sensor cable. This influence was reduced by affixing the cable and module to a long board, leaving about 2 ft free to extend to the sensor. Another disturbing problem was the shifting of the sensitivity for no apparent reason. Figure A.1 shows the setup and sensitivity for the sensor before using it in a test and the calibration immediately afterwards. Correlation was good up to about 25 mil, but beyond this, the sensitivity after the test increased nonlinearly. In comparison, the sensitivity before the test was linear up to approximately 55 mil. This particular test was at a moderate drop and, by using the pretest sensitivity, the diplacement was 52 mil. However, using the latter sensitivity, it would be 43.5 mil. This represents a variation of roughly 10% from the mean. This discrepancy was more extreme than was usually noticed, but it certainly diminished the confidence in the sensor. The combination of cable shifting and influence of surrounding metal, despite the precautions taken, probably caused this change. This same type sensor was used at position D2 and eventually at D2' (see Figure 7). The accuracy of the measurement at either of these positions was not critical, however, as will be discussed.

Because of the erratic performance and limitations of the eddy-current sensor, it became apparent that an alternative type was needed to measure the LPD. Thus, a basically different system was obtained on a temporary basis for evaluation, and eventually this system was purchased. As described in the text, this system was a

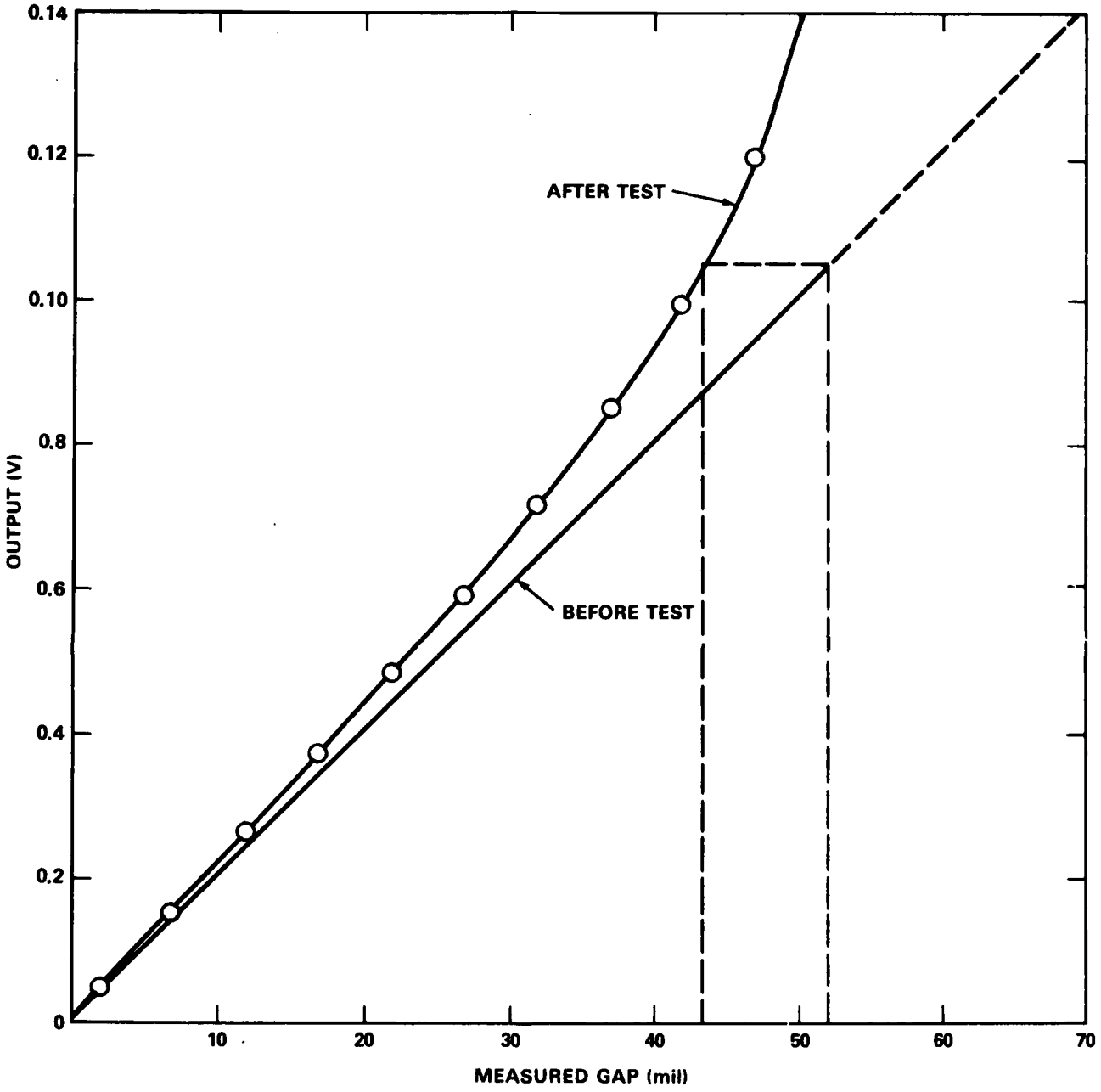

Figure A.1 - Sensitivity Change in LPD Sensor Before and After Use in Test

Fotonic sensor, series KD320 with a KDP109 CTI probe, manufactured by Mechanical Technology, Inc. The sensing probe contains two sets of fiber optic filaments. The system had a frequency response from DC to 125 kHz according to specifications. The probe was flexible except for a 6-in. steel jacket at the sensing end. The sensor had to approach from the side and enter the specimen from the top. For the first attempt the probe was custom configured to include a right-angle bend near the end so that with some care it could be adapted to the specimen. This arrangement was too susceptible to damage and, after consultation with the manufacturer, it was determined that the rigid section could be shortened and, after some machining operations to provide more clearance, the flexible cable could take the necessary bend. By using an adaptor this sensor was mounted in the same hole; it was targeted on the bottom of the notch.

During a test the specimen can be evisioned as hinging in the ligament section with the upper and lower halves counterrotating with respect to each other. For a realistic test the included angle from this rotation can approach 4^{o}. This means that target face does not remain perpendicular to the sensor and the impinging light from the surface would tend to be scattered during the test and influence the sensitivity. This factor, of course, must be considered during calibration and adjustment of the measuring system prior to use. The micrometer fixture again was used to adjust and calibrate the system, although a modification was incorporated to simulate this rotating effect (Figure A.2). Note the hinge installed in this fixture, which pivots with motion of the micrometer head. The length L corresponds to the distance between the sensor and the estimated hinge point in the specimen when loaded as computed from information in Reference 21. Figure A.3 shows a typical calibration curve. Note there are front slope and back slope operating regions.

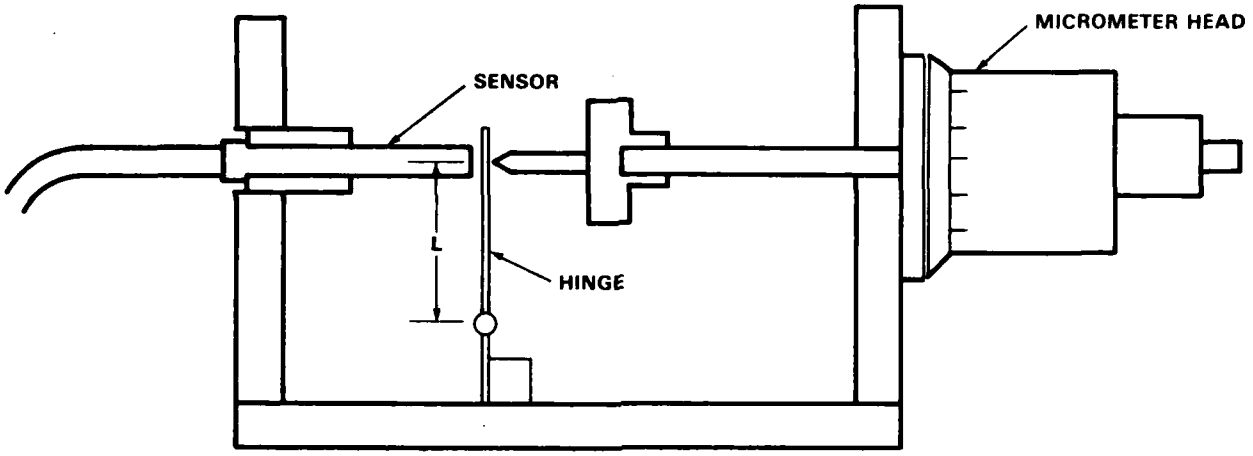

Figure A.2 - Procedure for Calibrating Fotonic Displacement Sensor

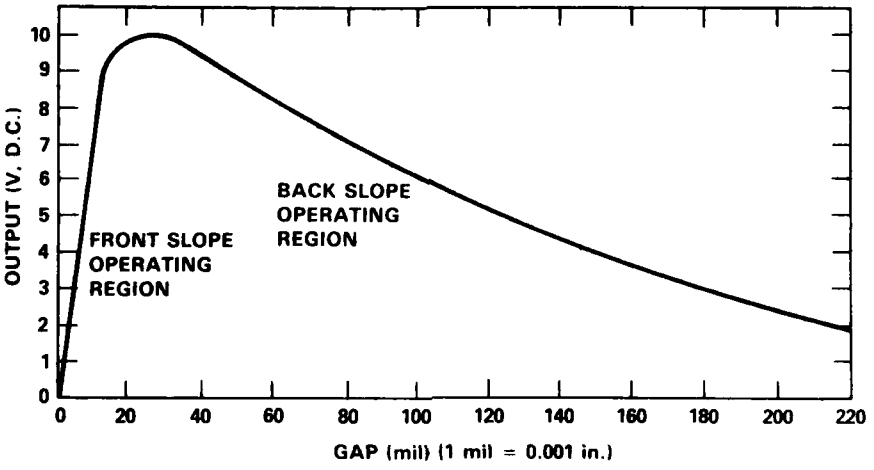

Figure A.3 - Typical Characteristics of the Fotonic Sensor

The rear slope would be used in situations such as these dynamic tests, where larger displacements are involved.

Different probe diameters and arrangements for the optical fibers influence the operating ranges. For this application it was necessary to use the smallest available probe (0.109-in. diameter) and, as a result, the available displacement range was sacrificed. The probe had a concentric fiber distribution where the transmitting fiber formed the inner core and the perceiving fibers the outer ring. This arrangement was chosen because it was less sensitive to the nonperpendicular target face. Figure A.4 shows a typical sensitivity curve for this sensor where the target face remains perpendicular to the sensor and a second curve where the target face is initially perpendicular and then rotates to match the situation in the test specimen. Note that the rotating target face affects the relationship, especially the sensitivity in the back slope region. Also, the sensitivity peaks at a different displacement for the two target face arrangements. To operate in the linear range of the back face slope region, an initial gap of 70 to 90 mil is required. Because of this and also because in the specimen the target face is initially perpendicular at the time of loading, an additional step is required to obtain a valid sensitivity. Repeated calibrations for different initial gaps indicated that 80 mil gave optimum useful range (Figure A.5). The sensitivity is calculated, and within the $\pm 5\%$ bounds, this calculated figure is valid for more than about 140 mil displacement. In practice, the sensor was therefore installed with an 80-mil gap and, through a control on the instrument, the light intensity was adjusted to give the corresponding output voltage. This adjustment was necessary to compensate for different remissivity between target surfaces. To minimize this effect, a highly reflective shim material was always bonded to the target face both during the calibration and the testing sequence.

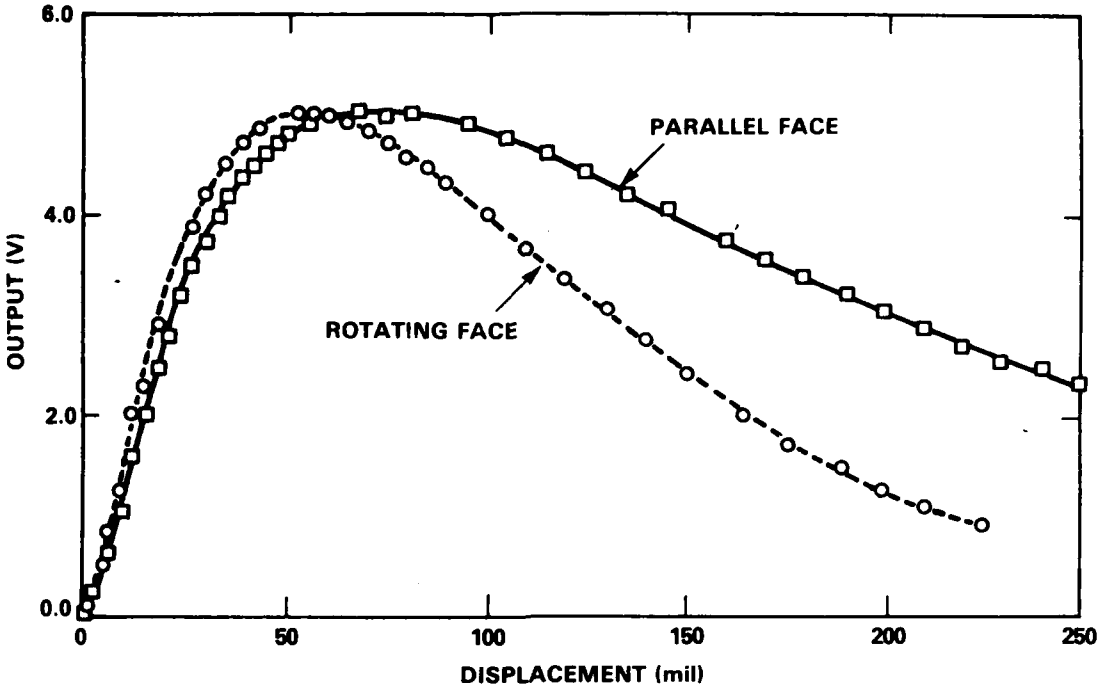

Figure A.4 - Fotonic Sensor Calibrations for Different Target Conditions

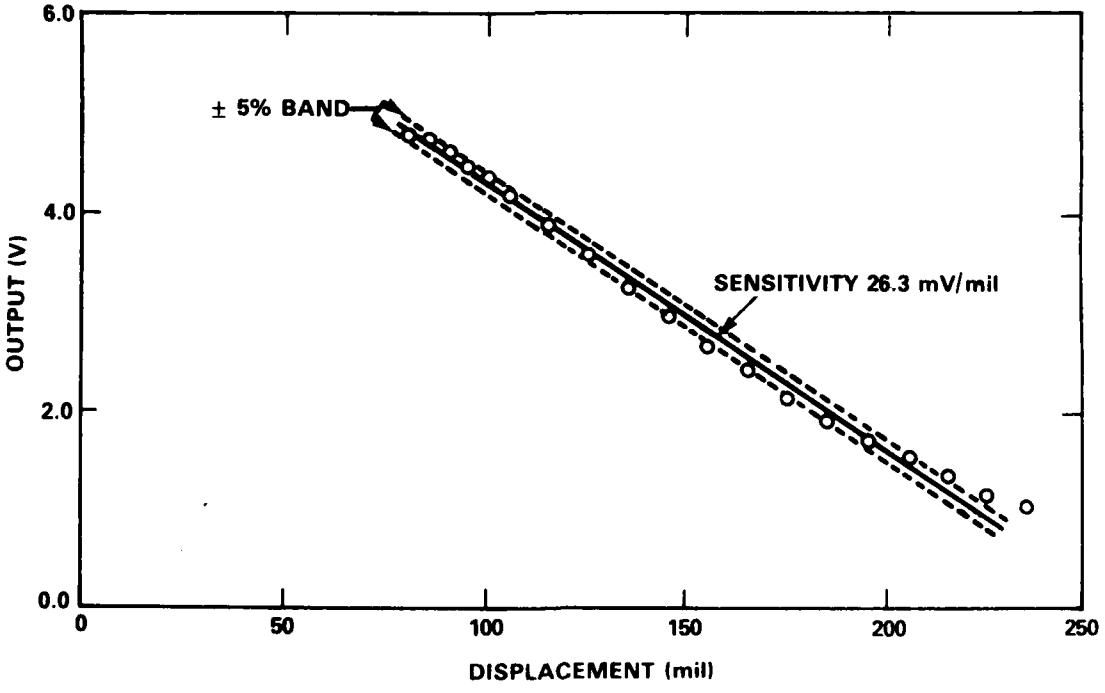

Figure A.5 - Sensitivity of Fotonic Sensor for Simulated Test Condition

To evaluate the Fotonic sensor under actual tests, a third tranducer was added to the specimen and was also recorded during several runs. This additional sensor was a linear variable differential transformer, LVDT; it was epoxied to the front face and also measured the displacement. To compare results, we again assumed that the specimen hinges in the ligament about a calculated center of rotation. Reference 21 discusses how this rotation point can be determined. It states that for an elastic strain at the crack tip this rotation would occur at a point 10% through the ligament from the crack tip and for a large amount of plasticity at roughly 33% of the ligament length. The displacement magnitudes indicated by each sensor would be proportioned to its distance from the center of rotation along a base line. In Figure A.6 the results from these three sensors are plotted at corresponding locations for two different static loads on one specimen and for an actual drop test on a second specimen. Note that for the static test the correlation was very good, but for the impact test the Fotonic sensor was 8% higher than expected. In Figure A.6b the displacements observed after the test (set values) are shown and the correlation between the three sensors is good. This certifies that the sensitivities for the sensors were correct. Thus this 8% disparity in the test values is difficult to explain. It cannot be attributed to nonlinearity because the calibration curves show a constant relationship over this range. Based on this study, as well as many similar cross checks made between the displacements thoughout the test, it appears that the LPD measurement using the Fotonic sensor can be considered accurate to within 10%.

CRACK INITIATION

The next section is devoted to the various procedures attempted to detect crack initiation. A crack would be expected to initiate at midthickness and this was a

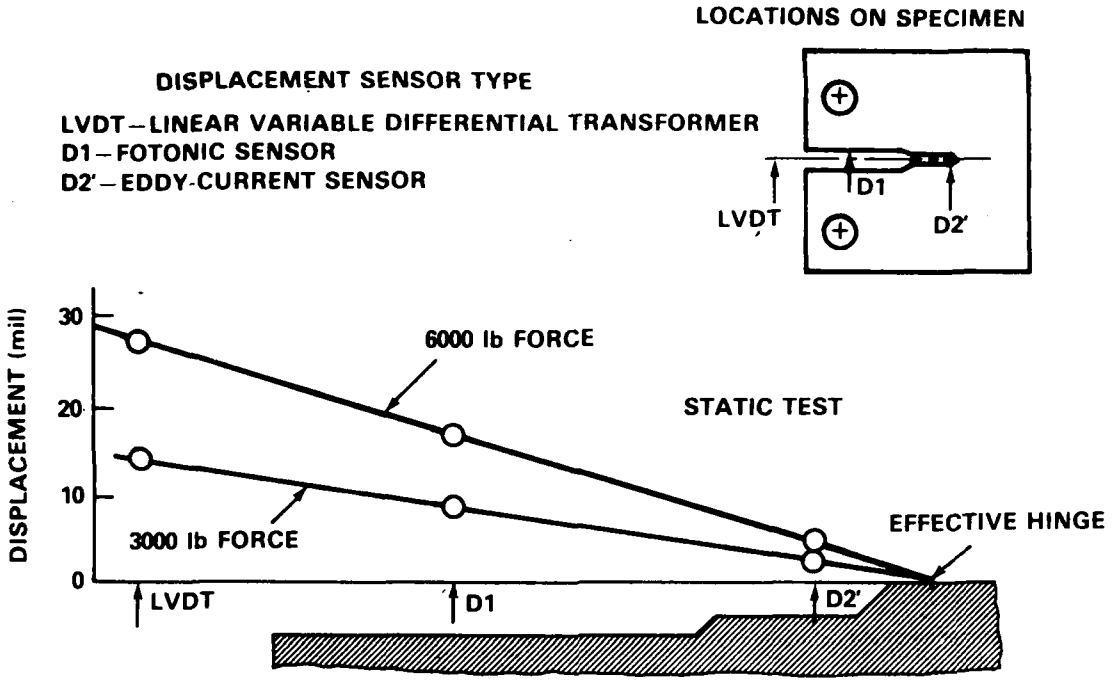

Figure A.6a - Displacement Measured Under Static Load

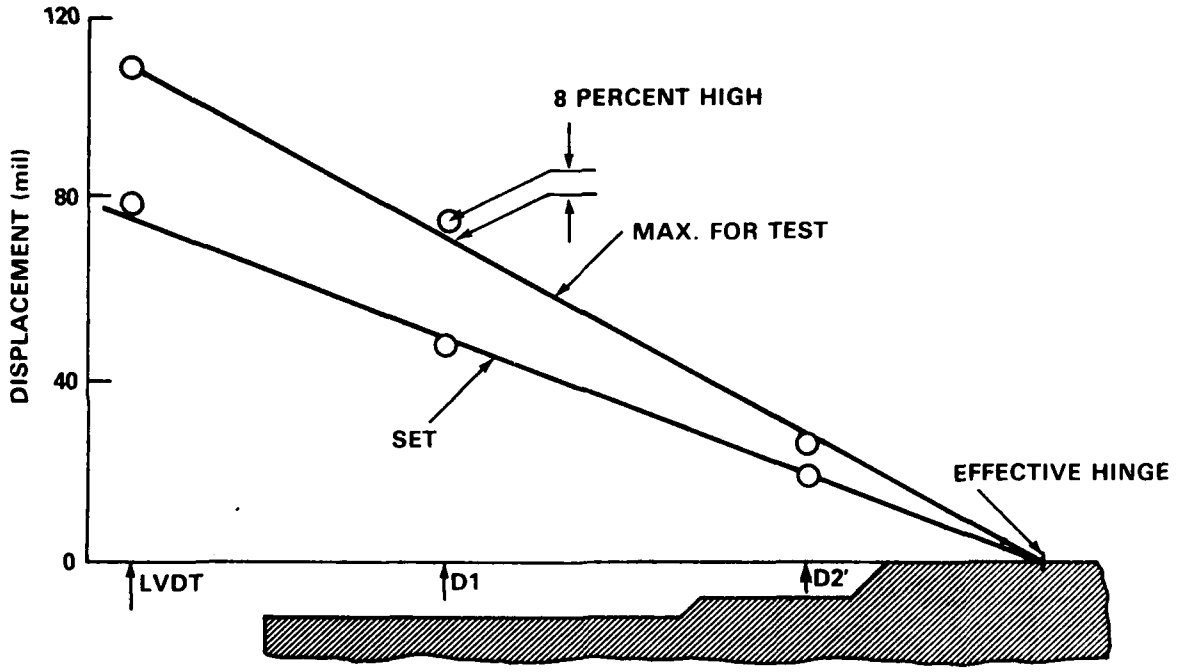

Figure A.6b - Peak Readings and Set Displacements from Actual Tests

Figure A.6 - Validation of Fotonic Sensor Used for LPD Measurement

consideration in the original plans. At first we used an eddy-current sensor identical to the one discussed earlier in connection with the LPD measurement. It was threaded into a blind hole from the top of the specimen into the ligament section. This sensor, designated D2, targeted the bottom of the hole ahead of the crack front; Figure A.7 shows this location and also the method by which we hoped to detect the crack initiation. This ligament displacement, LD, and the LPD are taken from the record and plotted at corresponding time increments. A sudden change in the slope would indicate the onset of fracture. After several tests we concluded that the ligament gage was insensitive to crack initiation and any significant response occurred only when the crack actually reached the sensor; this was evident from inspection of the specimen, from time relations, as well as from the magnitude of the measurement. Figure A.8 is a continuous record of the applied load, the load point displacement, and the ligament displacement recorded during a test. Note that there is no signal on the LD trace until nearly 5 ms, after which the displacement steadily increases and peaks at roughly 25 mil in another 5 ms. Visual inspection revealed that the crack in the specimen obviously had extended beyond the sensor, accounting for this large displacement. Attempts to shift the ligament gage closer to the crack tip for more sensitivity were unsuccessful. There was concern that the sensor mounting hole, if located closer to the crack tip, would cause premature fracture, and therefore the approach was changed. Instead of being placed in the ligament the sensor was located at the root of the machined notch and targeted on the lower face. Figure A.9 shows results for this configuration from two tests where it was evident from examination that both specimens had cracked. Slope did not change definitively even though fracture occurred.

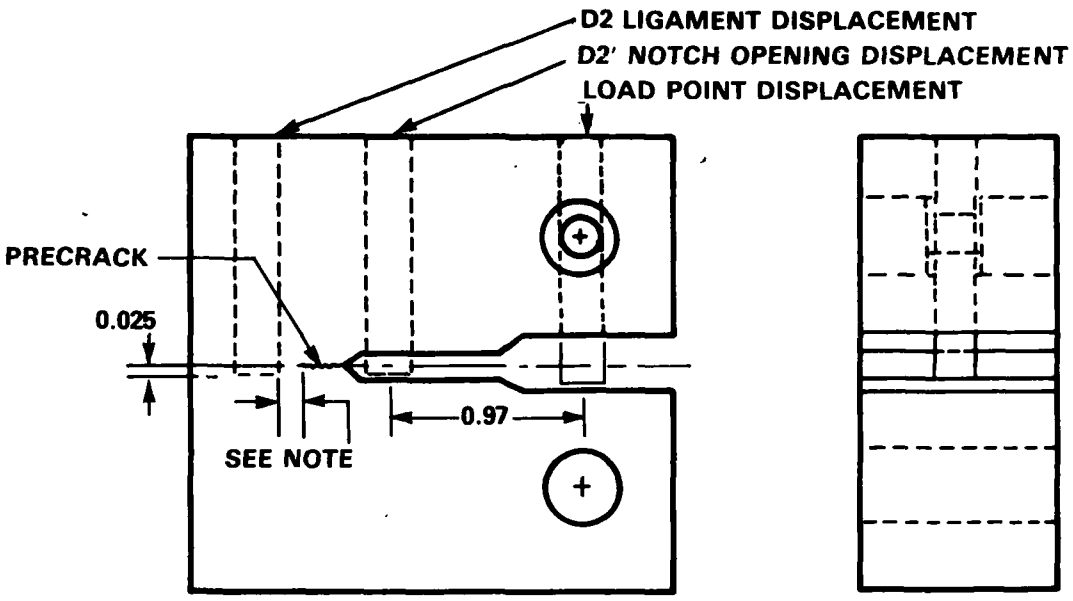

NOTE: DISTANCE VARIED FROM 3/32 TO 1/8 in.

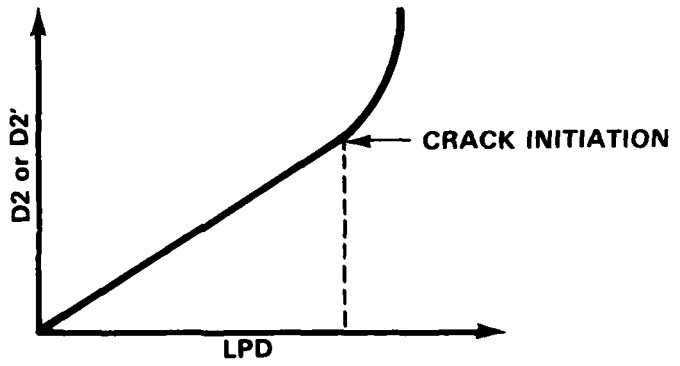

DATA PLOTTED AT CORRESPONDING TIME INCREMENTS

Figure A.7 - Initial Method for Determination of *Crack Initiation*

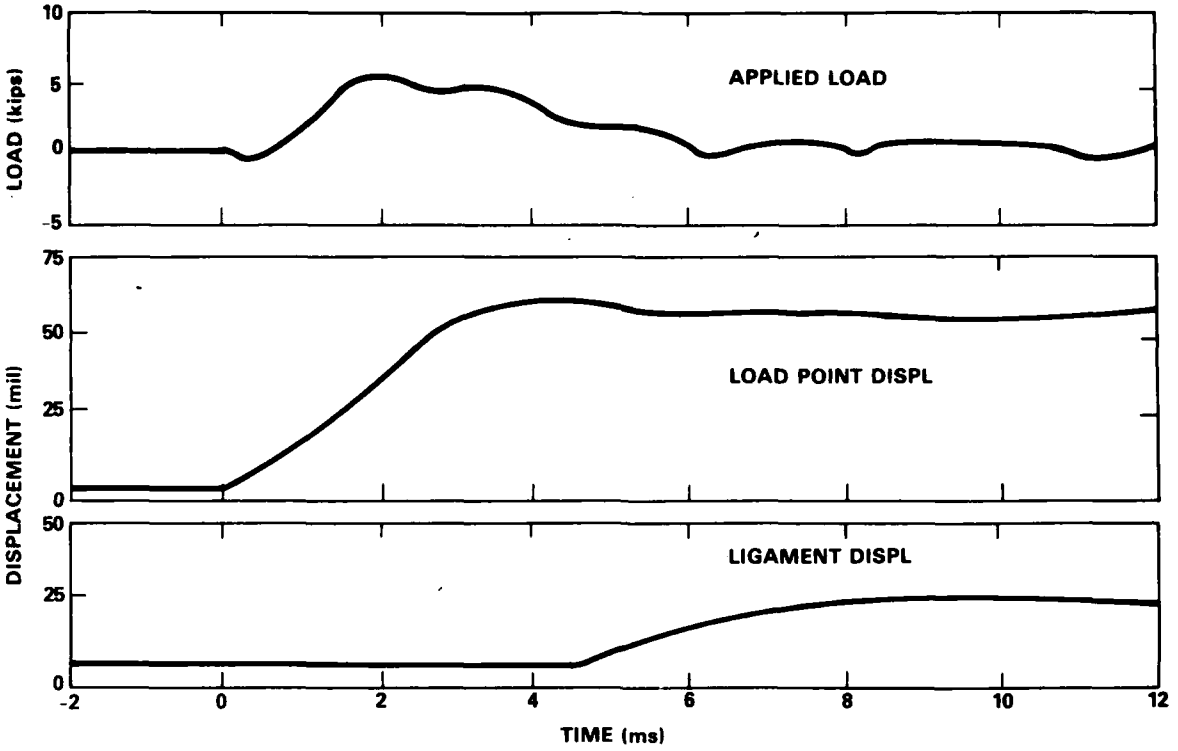

Figure A.8 - Attempt to Measure Crack Initiation with Sensor Located in Ligament

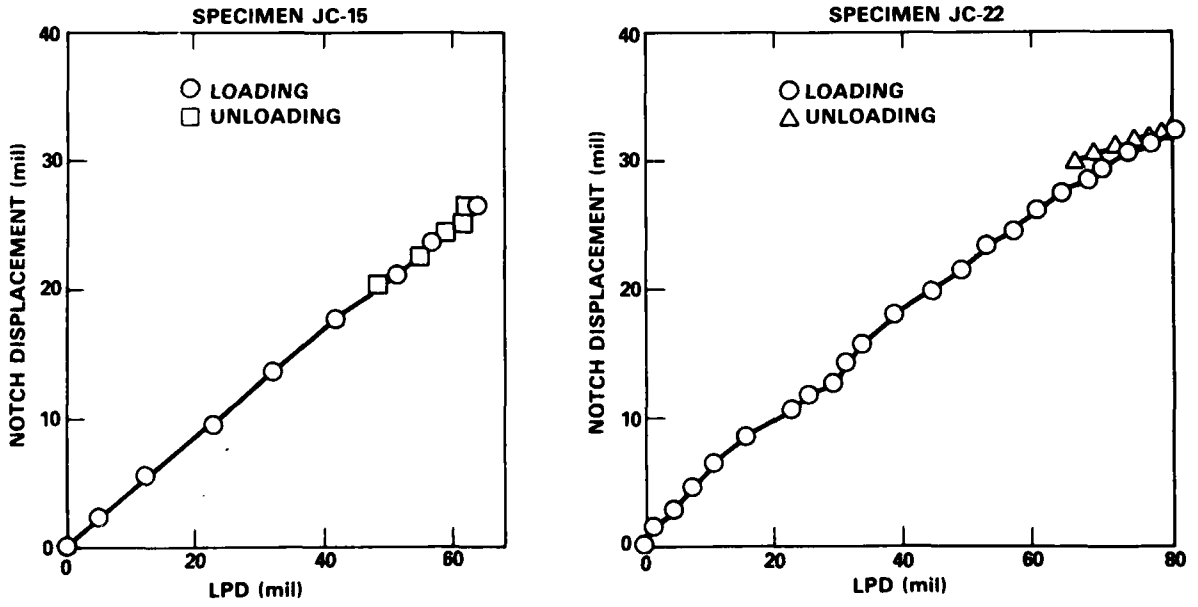

Figure A.9 - Attempts to Measure Crack Initiation with Sensor Located in Notch

At this point the emphasis was shifted to evaluation of a number of different procedures; they included using crack detection and crack propagation gages, moiré fringes, and finally the potential difference (PD) method.

A number of different types of gages were bonded to the sides of the specimen in the vicinity of the crack, as shown in Figure 10 of the main text. At the very beginning of this test program, a bonded gage was tried briefly with the idea of providing supplemental data; see Figure 10a. This was a crack propagation gage and consisted of a pattern of resistance strands connected in parallel. It was bonded with the strands running normal to the crack front. Progression of the crack causes successive interruptions of the strands, accompanied by an increase in resistance. With proper circuitry, this change is recorded as discrete steps from which the crack front can be tracked. After tests on the first specimen it was observed that strands had broken ahead of where the crack terminated and there was no further use of this gage type.

When work was resumed using bondable gages, several specimens were prepared with a small strain gage installed on the side faces in the vicinity of the crack tip. This was attempted both with the side surfaces flat and with the wide side grooves. The thought was that with this gage in close proximity to the crack tip, there would be a strain release at crack initiation which would be evident on the record. Figures 10b and 10c show the layout for these bonded strain gages. Another procedure using "Krak" gages was also tried in an effort to detect crack initiation. Figure 10d shows the installation arrangement where the gage was placed directly over the crack tip to follow the fracture propagation in the specimen. This gage consisted of conducting foil on a thin backing material. It was bonded using conventional material and techniques and it operated in a Wheatstone bridge fashion using a constant current excitation.

It soon became evident that bonded gages were not satisfactory; they almost invariably came loose during the test. The data showed this problem, and some gages were actually visibly separated from the specimen. Figure A.10 shows records from a strain gage and a "Krak" gage located on opposite sides of the specimen along with the applied load taken during a test. In this paricular test the specimen did not fracture, although there is a sudden jump in each trace. Note also that for the crack gage the signal occurs early in the event when the load is roughly one-half the peak value, nearly 1 ms ahead of the strain gage. Both gages obviously came unbonded. In some cases there was evidence that the strain gages did not always come loose. For example, Figure A.11 shows results for a strain gage bonded in each groove. This specimen did not crack and there is no sudden shift in the signal (perfect correlation). However, Figure A.12 is a similarly prepared specimen where crack initiation occurred, and this shows an entirely different problem. One gage showed a sudden unloading while the other did not and was obviously insensitive to crack initiation. Thus it was apparent from this work that bonded strain gages were not a solution. They were either insensitive or they came unbonded and gave meaningless data.

A number of other problems were noticed with the "Krak" gages, several of which also substantiated this bonding difficulty. These gages were installed after the specimen had been precracked, and therefore the specimen had to be exercised for several cycles to produce a corresponding crack in the gage. In a number of cases it was apparent that the crack in the gage was not following the crack in the specimen, and in fact the gage had come loose near the crack tip. In one case the gage came unbonded during the initial loading without a crack even starting. When bonding problems were detected the gages were replaced until installation seemed to

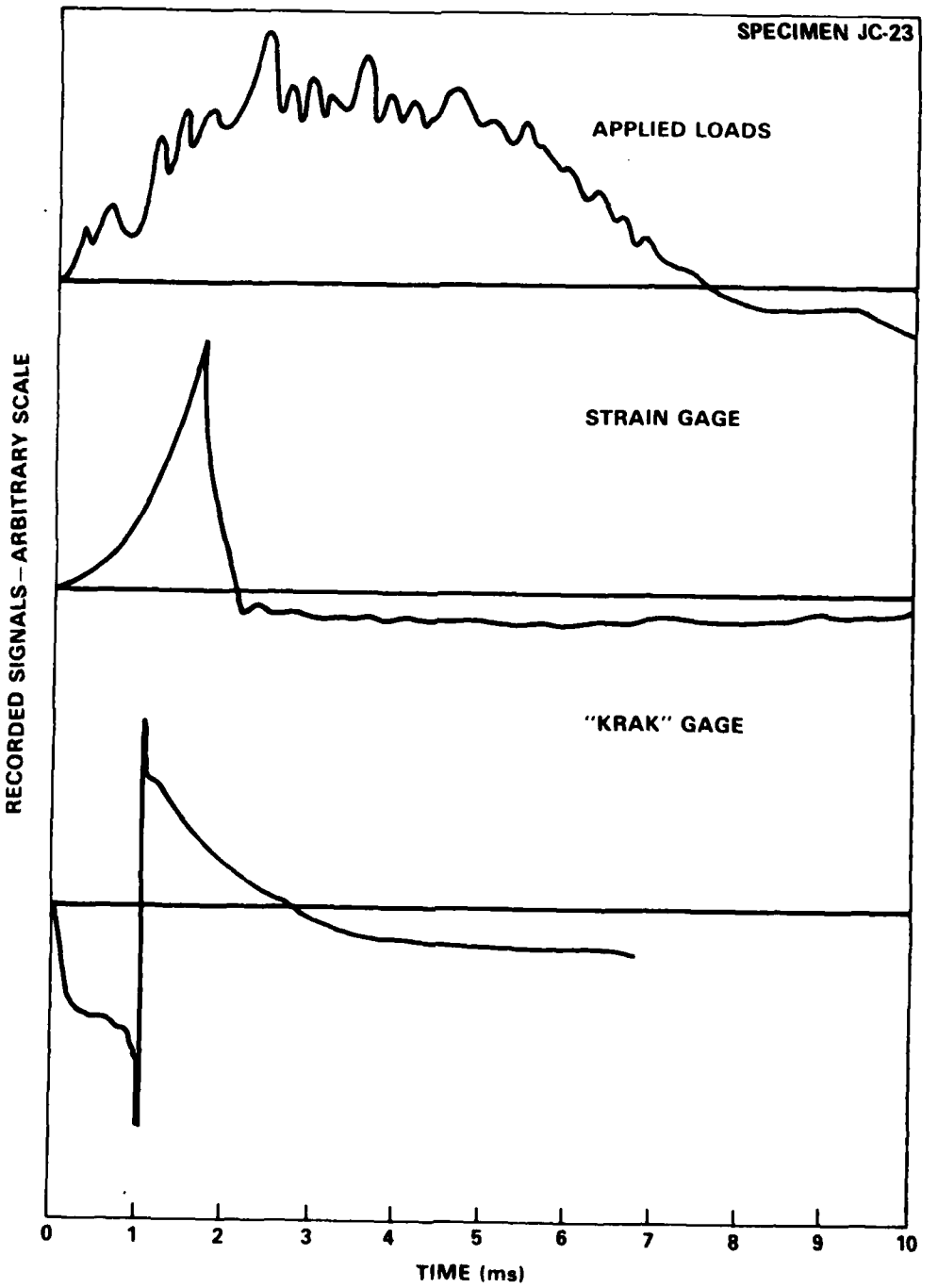

Figure A.10 - Example Showing Erroneous Indication by Crack Detection Gages (No Crack Extension)

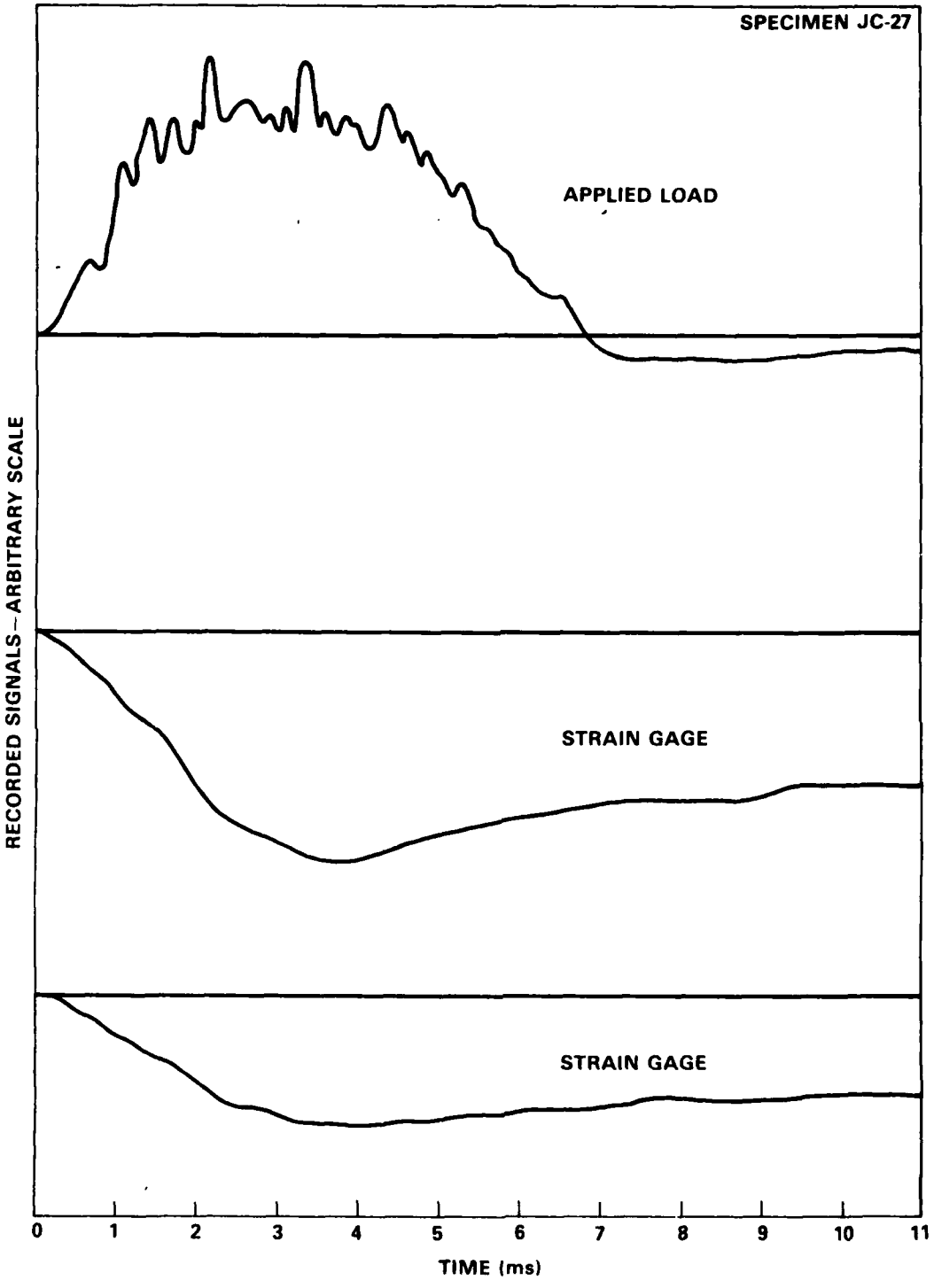

Figure A.11 - Example Showing Good Correlation Between Crack Detection Gages (No Crack Extension)

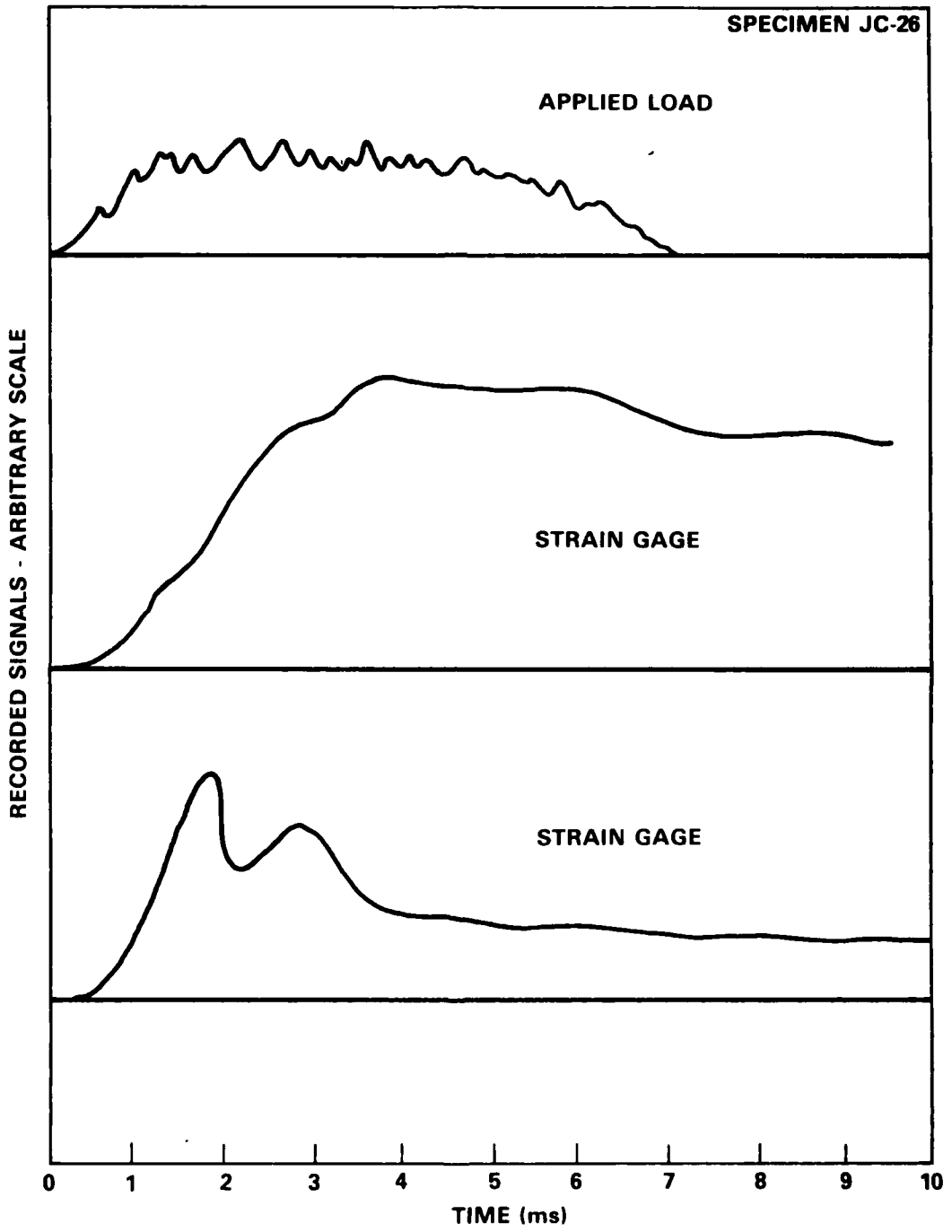

Figure A.12 - Example Showing Discrepency Between Crack Detection Gages (Crack Extension Measured in Specimen)

be satisfactory. For installation the gages were fitted into the groove, which seemed to compound the problem, as there was tendency for the gage to separate over a wide area. Another problem was the tendency during installation for the gage to open and lose continuity in the narrow sections where the gage wraps over the outside corner of the specimen, even though rather large radii had been ground at these locations. A smaller gage which essentially fit into the groove was subsequently used to solve this problem. The original gages had a 10 mm useful length. The smaller gage had a 5-mm length, which was adequate, but it had to be more carefully placed. Another difficulty was that once the crack developed and the load was removed, the gage actually closed so that electical conduction was restored and indicated no crack growth. Figure A.13 shows results from two instrumented specimens that had previously been exercised to produce cracks in the gages. The gages were monitored as the load was applied; note that a load of roughly 800 lb was required before the gages were fully opened to indicate the true crack length. In an attempt to offset this effect, two specimens were held under a compressive preload while the gages were installed. Based on compliance relations, this preload was roughly 1000 lb. Still, after the gages had been exercised, they also effectively closed when the load was dropped. A high gain in the recording channel was desired in order to detect crack initiation, but this was not possible without special equipment to suppress this significantly larger precrack signal. Therefore, the choice was made to separate the crack faces by raking the gage with a small scribe. This was done with the aid of a microscope and the gage was monitored so that the final indication observed during the exercising process was obtained. This procedure was tedious; furthermore, the possibility of precisely matching the crack was questionable. In the end it was apparent that crack gages were <u>not</u> a viable solution for detecting crack initiation in this application.

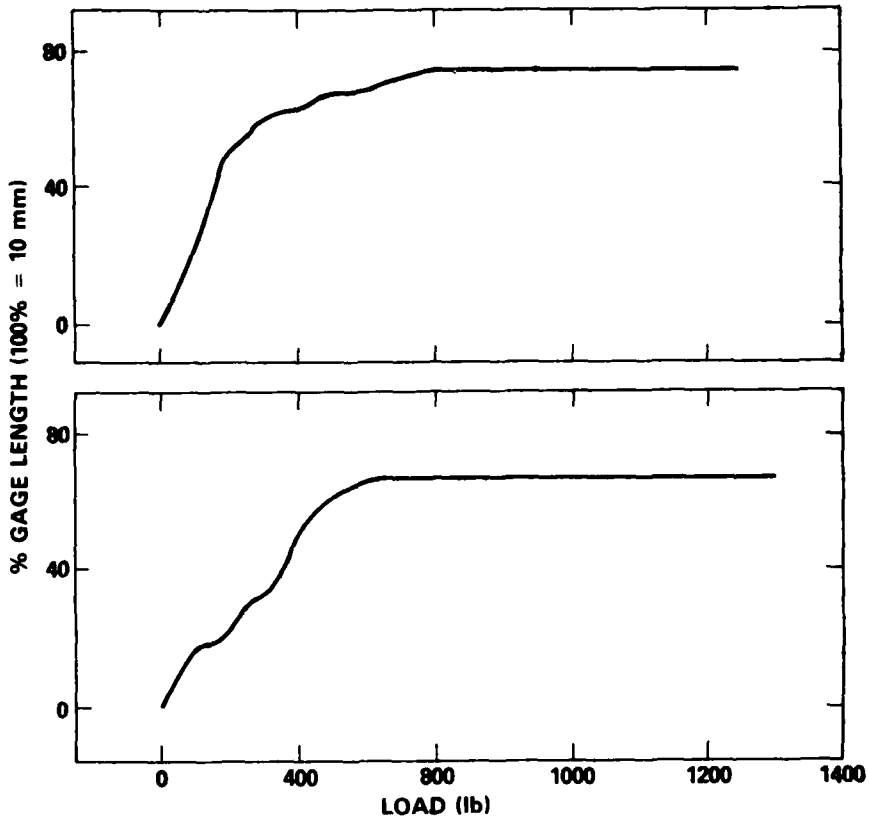

Figure A.13 - Load Required to Open "Krak" Gage After Precracking

The moiré fringe technique was used briefly with the idea that strains as well as crack initiation could be detected. This method uses an optical effect caused by a grid that is distorted along with the surface and interacts with a second stationary grid. In this application one grid is cemented over the crack tip section of the specimen and the second grid overlaid and supported separately; they are referred to as the working and the master grid, repsectively. These grids consist of unidirectional lines; as the specimen distorts, the superposition causes interference and moiré fringes appear. If no other influence is present, these

fringes represent a map of the strains in the direction perpendicular to the lines in the master grid. The magnitude for these strains can be determined from

$$\varepsilon = P/d$$

where ε is the strain, P is the spacing for the master grid and d the distance between observed fringes. The spacing for the master grid was 200 lines/in. and 5% was taken as a resonable strain at the crack tip. This strain would produce fringes 0.01 in. apart. Thus this approach seemed suitable for measuring the plastic strain around a crack tip. High speed 16-mm films were taken of these fringes during some tests. High intensity flood lamps were used, and by forcing the developing process, films of reasonable clarity were obtained, but resolution was not good enough to give all the desired information. Fringes were observed but they were related to another phenomenon more dominate than that associated with tip strains. The specimen halfs tend to counterrotate as two sections due to the bending moment at the time of loading. Fringe patterns consisting of a series of continous parallel lines are developed as a result of this rotation. In Figure A.14 are two enlargements obtained from the 16-mm film showing the zero time and this fully developed condition. The distance between the fringes, d, is related to this angle of rotation, θ, by

$$d = \frac{P}{2(\sin \theta/2)}$$

A typical value for the included angle of rotation is 4^{o} and where P = 0.005 (200 lines/in.) the value of d would be 0.14 in. This is an order of magnitude greater than the separation expected at the crack tip, thus overwhelming the fringe pattern. A time study was made of this angle for some specimens. Through geometrical relations, the angle was transformed into displacement for correlation with the

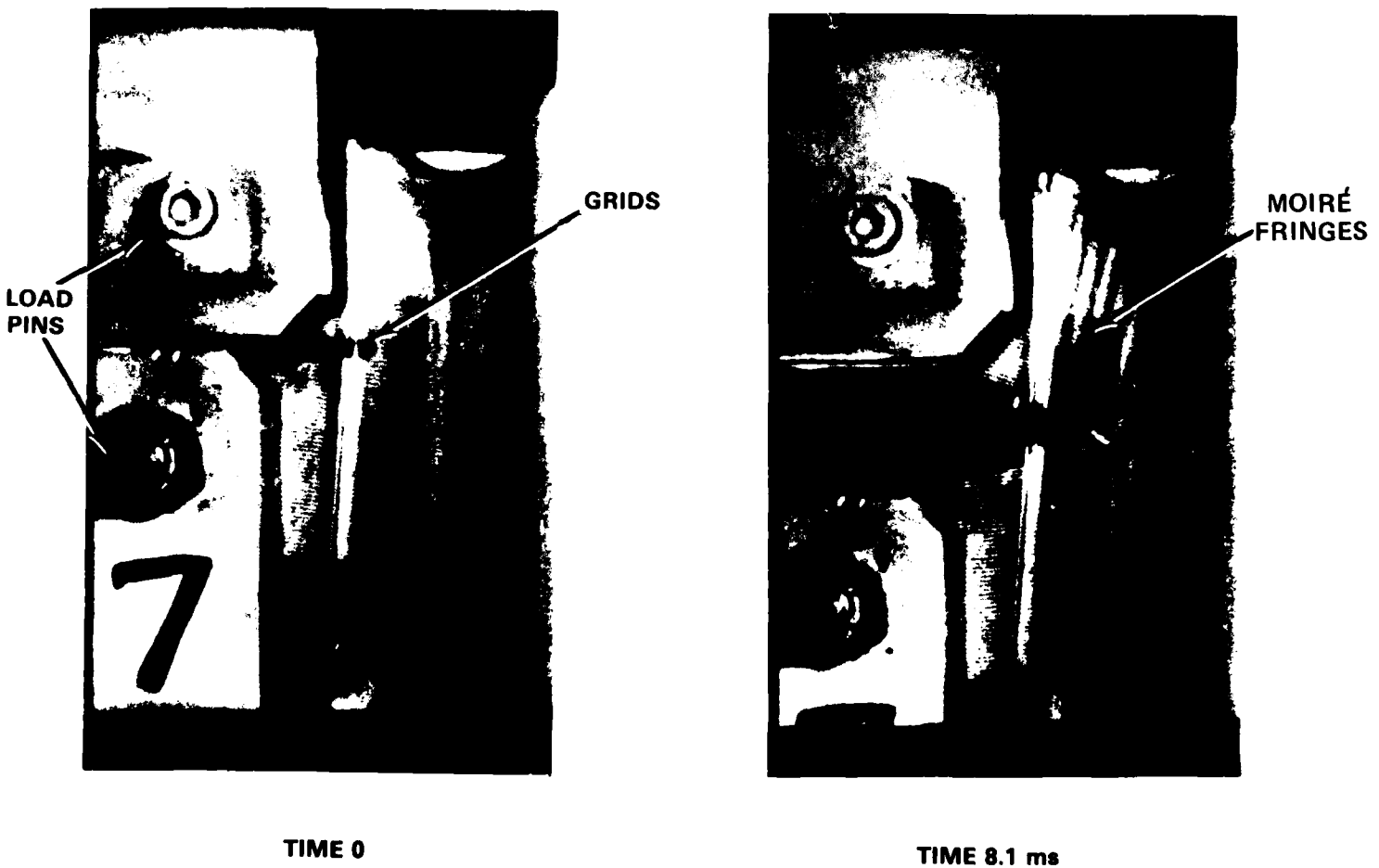

Figure A.14 - Moiré Fringes Produced During a Severe Specimen Test

measured load point value; see Figure A.15 for typical results. In this figure the LPD measured by the instrumentation is compared with results from the high speed film that included the moiré grid conversion and the direct measurements. The values from the instrumentation and directly from the film are comparable, considering that the magnitude is in the range where the accuracy of the eddy current sensor is suspect (see Figure A.1). The displacement from the moiré fringe pattern is roughly 17% low. This discrepancy is probably due to the inaccuracy of reading the spacing of the fringe because of poor contrast and broad lines on the image (see Figure A.14).

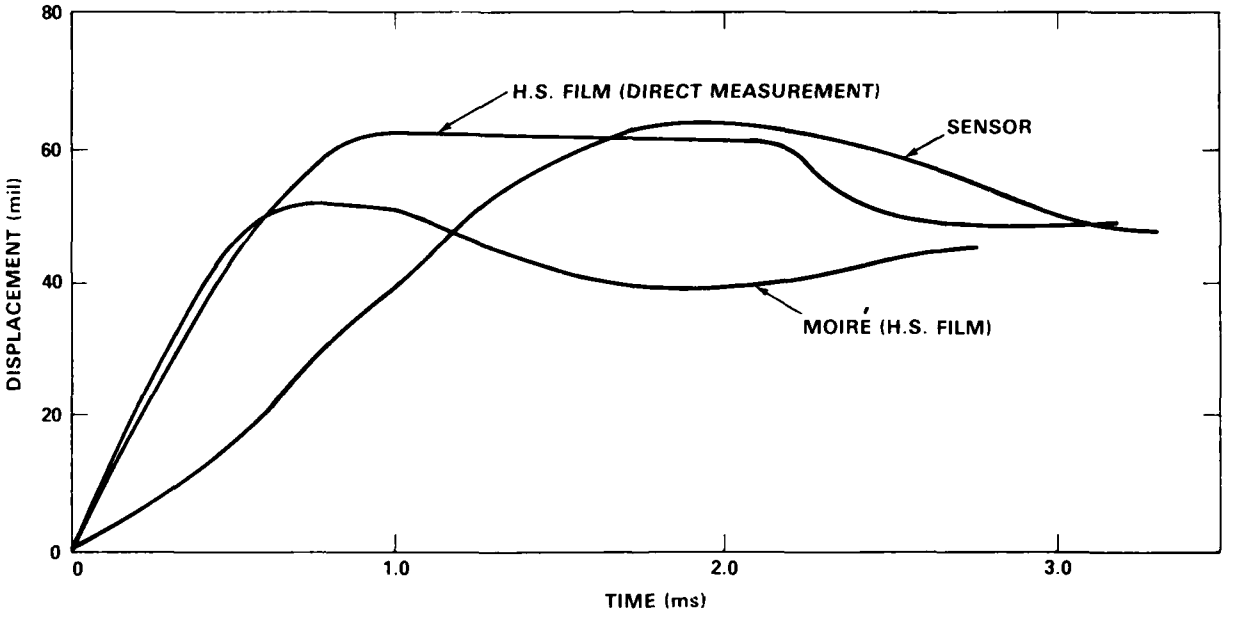

Figure A.15 - Comparison of Measurements from High Speed Film and LPD Sensor for Specimen JC-15

The potential difference, PD, was the final method tried in the effort to detect crack initiation. This technique relies upon the increase of resistance as the cross-sectional area decreases as in the case for crack growth in the CT specimen. A direct current is passed through the specimen to produce a potential related to

this uncracked area. Crack initiation would of course be indicated when the potential exceeds the final level observed during precracking.

In Reference 22, an analytical solution was derived to express the PD through a thin bar type specimen containing a small crack (a machined slot in this case). By solving Laplace equations for initial conditions and using conformal mapping procedures the potential distribution for this bar is

$$\frac{V_a}{V_{a_o}} = \frac{\cosh^{-1}\left(\frac{\cosh \pi Y/W}{\cos \pi a/W}\right)}{\cosh^{-1}\left(\frac{\cosh \pi Y/W}{\cos \pi a_o/W}\right)}$$

where V is the potential difference between two points on the specimen center line spaced a distance Y on either side of the crack, a_o is the initial crack length and a, the length after growth. Solutions have been expanded to cover more complex sections and results have been confirmed experimentally. The CT specimen is too geometrically complex for a similar approach but numerical solutions using finite element methods have been successful and results have been confirmed experimentally (Reference 24). In the experimental work, the length, a, was simulated by saw-cutting the specimen in incremental steps and measuring the corresponding potential change. Reference 22 showed that the attachment position for the probes has a large effect on the sensitivity of the signal. Following these guides, the potential probes were located directly across the plane of the crack, because this location produces a relatively high potential change with crack growth. To determine the influence of the current probes on sensitivity, some preliminary work was done where two different locations on the top and bottom surfaces were investigated (see Figure 11). Ring lugs were soldered to the ends of the cables and connections were made with screws that were threaded into the specimen. A block diagram of the circuit

used in this testing is shown in Figure A.16. The PD characteristic was observed during the fatigue cracking of a number of specimens. Compliances were measured during this operation, and by use of the empirical relations described in Reference 25 the crack growth could be determined. In Figure A.17 the voltage observed periodically at peak load and the normalized crack growth are plotted for two specimens, with the current probes located at the two different positions shown in Figure 11. Note that the voltage differed by a factor ranging from 2.2 to 2.0 when the probes were located 1-1/2 in. rather than 1/4 in. from the back edge of the specimen. On another specimen, which was already precracked, this influence was determined by shifting these connections between the two locations. The specimen was installed in the fixture but there was no applied load at the time of the readings. The voltage was greater by a factor of 2.1 to 1, which agrees with this earlier observation. In Figure A.18a the potential difference is plotted against the crack growth obtained during precracking where the current probes were located 1-1/2 in. from the back edge of the specimen. Both parameters have been normalized to the initial potential and the width of the specimen, respectively. For comparison, similar experimental results taken from Reference 24 are also shown. At the bottom of the figure the dimensions for these two specimens are compared. Note they are very similar except for the notch depth, and this accounts for the two different a/W realms in the plot. Both studies show similarity in that the potential varies exponentially. Where the a/W ratios coincide, you might expect the slopes to agree; however, note that the curve from the present data is somewhat steeper. This may be attributed to a number of factors, primarily the connection points for the input current (compare Figures 11 and A.18b for details). The test fixture characteristics can also affect this sensitivity, as it provides a parallel electrical path.

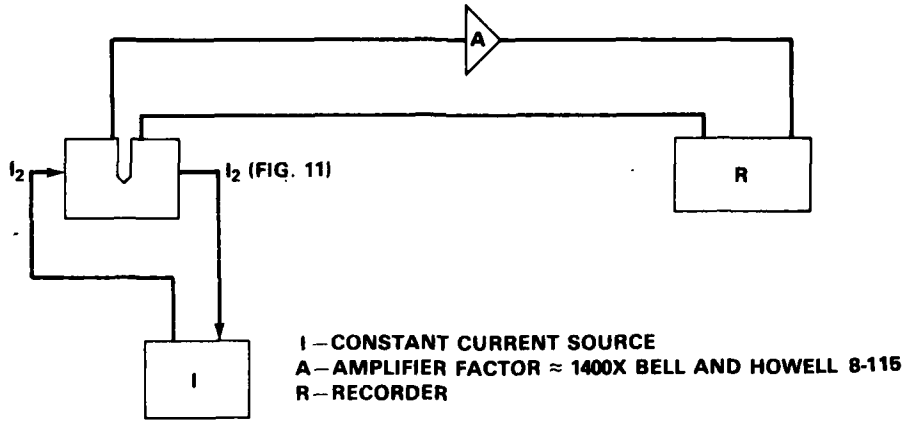

Figure A.16 - Circuitry for Potential Difference Measurements

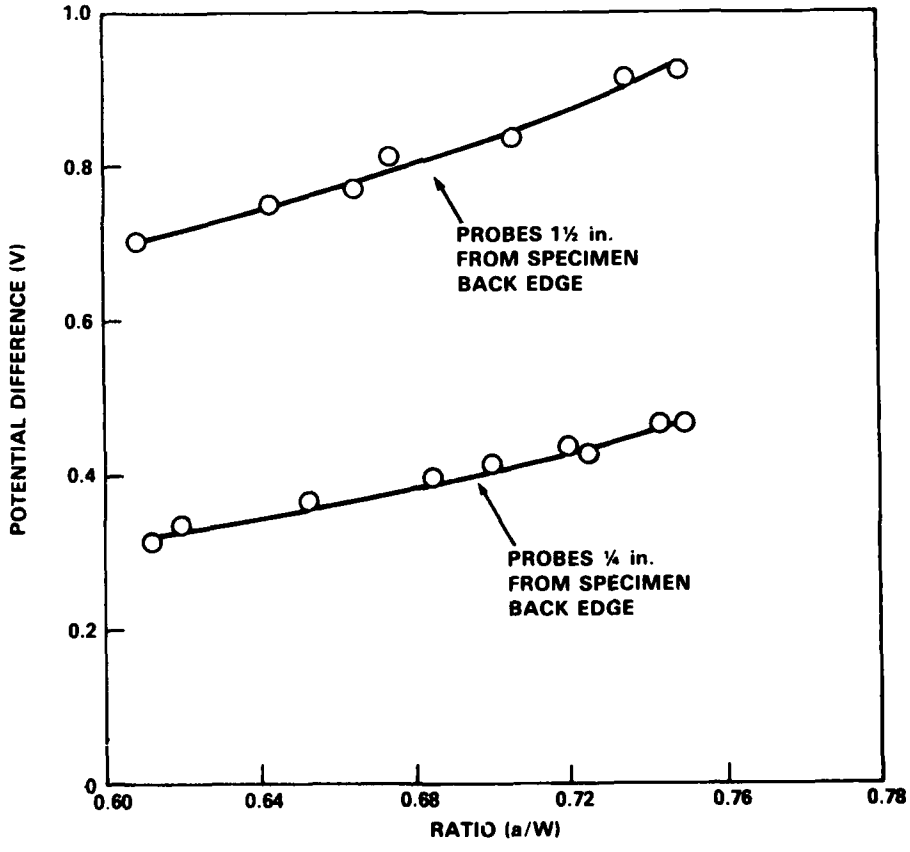

Figure A.17 - Effects of Current Probe Location on Output Voltage

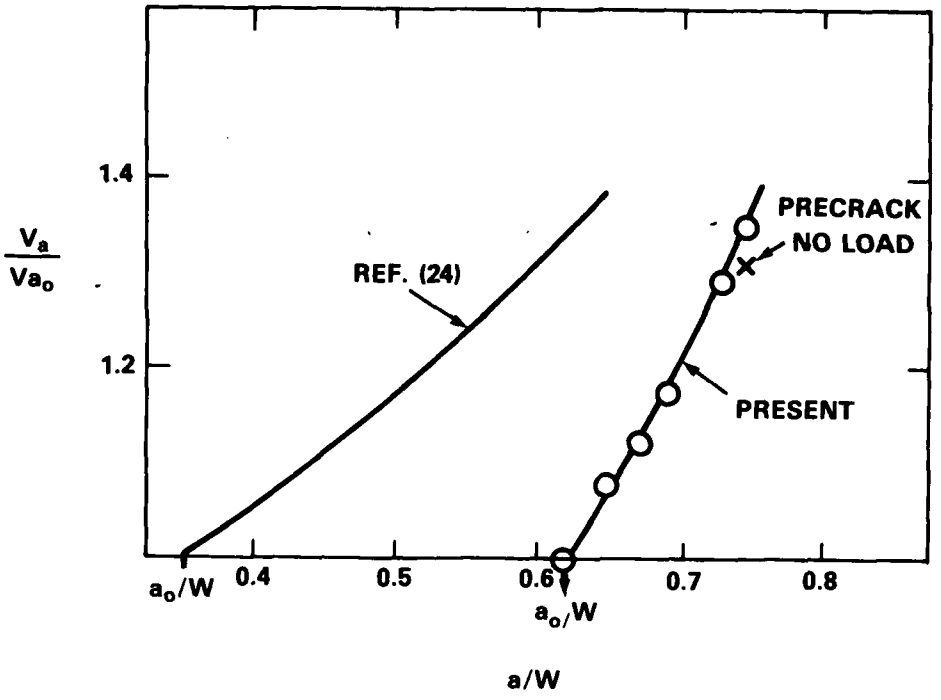

Figure A.18a - Comparison of Present and Referenced Data

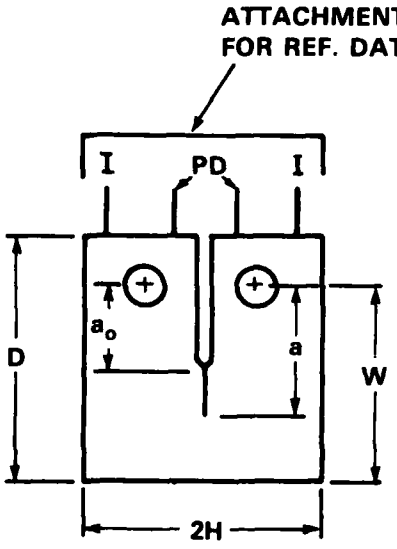

DIMENSIONS, in.:

SYMBOL	REF.	PRESENT
W	1.97	2.00
a_o	0.69	1.25
2H	2.36	2.40
D	2.46	2.50

Figure A.18b - Comparison of Dimensions

Figure A.18 - Specimen Potential Drop Characteristics for Present Test and Referenced Results

Another was that, once the specimen was precracked and the load dropped, the crack faces in general did not make perfect electrical contact, and in some cases, there was little difference in the potential between the peak cyclic load and no load. Of nine specimens tested, eight showed a drop of less than 7%. Halliday and Beevers[23] discussed this crack face contact problem and inconsistencies in behavior during cyclic loads. These same authors caution that this method may be less accurate when a very irregular crack front is present or where there is elastic and plastic crack tip deformation, which in these particular tests is significant.

Since the effects of the crack face closure varied among specimens, the plan was to observe the potential at the final precrack load, and then, during the actual test, assume that fracture occurred when this potential was exceeded. Figure A.19 shows actual signatures obtained from two tested specimens to date, namely JC-31 and 32. The basic difference between the tests was that JC-31 was tested at a 10-in. and JC-32 at a 12-in. drop. Note that their general appearance is similar; there is initially a very large negative signal (actually overloading the recorder) followed by a positive phase. Based on the previous static and fatigue work, there is no reasonable explanation for the large negative peak. In Figure A.20 this PD trace is shown, along with the corresponding load history for the drop tests on JC-32. The approach was to disregard this negative peak and, based on fatigue data assume that crack initiation essentially occurs when the trace becomes positive (or roughly 5 mV). This occurs at about 5.8 ms, at about the time that the applied load begins to drop off, which provides some indication that these data are reasonable. Note in Figure A.19 that for specimen JC-31 the signal becomes positive at roughly 2.9 ms. The applied load was not determined, unfortunately, due to faulty circuitry. However, specimen JC-27 was tested at similar conditions and the applied load for that test is combined with the PD signature in Figure A.21. Again, crack initiation is

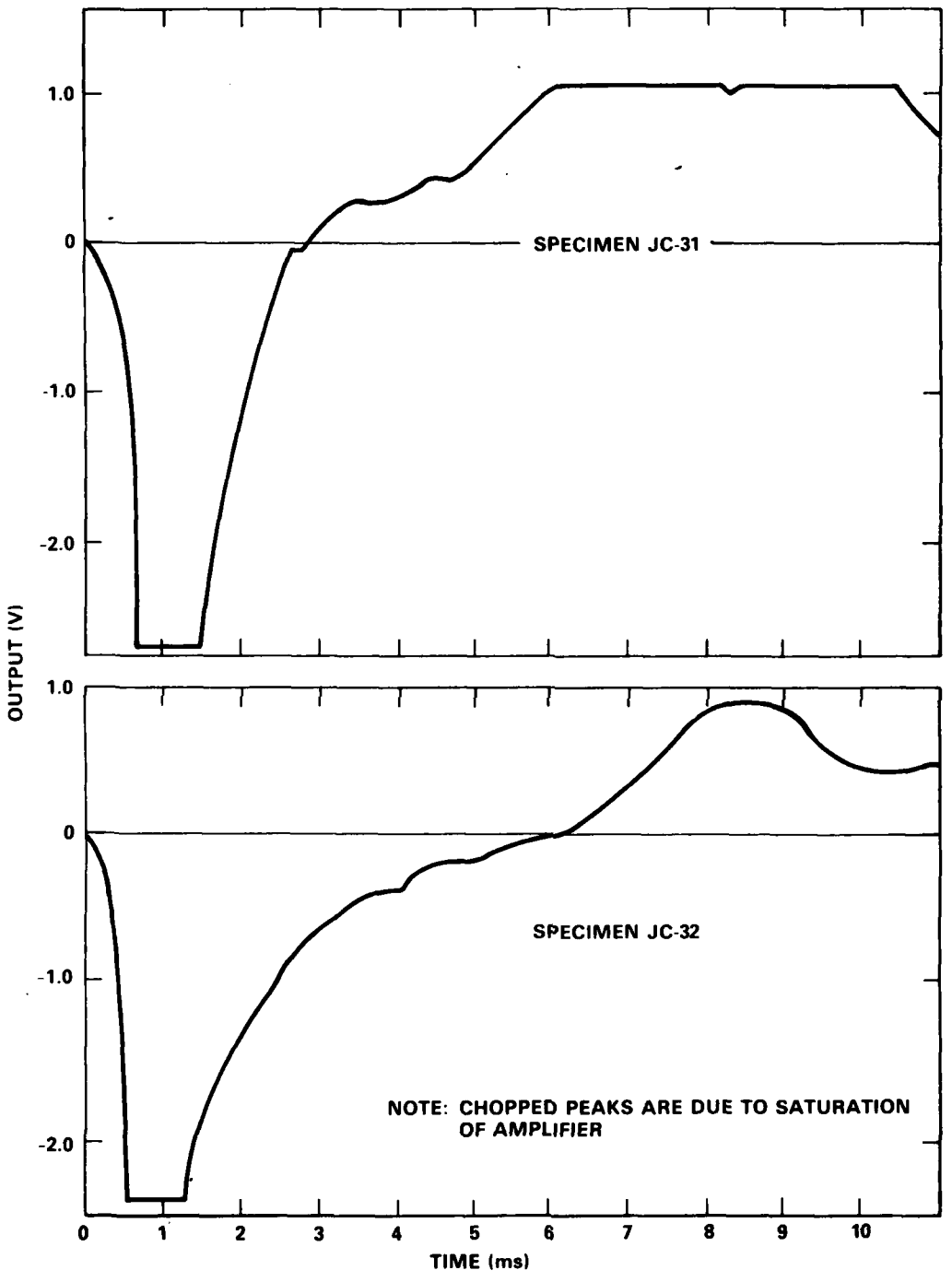

Figure A.19 - Potential Difference Signatures from Two Specimen Tests

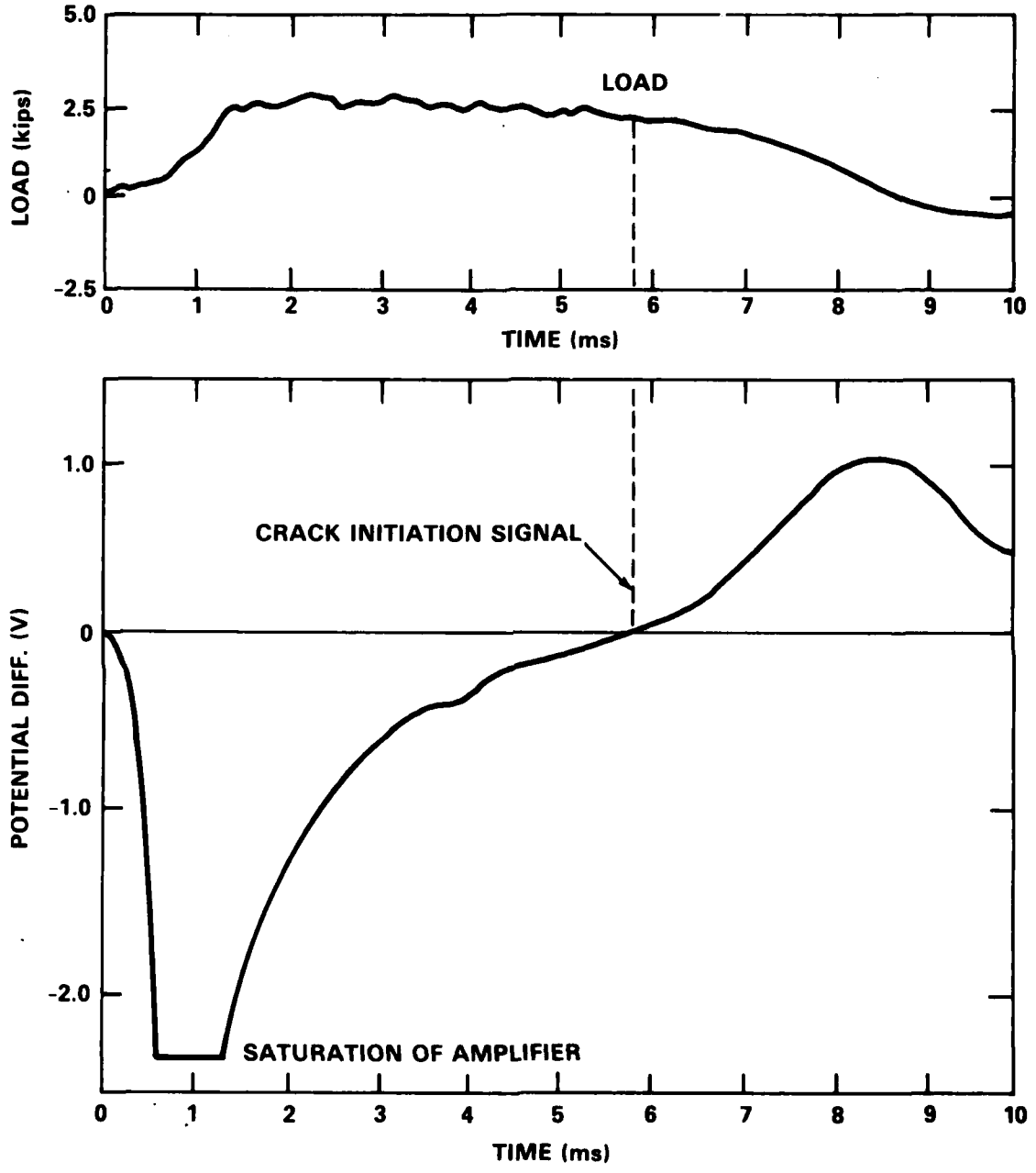

Figure A.20 - Applied Load and Corresponding Potential Difference Histories for Specimen JC-32

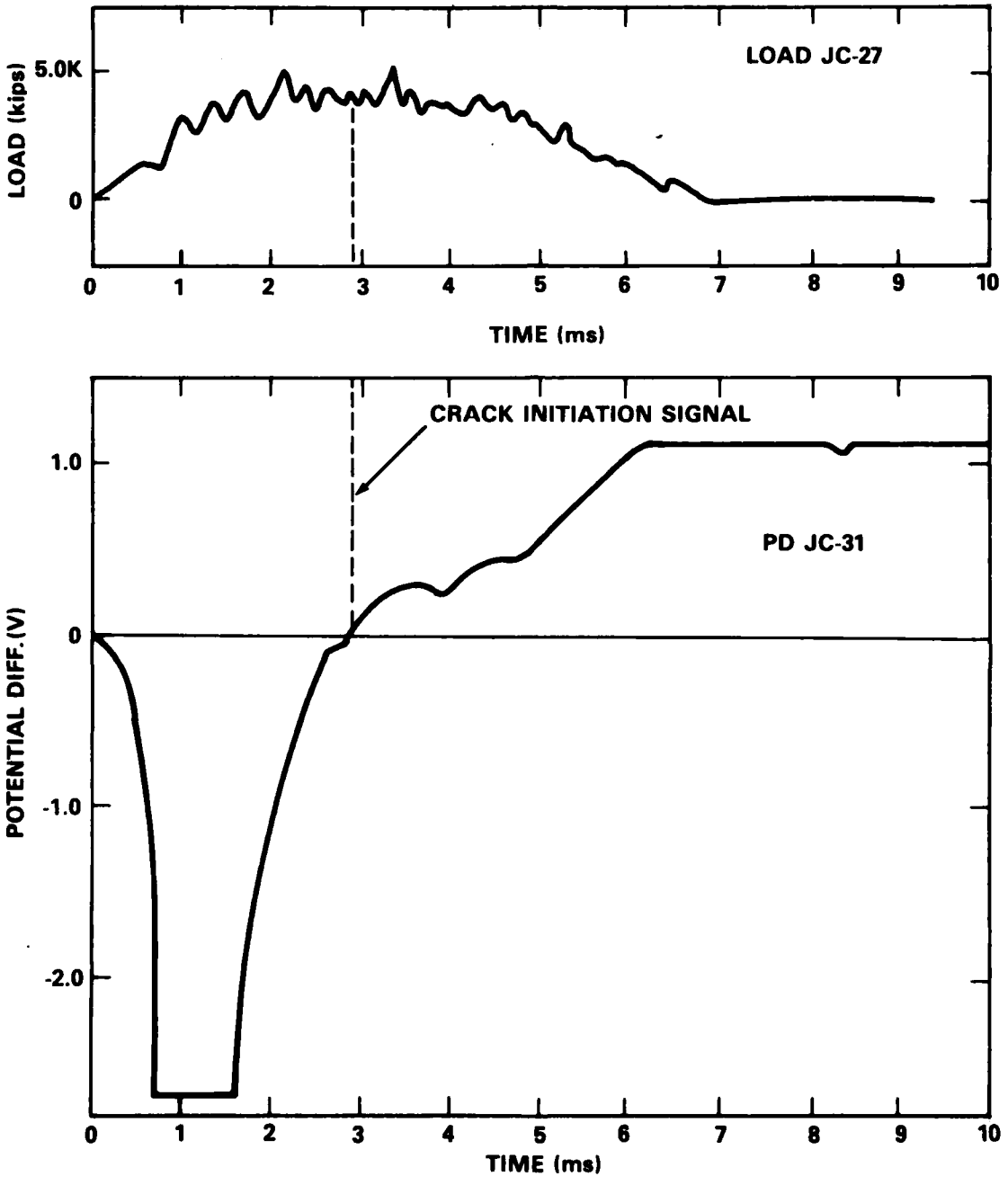

Figure A.21 - Comparison of Potential Difference Record with Applied Load for Tests at Comparable Conditions

indicated when the signal becomes positive. This indication comes early in the loading phase about the time of maximum load. It could not be certified that JC-31 sustained crack extension because it was used in subsequent tests before it was broken and examined. It was determined, however, that specimen JC-27 did not fracture. In the static and fatigue crack work this procedure looked promising, yet in the dynamic tests the results were questionable. There is no explanation for the large signal in excess of 1 V obtained during the tests since during fatiguing the signal was comparatively smaller. There was roughly a 1/4-in. crack extension and the voltage change was only 0.25 V. Also, there is no reason for the initial large negative spike. The test fixture was always insulated from ground, yet all the instrumentation is common to ground and this may be causing some problems. The technique needs more exploration before a valid assessment can be made.

REFERENCES

1. Vandervelt, H.H. and J.P. Gudas, "Application of Fracture Control Technology in Navy Ships and Submarines," in Fracture Mechanics, University of Virginia Press (1978).

2. Palermo, P.M., "Structural Integrity Procedures for Naval Ships," Trans. Am. Soc. Mech. Eng., J. of Eng. Materials and Tech., Vol. 102, No. 1, pp. 7-14 (Jan 1980).

3. Judy, R.W. et al., "Review of Fracture Control Technology in the Navy," Naval Research Laboratory Memorandum Report 4170 (Feb 1970).

4. Pellini, W.S., "Principles of Structural Integrity Technology," Office of Naval Research, Arlington, Va. (1976).

5. Gifford, L.N. and A.J. Wiggs, "Submarine Hull Toughness Research-Rationale, Approach, and Status," DTNSRDC Report 82/067 (Sep 1982).

6. Rice, J.R., "Mathematical Analysis in the Mechanics of Fracture," in Fracture, Vol. 2, Academic Press (1968).

7. "J_{IC}, a Measure of Fracture Toughness," Am. Soc. Testing Materials (ASTM) Standard E813-81, Annual Book of ASTM Standards, Vol. 03.01 (1983).

8. Joyce, J.A. and J.P. Gudas, "Computer Interactive J_{IC} Testing of Naval Alloys," in Elastic-Plastic Fracture, ASTM Special Technical Pubblication (STP) 668, pp. 451-468 (1979).

9. "Standard Method of Tests for Plane Strain Fracture Toughness of Metallic Materials," ASTM Standard E399-83, Annual Book of ASTM Standards, Vol. 03.01 (1983).

10. Begley, J.A. and J.D. Landes, "The J-integral as a Fracture Criterion," in Fracture Toughness, Part II, ASTM STP 514, pp. 1-20 (1972).

11. Joyce, J.A. and E.J. Czyryca, "Dynamic J_I - R Curve Testing of HY-130 Steel," DTNSRDC Ship Materials Eng., Dept. Report SME-81/57 (Oct 1981).

12. Hasson, D.F. and J.A. Joyce, "The Effect of Higher Loading Rate on the J_{IC} Fracture Toughness Transition Temperature of HY Steels," J. Eng. Materials Tech., Vol. 108, pp. 133-141 (Apr 1981).

13. Wilkowski, G.M. et al., "Fracture of Circumferentially Cracked Type 304 Stainless Steel Pipes Under Dynamic Loading," in Elastic-Plastic Fracture, Vol. II, ASTM STP 803, pp. II-331-352 (1983).

14. Ahmad, J., C.R. Barnes, and M.F. Kanninen, "An Elastoplastic Finite Element Investigation of Crack Initiation Under Mixed Mode Static and Dynamic Loading," in Elastic-Plastic Fracture, Vol. I, ASTM STP 803, pp. I-214-239 (1983).

15. Landes, J.D. and J.A. Begley, "The Effect of Specimen Geometry on J_{IC}," in Fracture Toughness, Part II, ASTM STP 514, pp. 24-39 (1972).

16. Gifford, L.N. and P.D. Hilton, "Preliminary Documentation of PAPST-Nonlinear Fracture and Stress Analysis by Finite Elements," DTNSRDC Structures Department Report m-43 (Jan 1981).

17. Merkle, J.G. and H.T. Corten, "A J-integral Analysis of the Compact Specimen, Considering Axial Force as Well as Bending Effects," Trans. ASME, J. of Pressure Vessel Tech., pp. 286-292 (1974).

18. Clark, G.A. and J.D. Landes, "Evaluation of the J-integral for Compact Tension Specimens," J. of Testing and Evaluation, Vol. 7, No. 5, pp. 264-269 (Sep 1979).

19. Dynamic J-Integral Compact Tension Specimen, DTNSRDC Drawing B-1043 (29 May 1979).

20. Dynamic J-Integral Tester, DTNSRDC Drawings E17-3596-1 through 3 (14 May 1979).

21. Landes, J.D., "J Calculation from Front Face Displacement Measurement on a Compact Specimen," Internat. J. Fracture, Vol. 16, No. 4, pp. R183-R186 (Aug 1980).

22. Johnson, J.J., "Calibrating the Electric Potential Method for Studying Flaw Crack Growth," Material Research and Standard, Vol. 5, pp. 442-445 (1965).

23. Halliday, M.D. and M.D. Beevers, "The d.c. Electrical Method for Crack Length Measurement," Proceeding of the Symposium on the Measurement of Crack Length and Shape During Fracture and Fatigue, Birmingham, England, pp. 85-112 (1979).

24. Ritche, R.D. and K.J. Bathe, "On the Calibration of the Electrical Potential Technique for Monitoring Crack Growth Using Finite Element Methods," Internat. J. Fracture, Vol. 5, No. 1, pp. 47-55 (Feb 1979).

25. Holsberg, P.W., J.P. Gudas, and T.B. Cox, "Stress Corrosion and Hydrogen Assisted Cracking Behavior of HY-130 Steel Plate, Weldments, and Product Forms," DTNSRDC Report 76-0083 (Dec 1976).

26. Conn, A.F., S.L. Rudy, and S.C. Howard, "The Strain Rate Dependence of Three High Strength Naval Alloys," Hydronautics, Inc. Technical Report 7111-1 (Jun 1974).

27. Bathe, K.J., "ADINA--Finite Element Program for Automatic Dynamic Incremental Nonlinear Analysis," Mech. Eng. Dept., Mass. Inst. Tech., Cambridge, MA (1978).

28. Key, Samuel W., Zelma E. Beisinger, and Raymond D. Krieg, "HONDO II--A Finite Element Computer Program for Large Deformation Dynamic Response of Axisymetric Solids," Sandia Laboratories, Albuquerque, NM (Oct 1978).

29. Hammel, J.W., U.v. Bodisco, and C. Mattheck, "An Elastic-Plastic Finite Element Analysis of a CT Fracture Specimen," Computers and Structures, Vol 13, pp. 757-770 (Oct-Dec 1981).

30. Atluri, Satya N., and Michikiko Nakagaki, "J-Integral Estimates for Strain Hardening Material in Ductile Fracture Problems," Amer. Inst. Aviation and Astronautics J., Vol 15, No. 7 (Jul 1977).

31. Hilton, Peter D. and L. Nash Gifford, "Evaluation of Some Crack Tip Finite Elements for Elastic Plastic Fracture Analysis," DTNSRDC Report 79/052 (Jul 1979).

32. Green, A.P. and B.B. Hundy, "Initial Plastic Yielding in Notched Bend Bars," J. Mech. and Physics of Solids, Vol. 4, pp. 128-144 (1956).

33. Yeakley, L.M. and U.S. Lindholm, "Effect of Strain Rate on the Strength of Four Metals (HY-80, HY-130, HY-180, and Ti-100)," SWRI Project 02-3625, Southwest Research Institute, San Antonio, Texas (Jun 1973).

34. Ouyang, C., "On Path Independent Integrals and Fracture Criteria in Nonlinear Fracture Dynamics," Internat. J. Nonlinear Mech., Vol. 18, No. 1, pp. 79-86 (1983).

35. Nishioka, T. and S.N. Atluri, "Path-Independent Integrals, Energy Release Rates, and General Solution of Near-tip Fields in Mixed Mode Dynamic Fracture Mechanics," Eng. Fracture Mech., Vol. 18, No. 1, pp. 1-22 (1983).

36. "ABAQUS User's Manual," Version 4, Revised, Hibbitt, Karlsson and Sorensen, Inc., Providence, RI (Aug 1982).

37. Ayres, D.J., "Dynamic Plastic Analysis of Ductile Fracture--The Charpy Specimen," Internat. J. Fracture, Vol. 12, No. 4, pp. 567-578 (Aug 1976).

INITIAL DISTRIBUTION

Copies		Copies	
1	DDR&E, Tech Lib	1	NCSC
3	CHONR	1	NSWC, White Oak
	1 ONR 432 (A. Kushner)		
	1 ONR 432 (Y. Rajapakse)	1	NSWC, Dahlgren
	1 ONR 471 (B. McDonald)		
		1	NUSC
1	CNO, OP987 R&D Plans Div		
		1	NAVAIR, 320
3	NAVMAT		
	1 MAT 071	1	NAVFAC, 03
	1 MAT 0713		
	1 MAT 0714	1	CBC Port Hueneme CA CEL
2	USNA	2	SUPSHIP, Groton
	1 (J. Joyce)		1 General Dynamics, EB
	1 (D. Hasson)		1 Dept 443 via SUPSHIP
4	NRL	2	SUPSHIP, Newport News
	1 6380		1 Newport News Shipbuilding
	1 6382 (M. Jolles)		1 Code E12 via SUPSHIP
	1 6384 (T. Crooker)		
	1 6323 (R. Judy)	1	SUPSHIP PASCAGOULA
14	NAVSEA	1	NAVSHIPYD MARE/Code 138
	1 SEA 05M		
	1 SEA 05R	2	NAVSHIPYD PORTSMOUTH
	1 SEA 05R25		1 Code 138
	1 SEA 55X		1 Code 200
	1 SEA 55Y		
	1 SEA 55Y2	1	NAVSHIPYD CHARLESTON
	1 SEA 55Y22		
	1 SEA 55Y23	12	DTIC
	1 SEA 55Y3		
	1 SEA 92	2	BUSTAND, Boulder
	1 SEA 921		1 Lib
	1 PMS 393		1 (D.T. Read)
	1 PMS 395		
	1 PMS 396	2	BUSTAND, Washington
			1 Lib
1	NAVPGSCOL		1 (J.T. Fong)
1	USNROTC and NAVADMIN, MIT	1	USCG
1	NADC	1	DOE, Oak Ridge
1	NOSC	1	NASA/Goddard
1	NWC		

Copies

2 NASA/Langley
  1 Lib
  1 (J.C. Newman)

1 NASA Scientific Tech Info Ofc

1 NUC Reg Comm

1 Johns Hopkins Appl Physics Lab

1 Hibbit, Karlsson and Sorensen, Inc

1 EPRI (Dr. D.M. Norris)

1 Univ of Arizona
  Dr. R.H. Gallagher

2 Battelle Columbus Labs
  1 Lib
  1 (C.R. Barnes)

2 Brown Univ
  1 (Dr. L.B. Freund)
  1 (Dr. C.F. Shih)

1 General Elec Corp Res Ctr
  Dr. V. Kumar

2 George Washington Univ
  1 (Dr. H. Liebowitz)
  1 (Dr. J.D. Lee)

1 Georgia Inst of Tech
  Dr. S.N. Atluri

1 Harvard Univ
  Dr. J.W. Hutchinson

1 Univ of Kansas
  Dr. R.H. Dodds

1 Lehigh Univ
  Dr. G.C. Sih

1 Authur D. Little, Inc.
  Dr. P.D. Hilton

Copies

2 MIT
  1 (Dr. D.M. Parks)
  1 (Dr. K.J. Bathe)

1 Univ of Maryland
  Dr. G.R. Irwin

1 Univ of Mass.
  Dr. W.A. Nash

1 Northwestern Univ
  Dr. J.D. Achenbach

1 Ohio State Univ
  Dr. C.H. Popelar

2 Sandia Laboratories
  1 Lib
  1 (Dr. S.W. Key)

2 Southwest Res Inst
  1 Lib
  1 (Dr. M.F. Kanninen)

1 Stanford Univ
  Dr. J.R. Rice

1 VPI & SU
  Dr. C.W. Smith

1 Vanderbilt Univ
  Dr. G.T. Hahn

1 Washington Univ
  Dr. P.C. Paris

2 Univ of Washington
  1 APL
  1 (Dr. A.S. Kobayashi)

2 Westinghouse R&D Center
  1 (Dr. H. Ernst)
  1 (Dr. W.K. Wilson)

CENTER DISTRIBUTION

Copies	Code	Name
1	012.1	G. Remmers
1	012.3	D. Moran
1	012.4	J. Corrado
1	17	W. Murray
1	1702	F. Lev
2	1706	K. McCabe(m)
1	172	M. Krenzke
1	1720.1	T. Tinley
1	1720.3	K. Hom
1	1720.4	A. Wiggs
1	1720.4	J. Carlberg
15	1720.4	L. Gifford
15	1720.4	E. Rasmussen
1	1720.5	D. McDevitt
1	1720.6	R. Rockwell
1	1720.6	P. Dudt
1	173	A. Stavovy
1	1730.6	J. Beach
1	174	I. Hansen
1	175	J. Sykes
1	1750.2	B. Whang
5	1750.2	W. Carr
1	177	R. Fuss
1	1770	Tech Ref Center
1	1770.1	V. Bloodgood
1	1770.5	J. Wise
1	28	J. Belt
1	2801	J. Crisci
1	2803	J. Cavallaro
1	281	G. Wacker
1	2814	J. Gudas
1	2814	E. Czyryca
1	2814	E. Hackett
1	2814	M. Vassilaros
1	2815	C. Zanis
10	5211.1	Reports Distribution
1	522.1	TIC (C) (+1m)
1	522.2	TIC (A)

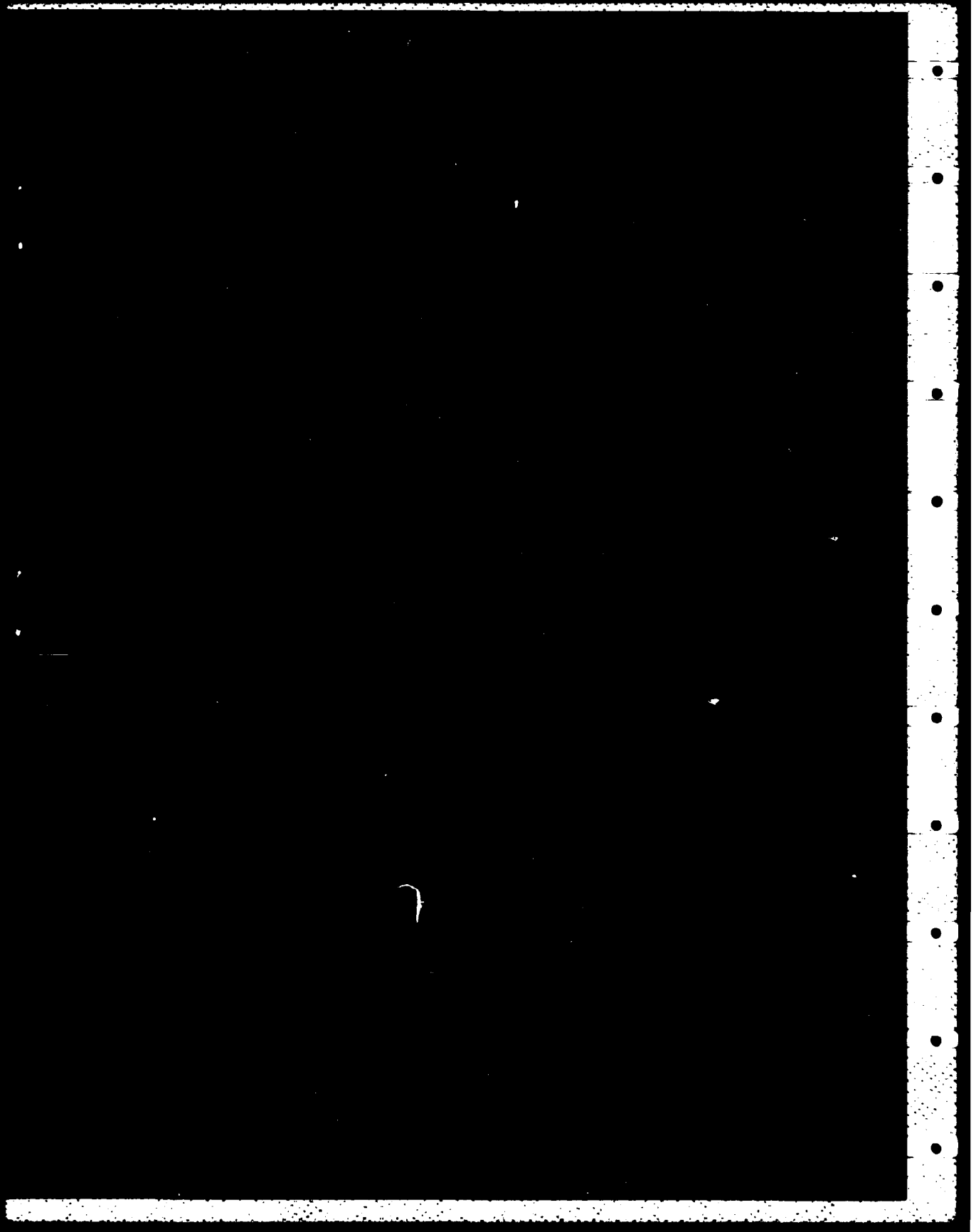

END

FILMED

8-85

DTIC